THE UNIVERSITY OF CHICAGO

EXPLORING ONTOGENETIC RELATIONSHIPS BETWEEN FORM AND FUNCTION

A DISSERTATION SUBMITTED TO

THE FACULTY OF THE DIVISION OF THE BIOLOGICAL SCIENCES

AND THE PRITZKER SCHOOL OF MEDICINE

IN CANDIDACY FOR THE DEGREE OF

DOCTOR OF PHILOSOPHY

GRADUATE PROGRAM IN INTEGRATIVE BIOLOGY

BY

HILARY ROSE KATZ

CHICAGO, ILLINOIS

AUGUST 2018

For my grandfather
Stanley Liss
1922 – 2014

TABLE OF CONTENTS

LIST OF FIGURES

LIST OF TABLES

ACKNOWLEDGEMENTS

I would not be the scientist that I am today without my advisor, Melina Hale. I would like to thank her for her incredible patience. As someone who gets easily distracted, I appreciated that she was quick to rein me in when I got too far out in the weeds. I am immensely grateful for her encouragement and support for my work at the Marine Biological Laboratory (MBL), which has become a huge part of my life. Under her guidance I have become a better thinker, writer, and mentor.

I want to thank my committee, Vicky Prince, Mike Coates, and Dan Margoliash, for sitting through what might be a record number of committee meetings. My work incorporated a number of different fields and techniques, and this group worked together perfectly to give me the feedback, advice, and constructive criticism that I needed.

I have to give a special thanks to everyone at the MBL for all of the help I received on my trips. I would like to thank Jennifer Morgan for being such a fantastic mentor and the entire Morgan Lab for making me feel like a part of the lab family. Special thank you to Kendra Hanslik for being my late night lab buddy, but also for getting me out of the lab from time to time. Thank you to Marko Horb, Marcin Wlizla, and everyone at the National Xenopus Resource for all of their help with my Xenopus work. They were amazing at making sure I had all of the frogs I needed at the right stages at the time of my visits.

Thank you to my fellow Hale lab members past and present, especially Brett Aiello, Adam Hardy, and Katie Henderson for putting up with me in my dark corner. I would like to thank our visiting high school student, Aden Goolsbee, for her help with frog digitizing and neuron tracing. Thank you to Berta Vasquez for being an amazing lab

manager and making all of our lives so much easier. A huge thank you to Evi Menelaou for her collaboration on the Rohon-Beard work. This chapter would not be what it is now without her electrophysiology skills and overall guidance. I would also like to thank her for the support and structure that she has brought to the lab since she arrived.

I don't know if I could have made it through grad school without the support of my fellow Darwinians, and special thanks to my Darwinian roommates, past and present. Thank you for being there through good times and bad.

Finally, I would like to thank my family. Thank you to my aunts, uncles, and cousins for your words of encouragement these past several years. Thank you to my sister, Julia, for distracting me with anything Disney-related and to my honorary sister, Tao-Tao, for being awesome. Thank you to my parents for always being there for me, and for working as hard as you have to support me. I am so lucky to have you.

ABSTRACT

Animals go through significant morphological and physiological change from hatching or birth to adulthood. Despite these transitions, fundamental behaviors such as feeding and locomotion must persist, but their performance may necessitate alternative strategies and structures. Relationships between anatomical structure and behavioral modality have been examined widely across species at the adult life stage, but less attention has been given to how these relationships change through life history. Examining relationships between structure and behavior across life history can provide insight into the evolution of behaviors as well as the functional plasticity that structures may exhibit. In this thesis, I utilize the Mauthner-based startle response in teleost fish and frogs as a model system for examining changes in morphology and behavior through life history. In fish, which have a well-characterized startle, I examine body shape and aspects of neural architecture and relate them back to what we already know about the behavior. In my second chapter I identify an ontogenetic change in body shape that is prevalent across ray-finned fish. In my third chapter, I characterize rostrocaudal regionalization within the larval mechanosensory cell population in zebrafish. Frogs do not have a well-characterized startle repertoire through metamorphosis, so in my fourth chapter I describe how a species of pipid frogs maintains a startle response as it transitions from axial- to limb-based locomotion. In my fifth chapter I discuss the teleost fish and frog systems, and propose experiments that could more directly examine the structure-function relationships that my findings indicate are changing through ontogeny.

CHAPTER 1

INTRODUCTION

To understand animal movement, we often study the relationship between morphology and function: the linkages of cranial bones and their association with jaw protrusion in fishes (e.g. Westneat 2004) or the shape and flexibility of a fin and its role in thrust generation (e.g. Feilich and Lauder 2015). Often these relationships are studied at a single stage of life history in a single species or by comparing structure and function among species (eg: Webb 1984; Eidietis 2006; Robovska-Havelkova et al. 2014). However, most animals undergo significant morphological change through ontogeny with related transitions in functions. As a result, animals must use different strategies to maintain necessary behaviors as they develop and in their adult form. To gain a better understanding of the evolution of behavior, it is essential that we study animals throughout their life history.

Life history stages are often studied in the context of development: the animal is an incomplete version of its adult form. But animals at intermediate stages also have unique pressures that are distinct from those of the adult stage. Ontogenetic, stage-specific adaptations allow animals to cope as relevant life history factors such as geographical location, predators, and diet, change with growth and maturation (reviewed in fish by Fuiman and Higgs 1997). For example, some amphibians transition from an aquatic habitat to a terrestrial one. Reef fish transition from a pelagic larval stage to a benthic adult stage when they settle on the reef (Leis and McCormick 2002). Biomechanics will also change with animal growth. For example, due to their small size,

larval fish experience intermediate Reynolds numbers where viscosity relatively high (Muller and van Leeuwen 2004; McHenry and Lauder 2006).

As animals undergo morphological changes associated with these life history factors they must maintain critical behaviors such as locomotion. Many larval fish locomote with undulatory waves propagated along the body axis, which allows the animal to efficiently move through an environment of transitional Reynolds numbers (Muller and van Leeuwen 2004; Mchenry and Lauder 2006). As they grow and enter the realm of high Reynolds numbers, locomotor strategies diversify among species. For example, they may transition from axial-based to fin-based locomotion. In this instance, different structures, body and fins, are utilized to maintain the behavior of swimming at different life history stages. This is particularly significant in the context of evolution because the same structure experiences different selective pressures across life history. Investigating post-natal or post-hatching development can provide insight into the evolution of the development of behavior as well as the functional plasticity that some structures exhibit.

In this dissertation, I examine relationships between structure and function and their impact on behavioral modality across life history stages. I focus on two animals that undergo distinctly different types of ontogenetic body shape change: teleost fish and frogs. The species that I will focus on are *Danio rerio* (zebrafish) and *Xenopus laevis* (African clawed frog). Zebrafish larvae and *X. laevis* tadpoles have many similarities. They both have an axial body plan, locomote via axial undulation, and have similar neural components such as a lateral line. However, they undergo very different trajectories throughout their post-larval ontogeny. Fish have distinct larval and adult

forms, but maintain their fundamental axial body plan of serial muscle segments through ontogeny, while frogs transition from an axial to a tetrapod body plan.

I use the startle system as a model to investigate relationships between morphology and behavioral modality in both fish and frogs. As startle is critical to survival, and therefore evolutionary fitness, this behavior is common and has been described in species spanning the animal kingdom. In fish, the startle behavior and neural circuit have been particularly well characterized (reviewed in: Stefanelli 1951; Korn and Faber 2005; Hale et al. 2016). The startle behavior in fish is also referred to as Mauthner-initiated startle, named for the pair of large reticulospinal neurons, Mauthner cells (M-cells), in the hindbrain that drive the behavior (Mauthner 1859). The cell bodies are located bilaterally in the hindbrain at the level of the eighth cranial nerve (Stephanelli 1951). M-cell axons project across the midline and extend along the length of the spinal cord, contralateral to the soma, making connections with motor neurons and interneurons. The somas receive and integrate input from many sensory systems including vestibular, visual, and mechanosensory. If a stimulus is strong enough to elicit a startle, an M-cell will produce a single action potential that travels down the spinal cord and elicits contralateral motor output, resulting in a "C-"shaped bend away from the stimulus. This "C-start" is the most common form of startle observed across fishes. This same general pattern of activity has been described in *Rana catesbeiana* (bullfrog) tadpoles (Rock 1980).

While the C-start is the most prevalent form of startle observed across fishes, there are several other forms of startle that specific types of fish have can perform. These modalities of startle behavior are associated with different body shapes (Hale 2002; Ward

and Azizi 2004; Liu and Hale, 2014). Highly elongate species (such as eels) perform a retraction response; animals with low (goldfish) to moderate (northern pike) elongation ratios perform a C-start response; and some moderately elongate species (northern pike) alternate between S- and C-starts (Hale, 2002; Ward and Azizi, 2004; Liu and Hale, 2014). An S-start can only be elicited by a caudal tactile stimulus. These different forms of startle are produced by different activation patterns of the Mauthner circuit (Hale 2002; Liu et al. 2011; Liu and Hale 2017).

Unlike the C-start, both M-cells must fire to produce an S-start, and the axial output is characterized by rostral motor output on one side and caudal motor output on the opposite side (Liu and Hale 2017). This results in two bends along the body axis, forming an S-shape for which the response is named. Figure 1.1 shows the activation pattern that produces the S-start in more detail.

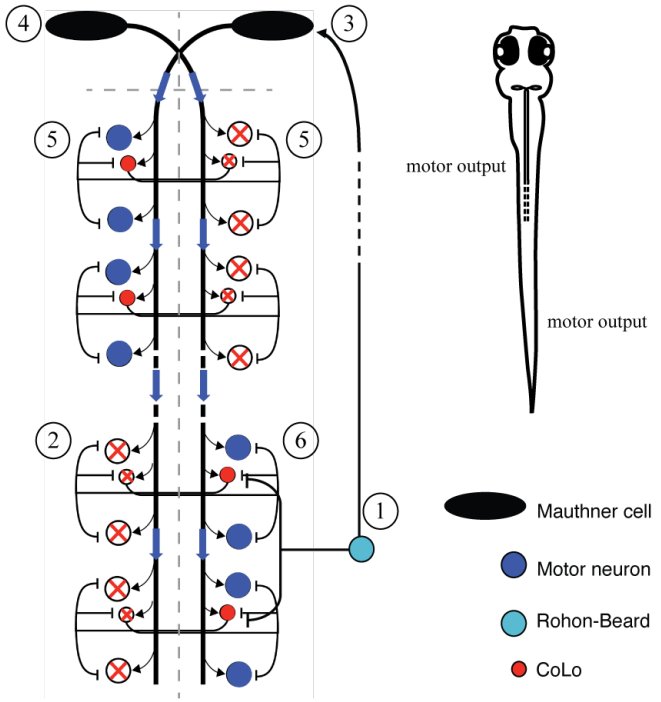

Figure 1.1: Schematic of the S-start activation pattern within the Mauthner circuit. (1) Rohon-Beard activation activates commissural contralateral inhibitory interneurons (CoLos) in the spinal cord, which (2) inhibit contralateral motor neurons and CoLos. The RB cells then indirectly (3) activate the ipsilateral Mauthner cell followed shortly by (4) the contralateral Mauthner cell. As the signal travels down the spinal cord, (5) the fist Mauthner activates contralateral motor neurons and CoLos, which hyperpolarize contralateral motor neurons and CoLos. As the signal from the second Mauthner cell follows, it is unable to bring these hyperpolarized cells to threshold. However, when these signals reach the caudal region of the body, the contralateral motor neurons and CoLos are still hyperpolarized. As a result, the second Mauthner cell is able to (6) bring the ipsilateral motor neurons and CoLos to threshold before the first Mauthner cell. This results in rostral motor output on one side of the body, and caudal motor output on the opposite side. Based on Liu and Hale (2017)

We specifically selected *X. laevis* for our study because it has been shown to have M-cells at both tadpole and adult stages (Will 1986). The Mauthner circuit is highly conserved across fish and some amphibians (Bierman et al. 2009). Up until about 30 years ago, it was thought that M-cells were only found in tadpoles, and disappeared in

frogs shortly after metamorphosis (Stefanelli 1951). However, Will (1986) showed that in some species, M-cells could be identified in mature adult frogs. Tadpoles perform a C-start response that has been well characterized and is very similar to the fish C-start (Rock 1980; Clarke et al. 1984; Laura Eidietis 2006). Physiological studies in bullfrog tadpoles indicate that the pattern of neural activation that drives the C-start is also very similar to what we see in fish: Mauthner cell activation results in primarily contralateral motor output (Rock 1980).

Based on electrophysiological evidence, frogs do not appear to have the contralateral M-cell inhibition that zebrafish exhibit (Rock 1980). This lack of inhibition in the hindbrain may be due to variation in a specialized structure known at the M-cell axon cap. Zebrafish, and all cyprinids examined, have what is referred to as a composite axon cap (Bierman et al. 2009). At the center of this structure are the unmyelinated axons of spiral fiber neurons, which wrap around the Mauthner axon hillock and form excitatory synapses with the contralateral M-cell (Scott et al. 1994; Koyama et al. 2011). The outer layer includes passive-hyperpolarizing potential (PHP) fibers. These neurons are activated by either the ipsilateral or contralateral VIIIth cranial nerve and inhibit the M-cell. These PHP neurons produce an extrinsic hyperpolarizing potential at the axon hillock which prevents the M-cell from firing multiple action potentials and also inhibits the contralateral M-cell (Furukawa and Furshpan, 1963; Weiss et al., 2008). Tadpoles as well as lungfish and other early-branching actinoperygii have a simple axon cap, which lacks these inhibitory PHP neurons (Will 1991; Bierman et al. 2009). This simple cap structure seems to be associated with a higher probability of bilateral motor output during startle (Westneat et al. 1998; Hale et al. 2002; Bierman et al. 2009). For the frog, this lack

of inhibition at the level of the hindbrain may be helpful for transitioning from axial startle to bilateral limb-based startle during metamorphosis.

Because zebrafish and *X. laevis* both have Mauthner cell-based startles, it allows for the unique opportunity to compare how the same neural circuit can accommodate two very different types of morphological change through ontogeny. I use each system to explore different aspects of this question. In the fish, I examine (1) how body shape changes through ontogeny across ray-finned fish, and (2) how axial mechanosensory cells play a key role in the regionalized motor output associated with a stage-specific startle modality. In the frog system, I examine how startle behavior is maintained as it transitions from an axial- to limb-based movement mechanisms through metamorphosis.

In my second chapter, I look for common trends in ontogenetic shape change across ray-finned fishes. In adult fish, the broad diversity of body shape is well established. This variation in body shape has been linked to differences in behaviors such as locomotion (Webb 1984). With such diversity, I wanted to know if there were common trends in how fish transition from their larval to adult forms. I surveyed a broad range of ray-finned fish species and compared body elongation at larval and adult stages. I included at least one species from every order of the subclass Actinopteri for a total of 108 species from 44 orders (Based on the Eschmeyer Catalogue of fishes accessed January 2015). I found that the vast majority of fish are more elongate at the larval stage than at the adult stage, and that adults display greater interspecies variation than larvae. These results indicate that much of the diversity observed in adults is achieved in post-larval stages, and suggest that larval morphology in the majority of fishes is subject to common constraints across the phylogeny.

Zebrafish larvae fall within the moderately elongate category and can perform both C- and S-starts, while adults have only been observed to perform C-starts (Liu and Hale 2014). The stage specific S-start response is characterized by one rostral and one contralateral caudal bend along the body axis (Hale 2002; Liu et al. 2012). This sort of regionalized motor pattern is unusual because the fish post-cranial body plan has traditionally been considered to be a series of repeated sections without significant region-specific variation in its control of axial movements (Rovainen 1967, 1974; Selzer 1979; Buchanan 2001). The spinal motor and interneurons have been studied extensively in larval zebrafish and show no evidence of rostrocaudal variation in distribution or activity that could account for regionalized motor output observed in the S-start. This led us to look within the mechanosensory population for rostrocaudal variation.

In chapter three, I examine the larval mechanosensory network as a potential neural mechanism for regionalized motor output associated with a stage-specific behavior in fishes. At the larval stage in fish and many amphibians, post-cranial mechanosensation is carried out by a population of neurons called Rohon-Beard (RB) cells. RB cell bodies are located dorsally along the length of the spinal cord. Their afferents project out of the spinal cord, and to the skin where they form complex arborization patterns. These cells can be found across ray-finned fish, lobe-finned fish (*Neoceratodus*), and amphibians (Carter and Fox 1994). We utilized imaging and electrophysiological techniques to look for rostrocaudal differences in RB physiology and morphology of the peripheral processes in zebrafish. Across the RB cell population, we found evidence of rostrocaudal variation in morphology and physiology. We observed no differences in intrinsic

properties of these cells, indicating that the regionalization in the physiology comes from the complex structure of the peripheral process.

There are a number of similarities between tadpoles and larval fish. Both locomote via axial undulation, have lateral line systems and RB cells, and perform Mauthner-based C-starts (Rock 1980; Clarke et al. 1984; Laura Eidietis 2006). Unlike fish, frogs transition from an axial to a tetrapod body plan through metamorphosis. The C-start behavior is well characterized in tadpoles (Will 1991) and a form of adult startle has been described (Videler and Jorna 1985; Will 1991), but the transition between the two modalities has received much less attention. This system provides us with the ideal model for examining changes in behavioral modalities through dramatic morphological changes.

In chapter four, I utilize the startle response in *X. laevis* to investigate how a behavior is maintained through dramatic ontogenetic changes in the body. I examined how the axial C-start and new limb-based response change as the former is lost and the latter develops. The C-start did not display any significant difference in performance across metamorphic stages until it was lost. The limb-based startle or "pushback" response performance increased through metamorphosis, but decreased post-metamorphosis. The C-start appears to maintain its high performance level until pushback performance reaches higher performance levels, at which point the C-start is lost.

In my fifth chapter, I discuss my results and propose future experiments to expand on my findings. In fish, based on the ontogenetic decrease in elongation I found across fish, I propose that the S-start may be more common across fishes than is currently

described, particularly in the larval stage. Additionally, I hypothesize that the loss of the S-start through ontogeny may result from the loss of the RB cells. Finally, I utilize what is already known from work in both fish and frogs to discuss possible neural mechanisms that might facilitate the axial- to limb-based startle transition.

CHAPTER 2

A LARGE-SCALE PATTERN OF ONTOGENETIC SHAPE CHANGE ACROSS RAY-FINNED FISHES

2.1 Abstract

Fishes exhibit a remarkable diversity of body shape as adults; however, it is unknown whether this diversity is reflected in larval stage morphology. Here we investigate the relationship between larval and adult body shape as expressed by body elongation. We surveyed a broad range of ray-finned fish species and compared body shape at larval and adult stages. Analysis shows that the vast majority of fish are more elongate at the larval stage than at the adult stage, and that adults display greater interspecies variation in elongation ratio than larvae. We found that the superorder Elopomorpha is unique because many species within the group do not follow the aforementioned elongation trends. These results indicate that much of the diversity observed in adults is achieved in post-larval stages. This trend in ontogenetic morphological change may be indicative of shifts in associated movement strategies. We suggest that larval morphology is subject to common constraints across the phylogeny.

2.2 Introduction

Comparing and categorizing species at their adult stage has shown that ray-finned fishes exhibit a wide diversity of body shapes (Ward and Brainerd 2007; Claverie and Wainright 2014; Ward and Mehta 2010). Studies investigating shape diversity at the larval stage indicate that there is less diversity in larvae than adults (Strauss and Fuiman

1985). However, such work at the larval stage has been limited to a handful of species in one environment or species within a single family (Strauss and Fuiman 1985; Fuiman 1979). In this study, we examine larval and adult body shape diversity on a broader scale. By surveying a wide range of species, we can investigate trends across the phylogeny. We can also identify outlier groups that may be of use as case studies for finding developmental mechanisms for shape diversification.

A particularly informative measure of body shape is body elongation (Ward and Brainerd 2007; Claverie and Wainright 2014; Ward and Mehta 2010) because it captures much of the axial diversity in adults (Claverie and Wainright 2014). The diversity of elongation is associated with a variety of factors including development, locomotion, and physiology. Early developmental processes of axial patterning may constrain larval body shape. Axial morphology could also have evolved to support particular locomotor strategies (Webb 1984) or to accommodate physiological and functional requirements such as respiration (Hale 2014), burrowing (Herrel et al. 2011), and feeding (Toline and Baker 1993).

One function that has been associated with body elongation is the escape response (Liu and Hale 2013; Ward and Azizi 2004). There are three behavioral subtypes of startle that appear to be linked with different elongation ranges. Highly elongate fish such as lampreys and ropefish perform a withdrawl startle response, which is characterized by the head retracting in towards the body via bilateral bending along the body axis (Currie and Carleson 1985; Bierman et al. 2004). Moderately elongate fish like muskellunges can perform two types of startle behavior: S- and C-start responses (Hale 2002). S- starts are characterized by two bends along the body axis, forming an “S” shape, while the C-start

has only a single bend resulting in the fish forming a "C" shape. Finally, fish with very low elongation ratios such as goldfish only perform a C-start response.

These associations between startle and body shape have been made, for the most part, with adult animals. One exception is zebrafish: larval zebrafish fall under the moderately elongate category and perform both the C- and S-start (Liu and Hale 2013), while adult zebrafish are less elongate and have only been observed to perform the C-start. This behavioral shift suggests that the relationship between startle and elongation may persist not only across adults, but also potentially within individuals across life stages.

Understanding larval body shape, its comparison to adult shape and trends across fishes, are fundamental to understanding fish biodiversity as well as development and evolution of body shape. Furthermore, these changes may give insight into potential behavioral shifts the animal might be experiencing through life history, and provide us with a model with which to investigate the evolution of this ontogenetic relationship between form and function. Here we set out to answer the following questions: Is the diversity in elongation observed in adult fish reflected in the early larval stage? Is there a difference in the variability of body shape between larval and adult stages? And are there different developmental trajectories by which the adult elongation state is achieved?

2.3 Methods

We collected images from at least one species of fish from every order of the subclass Actinopteri. Orders and families were based on Eschmeyer's catalogue of fishes (Eschmeyer et al. 2018). Images were collected from online databases (i.e. FishBase) as

well as the literature [Appendix I]. By far our largest source of images of larvae was Jones et al. (1978). Species from Jones et al. (1978) were selected randomly while others were selected based on availability to fill in gaps. Images were used from larvae that were as close to hatching as possible so that the larvae measured fell within the same life history stage. At least one image of a larval fish and one of an adult fish were collected for each species. In many clades, images of larvae at different stages are rare, and to be consistent across the sample, we selected one individual per species for use in analysis. If we were able to acquire multiple measurements for a species, we used three criteria to objectively decide which one to include. First, an image with a scale was taken over one without. Because we were measuring a dimensionless number, a scale is not necessary. Second, many of the images of larvae are only available as drawings or traces, particularly in the older literature. However, if a photo was available, we selected it over a drawing. Finally, an image from a primary source was selected over an image from a collection. It should be noted, however, that the results did not change when data were analyzed using averages of data from multiple images.

Elongation ratio was calculated as a ratio of body length to depth and is dimensionless. Length was measured from the center of eye to end of the caudal fin so that elongate snouts would not be included in the measurement. Depth was measured at the anus for larvae, and just anterior to anal fin for adults as described in Parichy et al. (2009). Depth did not include the fin fold in larvae or any of the median fins in adults. We did not include these structures in our measurements because our goal was to measure comparable structures at the larval and adult stages. Measurements were taken

in ImageJ (Schneider et al. 2012), and statistical analysis was completed in R (R Core Team 2013).

There were two extreme outliers in our data set: *Notacanthus chemnitzii* (snubnosed spiny eel) and *Eurypharynx pelecanoides* (pelican eel). *N. chemnitzii* had the greatest larval elongation ratio and was more than twice as elongate as the second most elongate specimen. *E. pelecanoides* had a very elongate adult form and an extremely low elongation ratio as a larva. We performed statistical analyses without these two species because we are interested in general group trends and these two species have very distinct characteristics. The results without these animals are presented below, but overall findings are consistent with or without the inclusion of these values.

2.4 Results and Discussion

We first investigated differences between life history stages by comparing elongation ratio between the larval and adult stage of each species (Figure 2.1). Most species achieve their final adult morphology by becoming less elongate than their larva (96 out of the 108 species sampled). The other 12 species became more elongate through ontogeny. Of these 12 species, five were anguilliformes, or true eels, while the other seven were scattered throughout the phylogeny. Of the 108 species, five showed less than a 10% change in elongation ratio. These five species were scattered across the phylogeny and have very different morphologies: *Euthynnus affinis* (Mackerel tuna), *Trichiurus lepturus* (Largehead hairtail), *Cheilopogon cyanopterus* (Margined flyingfish), *Poromitra megalops* (Ridgehead), and *Arius felis* (Hardhead catfish).

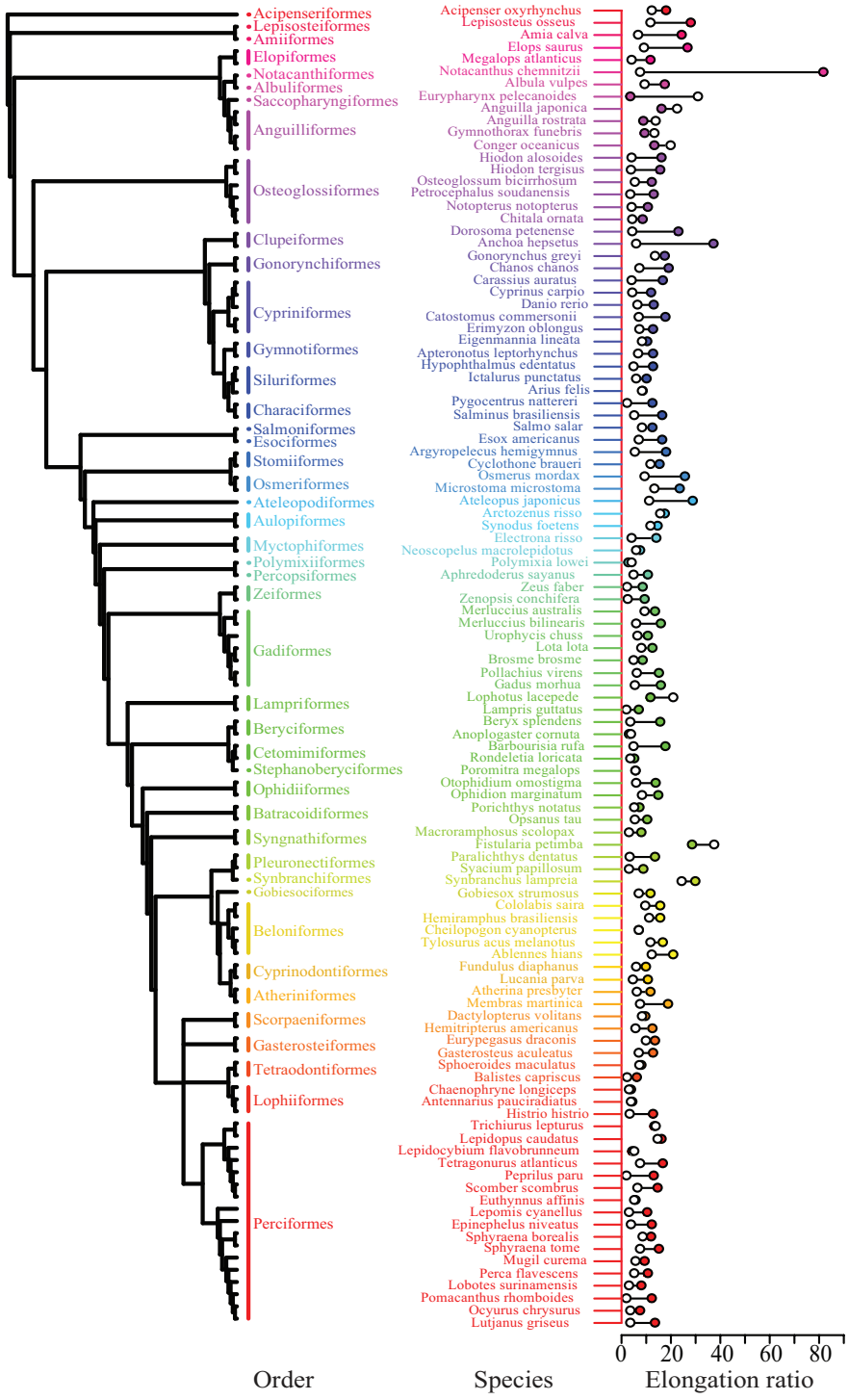

Figure 2.1: Individual larval and adult elongation ratios.

Figure 2.1, continued. The reconstructed phylogeny of all species utilized in this study: orders are indicated in different colors with arbitrary branch lengths. The phylogeny was assembled from several different phylogenies [Near et al. 2012; Near et al. 2013; Yoon et al. 2011; Miya et al. 2013; Sullivan et al. 2006; Inoue et al. 2010; Wang et al. 2012; Lavoué and Sullivan 2004). Genus and species name for every species measured in this study with corresponding larval (filled circle) and adult (open circle) elongation ratios (see S1 Table for exact values). The measurements plotted are the same as those used for statistical analyses (see methods section for selection criteria). Colors correspond to the orders from which the species were selected. Expanded views can be found in Figures S2.1 – S2.3.

We compared the average and distribution of elongation ratios of larval and adult stages, to determine whether the body shape diversity observed in adults is reflected in the larval stage. Larvae (mean±SE, 13.3±0.591) had a significantly greater mean elongation ratio than the adults (7.43±0.551) (ANOVA, $p<0.001$, Figure 2.2A), which is consistent with the decrease in elongation ratio observed in most of the species (Figure 2.1). This ontogenetic decrease in elongation ratio suggests that behavioral changes, like the shift in startle repertoire observed in zebrafish, may be more prevalent across the phylogeny. In fact, we found that 46 out of 96 species displayed an ontogenetic decrease in elongation ratio that was greater than or equal to that of the zebrafish (6.65). In looking for changes in startle behavior, this seems like it would be a good group of species to examine.

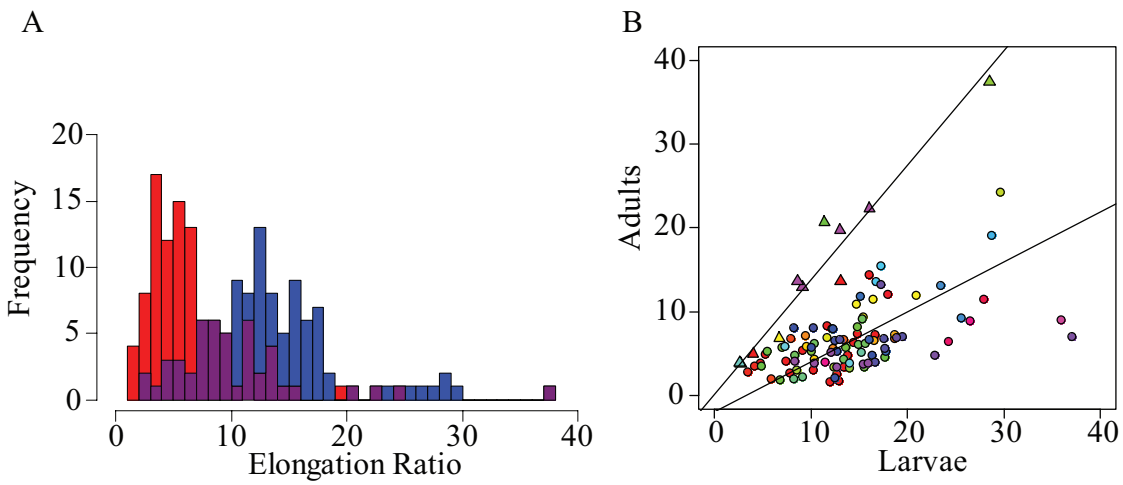

Figure 2.2: Comparison of larval and adult elongation ratios. (a) The distribution of larval (blue) and adult (red) elongation ratios. The number of species (x-axis) observed for a given elongation ratio (y-axis). (b) Larval elongation ratio plotted against adult elongation ratio. Each point represents a single species and colors correspond to the orders as presented in figure 1. The regression line is plotted for species that demonstrated a decrease in elongation ratio through ontogeny (circles) as well as for those species that demonstrated an increase in elongation ratio (triangles). Colors correspond to the orders as presented in figure 1.

The adults and larvae also had significantly different distributions of elongation ratios (Komogrov Smirnov test $p<0.001$; Figure 2.2A) with a greater coefficient of variation in adults (76.7%) than in larvae (46.1%). Our survey shows that this greater elongation diversity in adults is a broad trend across the fish phylogeny, and not limited to the handful of species that have been previously investigated (Strauss and Fuiman 1985). Because there is more diversity in elongation in adults than larval counterparts, these data suggest that much of the diversity observed in adults is achieved through post-larval development. This is in contrast to most investigations of the evolution of elongation across fishes, which propose that diversity in elongation is likely produced primarily by changes in the number or size of somites that are established at the embryonic stage (Ward and Brainerd 2007; Ward and Mehta 2010).

Differences in the diversity of elongation between larval and adult may be influenced by factors acting at different developmental stages. Early post-cranial anterior-posterior patterning is essential to ensure that the body is reliably segmented and cells are appropriately distributed between segments. Because of this patterning process, larval body shape may be constrained to the initial highly elongate form that is produced. Body shape may also be influenced by the locomotor demands of the environment. Larval fish experience primarily intermediate Reynolds numbers ($20 < Re < 1000$) (Müller and van Leeuwen 2004), where undulation is a particularly effective form of locomotion (Müller and van Leeuwen 2004). This form of locomotion benefits from a more elongate shape that can propagate waves along the entire body. As body size and swimming speed increase through ontogeny, fish spend more time at high Re ($Re >> 1000$) (Müller and van Leeuwen 2004; Webb and Weihs 1986), where they may utilize a broader range of propulsive strategies efficiently. Body shape may also be influenced by physiological factors such as respiration. Larval fish absorb oxygen and ions through the skin, which may constrain post-cranial morphology until they develop gills at the juvenile stage (Hale 2014).

To test for an association in elongation ratio between larval and adult stages, we performed a reduced major axis regression (Figure 2.2B). For species that showed a decrease in elongation through ontogeny, larval elongation ratio was weakly correlated with adult elongation ratio (R^2=0.322, slope=0.339, intercept = 1.70, $p<0.0001$), suggesting that the adult elongation ratio may be independent of the initial larval elongation ratio. However, there was a strong correlation between the two stages for the species that showed the reverse trend (R^2=0.943, slope=1.33, intercept = 0.516,

$p<0.0001$). Among species that show the reverse trend, the high R^2 value indicates that adult elongation ratio is highly predictable from larval elongation. This would suggest that there is a closer association between adult and larval elongation in animals that become more elongate than in animals that become less elongate. Elongate body forms may occur from an increase in vertebral length, number, or a combination of both (Ward and Brainerd 2007; Ward and Mehta 2010). For a given body size, these components are linked: increasing the number of somites will decrease the somite length (Ward and Mehta 2010). Of the 12 species that showed an increase in elongation through ontogeny, eight actually had elongate adult body forms (elongation ratio > 10). All of these species have very high vertebral counts recorded ranging from ~76 in *Fistularia petimba* (trumpet fish; McEachran and Fechhelm 1998) to ~138 in the order Lophotidae (oarfish; Richards 2005). These species may be reaching the maximum number of somites that can be fit into their respective bodies, and as a result, their adult form is very closely associated with their larval form.

The superorder Elopomorpha was uniquely variable among the taxa we examined. All anguilliform, or true eel, species sampled showed an increase in elongation ratio through ontogeny. *Notacanthus chemitzii* (snubnosed spiny eel) and *Eurypharynx pelecanoides* (pelican eel) were both major outliers. In contrast, *Megalops atlanticus* (atlantic tarpon) and *Elops saurus* (ladyfish) showed the more common decrease in elongation ratio. Unlike most of the other groups we surveyed, this superorder appears to use several different developmental strategies to achieve their diverse adult forms. The variability observed within this superorder may be related to its unusual and unique larval stage, known as leptocephalus, which is characterized by a ribbon-like, glassy appearance

(Miller 2009). Because of this remarkable morphological range in both larvae and adults, we suggest that Elopomorpha would be a valuable group in which to examine the development of body shape and elongation. Recent advances in captive breeding of certain true eel species (Sorensen et al. 2016) may allow for more in-depth ontogenetic behavioral studies. Since this group includes fewer species and has a well-supported origin (Near et al. 2012), phylogenetic comparative methods could be applied to tease out the phylogenetic signal in the relationship between larval and adult body shape.

CHAPTER 3

ZEBRAFISH MECHANOSENSORY AFFERENTS EXHIBIT MORPHOLOGICAL AND PHYSIOLOGICAL REGIONALIZATION ALONG THE BODY AXIS

Hilary Katz (HK) and Melina Hale (MH) conceived this study. HK and MH designed the Rohon-Beard population imaging experiments. HK, MH, and Evdokia Menelaou (EM) designed the single cell Rohon-Beard imaging experiments and electrophysiology experiments. EM performed embryo injections for sparse labeling of RB cells. HK performed all lightsheet and confocal imaging and analysis. EM performed electrophysiology experiments and data collection. HK analyzed the electrophysiology data with input from EM.

3.1 Abstract

Mechanosensory neurons play an important role in converting mechanical forces into the sense of touch. In zebrafish it is well established that Rohon-Beard (RB) neurons serve this role at the larval stage. Previous work has shown differences in spinal neural circuit activity between rostral and caudal regions of the spinal cord. This rostrocaudal variation has been suggested to be due to differences in mechanosensory input. In this study we assessed RB morphology and physiology along the body to address whether RB heterogeneity could account for such variation. We found that RB neurons exhibit morphological and physiological variation related to their location along the spinal cord. RB neurons located rostrally have peripheral afferents that exit the spinal cord within one body segment of the soma and their area of arborization is narrow. In contrast, RB cells

located caudally may exit the spinal cord much further away from the soma and, on average, have broader areas of arborization. At the level of the skin, we found that more caudal RB soma tended to have more longitudinal processes that extend further caudally. The receptive fields established electrophysiologically matched the morphological arborization ranges: rostral cells respond to stimuli close to the soma, while caudal cells respond to more distant stimuli over a broader area. The caudal fin in particular was found to be an area of high sensitivity. This regionalization of the zebrafish mechanosensory system can provide insights into how sensory information is encoded in the periphery and how spinal circuits transform touch information into behavioral outputs.

3.2 Introduction

The post-cranial body plan of fish has historically been considered as a series of repeated segments with little to no variation among them (Rovainen 1967, 1974; Selzer 1979; Buchanan 2001). However, recent physiological studies have shown complexity in body bending and suggested antero-posterior variation in the neural control of axial muscles (Liu et al. 2012; Liu and Hale 2017). The spinal interneurons and motor neurons that drive axial bending have been described morphologically and physiologically (Bernhardt et al. 1992; Hale et al. 2001; Bhatt et al. 2007; Bagnall and McLean 2014), and exhibit relatively consistent morphology and distributions along the spinal cord. We hypothesized that variation in sensory input along the body axis may provide a mechanism for driving variation in axial movement. In this study we examine the main population of mechanosensory neurons in larval zebrafish, the Rohon-Beard (RB) cells.

The RBs provide an opportunity to map a population of mechanosensory cells along the body and investigate the potential source of regionalized variation in motor activity. The RBs are a more accessible model for investigating mechanosensation in vertebrates than analogous neurons in mammalian models. RBs may provide insight into how regionalization of the spinal cord, which is significant in terrestrial vertebrates, may have arisen in systems with less-differentiated spinal cord circuits.

Identifying the morphological features of sensory neurons and their afferents, and characterizing their physiological responses to stimuli are critical to understanding any sensory network. In vertebrates, physiology is also used to identify sensory neurons as morphological access is limited. Cell bodies for most vertebrate mechanoreceptors are contained within the dorsal root ganglia (DRG), which are partially covered by the vertebral column making them challenging to access (Djouhri et al. 1998). Studies that have performed *in vivo* whole cell recordings from DRG cells have identified differences in spike features that correspond to functionally distinct afferent types, particularly nociceptors and low-threshold mechanoreceptors (Djouhri et al. 1998; Fang et al. 2005). For studying the encoding of stimulus features, extracellular recordings on single primary afferent fibers (first described in Talbot et al. 1968) are commonly utilized. These extracellular techniques are often used to examine how stimulus features are encoded via spike number, rate, and/or latency. Afferent fibers are often more accessible than the soma, facilitating *in vivo* experiments. Extracellular afferent nerve recordings may also be performed *in vitro* for more controlled stimulus manipulation (Zimmermann et al. 2009). Along with physiological studies, new molecular tools have allowed researchers to identify ion channels and receptors that are specific to mechanoreceptors (Reviewed in

Walsh et al. 2015). The identification of subtypes of channels and signaling molecules has facilitated the generation of transgenic mouse lines with different mechanosensory populations labeled (Hasegawa and Wang 2008; Li et al. 2011). This allows for targeted investigations of specific mechanosensory sub-types without the need to use physiological recordings to identify the cells of interest.

One of the major challenges in studying mechanosensory networks involved in touch and local body movement in tetrapods is that the peripheral processes are embedded in the skin, and can only be visualized from extracted tissue (eg: Marshall et al. 2016). However, certain morphological features can be characterized with electrophysiology. Peng et al. 1999 describes a technique for characterizing branching structure between two points on the skin. Breifly, this can be done by recording from a nerve trunk afferent and stimulating two locations. A branching point can be calculated from the conduction time from each stimulus location to the recording electrode and the distance along the process between the two stimulus locations (described in Peng et al. 1999). This type of study is immensely valuable for understanding the role that branching plays in peripheral processing, but it is impractical as a tool for studying gross morphology because of the sheer number and complexity of afferent branches and the distributions of their endings. Extracellular afferent nerve recordings *in vitro* can be utilized to relate the morphology of peripheral processes back to the physiology by staining the stimulated patch of skin (Zimmermann et al. 2009).

The mechanosensory network consisting of RB neurons is a model for mechanosensory research that addresses many of these challenges in tetrapod system by allowing for *in vivo* visualization of both the cell bodies in the spinal cord for

electrophysiological recording and the peripheral processes in the epidermis for simultaneous targeted stimulation. The RB cell bodies are located dorsally along the length of the spinal cord (Metcalfe et al. 1990). Their size and location make RB cells relatively easy targets for electrophysiological recordings as compared to the DRG cells that are embedded in ganglia. They are traditionally associated with three projections: two within the spinal cord (one extending rostrally and the other caudally), and one afferent fiber that projects dorsally out of the spinal cord to reach the epithelium. Once the peripheral projection reaches the skin it undergoes extensive branching and forms a dense network of arbors (Metcalfe et al. 1990; O'Brien et al. 2012). Recent work suggests that the RB population maybe more complex. Molecularly distinct sub-groups of RB cell type have been identified, but not yet linked to any functional or morphological sub-types (Palanca et al. 2013). Variation in the central axon projection has been identified along the body axis. Projections from cell bodies in the rostral region are more likely to reach the hindbrain than cells from the caudal region (Palanca et al. 2013; Umeda et al. 2016). Variable behavioral responses suggest they have regionalized sensitivity to stimuli (Umeda et al. 2016; Liu and Hale 2017).

A major gap in research on zebrafish RB cells has resulted from the lack of biologically relevant stimuli utilized in electrophysiology experiments. Because patching is so sensitive to mechanical disruption, experiments that require any additional manipulation near the recording site are extremely challenging. For this reason, current injections in the soma are commonly used to excite RB cells when examining their synaptic connections. While this technique can be utilized to examine downstream synapses, it leaves out arguably the most important component the mechanosensory

neuron: the afferent input. The importance of afferent input to RB activity has been demonstrated in tadpole RB cells, where somas can produce multiple spikes in response to a tactile stimulus on the skin, but will always produce a single burst response to current injection (Roberts and Hayes 1977; Clarke et al. 1984).

Here we examine RBs along the length of the spinal cord to describe their afferent anatomy and physiological response to touch stimulation and to determine whether there are regional differences in RBs that may have functional implications. We ask (1) do afferents of individual RB cells exhibit morphological differences associated with the antero-posterior location of their soma? (2) How do RBs in larval zebrafish respond to touch stimulation? (3) How do the physiological responses of individual RBs reflect regional morphological variation?

3.3 Methods

Fish

Experimental protocols were approved by the University of Chicago Institutional Animal Care and Use Committee. Zebrafish larvae and embryos were housed in 10% Hanks solution in a temperature controlled incubator at 28.2 ^{o}C under a 12 – 12 h light-dark cycle. Imaging was done between four to six days post-fertilization, while electrophysiology was performed between four and five days post-fertilization. Islt2b:GFP line of zebrafish were used for whole fish imaging and electrophysiology. To achieve sparse labeling for imaging single cells, we used the Islt2b:gal4 zebrafish line and injected the embryos at the one cell stage with either UAS:mcd8GFP or UAS:ptagRFP construct.

Imaging

For population imaging, we imaged the entire length of islt2b:GFP larval fish on a Zeiss Lightsheet Z.1 with a 20x/1.0 water dipper, which uses 10x NA 0.2 dry illumination objectives. Live fish were sedated in 0.02% trimethyl-sulfate (ms-222) in 10% Hanks solution and embedded in 1.4% agar. The animals were suspended in the imaging chamber in 0.01% ms-222 in 10% hanks solution.

For single cell imaging, we imaged islt2b:gal4 larva injected with either UAS:mcd8GFP or UAS:ptagRFP on a Zeiss Upright LSM 710. Again, live fish were sedated in 0.02% trimethyl-sulfate (ms-222) in 10% Hanks solution and embedded in a glass bottom dish in 1.2% agar. Fish were imaged with a 40x/1.0 numerical aperture water immersion objective. To capture the morphology of RB cells, we created a tiled image with 15% overlap. Tile stitching was performed in Fiji with the grid/pairwise stitching tool (Preibisch et al. 2009)

Analysis

We collected measurements of RB cells from a total of 102 cells from 8 larval Islt2b:GFP fish. Images were post-processed in Fiji (Schindelin et al. 2012) by increasing the gamma and subtracting the background to optimize visibility of fine nerve endings. Maximum intensity projections were stitched in order to count segment numbers. The initial trajectory of peripheral projections shortly after they enter the skin was analyzed for the RB population by performing semi-automated tracing in Fiji with the Simple Neurite Tracer plugin (Longair et al. 2011). All cells that had a clear projection to the

imaged side of the body were traced until the dendrites became ambiguous or ended. Trajectory measurements were taken at 200μm along the traced dendritic branch. This distance was selected because it was long enough that the projection was well into the skin, but short enough that we could reliably trace this far in most of the visible projections. If there was a branching point before the 200μm point, the branch that projected more caudal was followed. Any traced cells that did not reach 200μm were excluded. At the 200μm point, we measured the longitudinal distance from the soma and the projection angle (Figure 3.1).

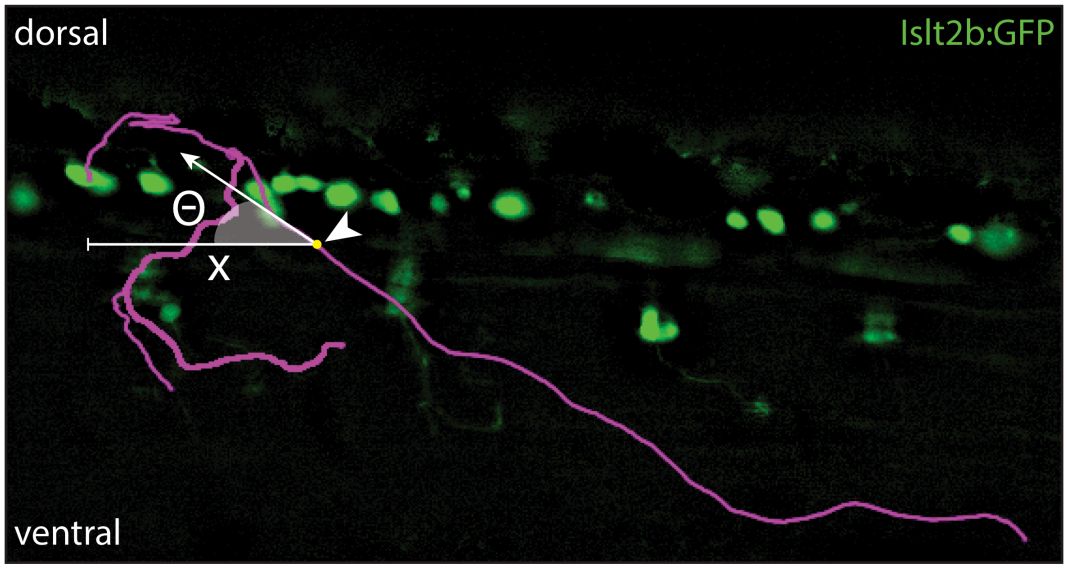

Figure 3.1: Morphological measurements taken at 200μm from the soma (white arrow) along the peripheral process. Purple lines indicate traced peripheral RB processes. This position always occurred after the process had reached the skin. We measured longitudinal projection distance from the soma (x) and projection angle (Θ, shaded angle).

From the images of single RB cells (n=21), we performed the same tracing and measurement analysis of the peripheral projection as described above for the population images. Our single cell measurements showed the same trend as our population

measurement, which suggests that these measurements taken 200μm from the soma along the peripheral processes are indicative of gross morphology. To quantify the range of peripheral innervation of RB processes, we extracted the rostral-most point and the caudal-most point from the peripheral projections from single-labeled RB cells. The longitudinal distance from these points to the level of the soma was taken to plot the projection distances of the peripheral processes. Projections in the finfold were not included. The segment that the soma was located and the distance from the soma at which the central projection exited the spinal cord were also measured. Statistical analyses were performed in R (R Core Team 2013).

Physiology

Electrophysiological recordings in zebrafish larvae were performed based on techniques described previously (Menelaou and McLean 2012) with some modifications. Isl2b:GFP or islt2b:gal4 injected with UAS:mcdGFR zebrafish larvae were immobilized using α -bungarotoxin (10mg/ml in recording solution;composition in mM: 134 NaCl, 2.9 KCl, 1.2 $MgCl_2$, 2.1 $CaCl_2$, 10 HEPES, 10 glucose, adjusted to pH 7.8 with NaOH). The immobilized larva were transferred to a glass bottom plate coated with Sylgard and were pinned through the notochord using two custom-made tungsten pins on the left side. A small patch of skin on the right side was removed using fine forceps, and the muscle over two spinal segments was removed using a custom-made tungsten dissecting tool. The two pins were carefully removed and the larvae were pinned on the opposite (right) side on a small block of Sylgard secured to the underlying Sylgard by three large pins. In order to orient the fish dorsal side up, the pins that secured the small Sylgard block were removed,

the block was tilted 90 degrees and then secured again on the underlying Sylgard with three pins.

The preparation was then moved onto the electrophysiology rig for whole cell recordings. Recording electrodes were made from standard-wall 1mm outer diameter borosilicate capillaries (Warner Instruments) using a micropipette puller (P-97; Sutter Instrument). Whole cell recordings were performed using a motorized manipulator (PatchStar; Scientifica) on an upright Olympus BX51 microscope equipped with a 40x/0.8 numerical aperture water immersion objective. Electrodes were filled with intracellular solution (composition in mM: 126 K-gluconate, 2 $MbCl_2$, 10 EGTA, 10 HEPES, 4 Na_2ATP, adjusted to pH 7.2 with KOH) and positive pressure (30 – 40 mmHg) was maintained using a pneumatic transducer (DPM-1B; Fluke Biomedical) while the pipette was advanced into the spinal cord.

The dissected side of the fish was used as an entry point into the spinal cord to target GFP-positive RB neurons, while the tactile stimulus was delivered on the intact side of the fish (see schematic in Figure 3.5A). Whole cell recordings were acquired using a Multiclamp 700B amplifier, a Digidata series 1440A digitizer and pClamp software (Molecular Devices). Signals were filtered at 30kHz and digitized at 63 kHz at a gain of 10 (feedback resistor, 500 MΩ) and standard corrections for bridge balance and electrode capacitance were applied. Recordings were performed in current-clamp mode and upon breaking into the cell hyperpolarizing and depolarizing steps of current were delivered into the soma to assess input resistance and determine rheobase and spiking pattern of the cell. The intracellular solution contained AlexaFluor 546 fluorescent dye to allow the cell to fill and examine its morphology at the end of the recordings. We

recorded from a total of 17 RB neurons at each rostrocaudal location (rostral: segments 10-16 & caudal: segments 21-26). We defined rostral as segments one through 16 and caudal as segments 17 and on. These designations were based on regions where rostral and caudal motor output were recorded during an S-start startle response (Liu et al. 2012).

Stimulus

We collected piezo-evoked responses at different locations along the body in six of 17 rostral and six of 17 caudal RB neurons recorded. For delivering the mechanical stimuli along the body of the fish, while simultaneously recording from RB cells, a second motorized manipulator (Patchstar; Scientifica) was used to guide a glass pipette (fire polished beveled tip size 50-80 μm) mounted on a piezo electric actuator. The piezo was driven by an external stimulator (A-M Systems). Increasing voltages drove larger deflection of the glass capillary resulting in a larger mechanical stimulation on the skin.

The tip of the glass probe was positioned at the midline of the fish along the horizontal myoseptum apposed to the skin but without any clear skin indentation. At each rostrocaudal location, the piezo probe was driven at different voltages while simultaneously recording the voltage responses from RB neurons. At each position 5 trials were performed for each voltage. For each trial, the stimulus was presented for 200ms at 0.33 Hz (every 3 seconds). The voltage was set low at first and was gradually incremented until the stimulation threshold was determined at each location.

To assess the piezo-evoked responses of RB neurons with respect to soma location, the 40x objective was carefully lifted out of the recording solution and a 10x/0.3

water-immersion objective was then lowered into place slowly to avoid disrupting the whole cell recording. At this lower magnitude, we recorded a short video (cellSens camera) of the preparation with both the patch electrode and the glass probe in the field of view to document the magnitude of the deflection and the exact location of the piezo glass in reference to the location of the soma.

Analysis

All the electrophysiological data were analyzed in Igor Pro using custom written scripts. All current evoked measurements were taken for the first spike at rheobase in current protocols. Spike threshold was determined by taking the peak of the third derivative of the spike waveform, which provides a good measure of the fastest change in voltage. Measures of spike amplitude are from threshold values to the peak of the spike for current-evoked and piezo-evoked firing. For the spike afterhyperpolarization (AHP), we calculated the voltage deflection from the trough of the AHP to spike threshold (fast AHP). A slow AHP was evident and was measured from the trough of the slow AHP from to resisting membrane potential (slow AHP). Spike half-widths represent the duration of the spike at one-half of the spike height. Spike latency was measured from onset of current step to spike threshold.

The distance of the piezo glass from the RB soma was measured in Fiji and was taken as the absolute distance in micrometers from the tip of the patch electrode to the center of the glass probe. Piezo-evoked spike latency was taken from the onset of the piezo stimulus to spike threshold at different piezo amplitudes. R was used for generating

plots and running statistical tests (R Core Team 2013). Figures were organized using Adobe Illustrator.

3.4 Results

Morphology

Across individual RB cells, we examined variation along the rostrocaudal axis. We also looked for differences between cells in rostral (segments 1-16) and caudal (segments >16) regions. We found that the absolute caudal projection distance, from the soma to the most caudal position that the peripheral process reaches, was greater the further along the body the soma was located (Figure 3.2C, $p<0.001$, $R^2 = 0.527$, Pearson test). We found that in several cells (five out of 21), the primary branch projected across several segments caudally within the spinal cord before exiting to the skin (473.4μm±183.5 Figure 3.2B), while all others exited close to the soma (19.91μm±15.47). None of these long-projecting cells were found before segment 19. This would suggest that the cells that project within the spinal cord before exiting to innervate the skin may be part of a subpopulation of RB cells that are only found in the caudal region. At the level of the skin, most rostral cell arborization appeared to exhibit clear boundaries (Figure 3.2A). This area often extended both rostral and caudal to the soma. Based on these observations, in the rostral region, the soma is located in the same rostrocadal area as its peripheral processes, while in the caudal region, the soma position may be rostral to the innervated area.

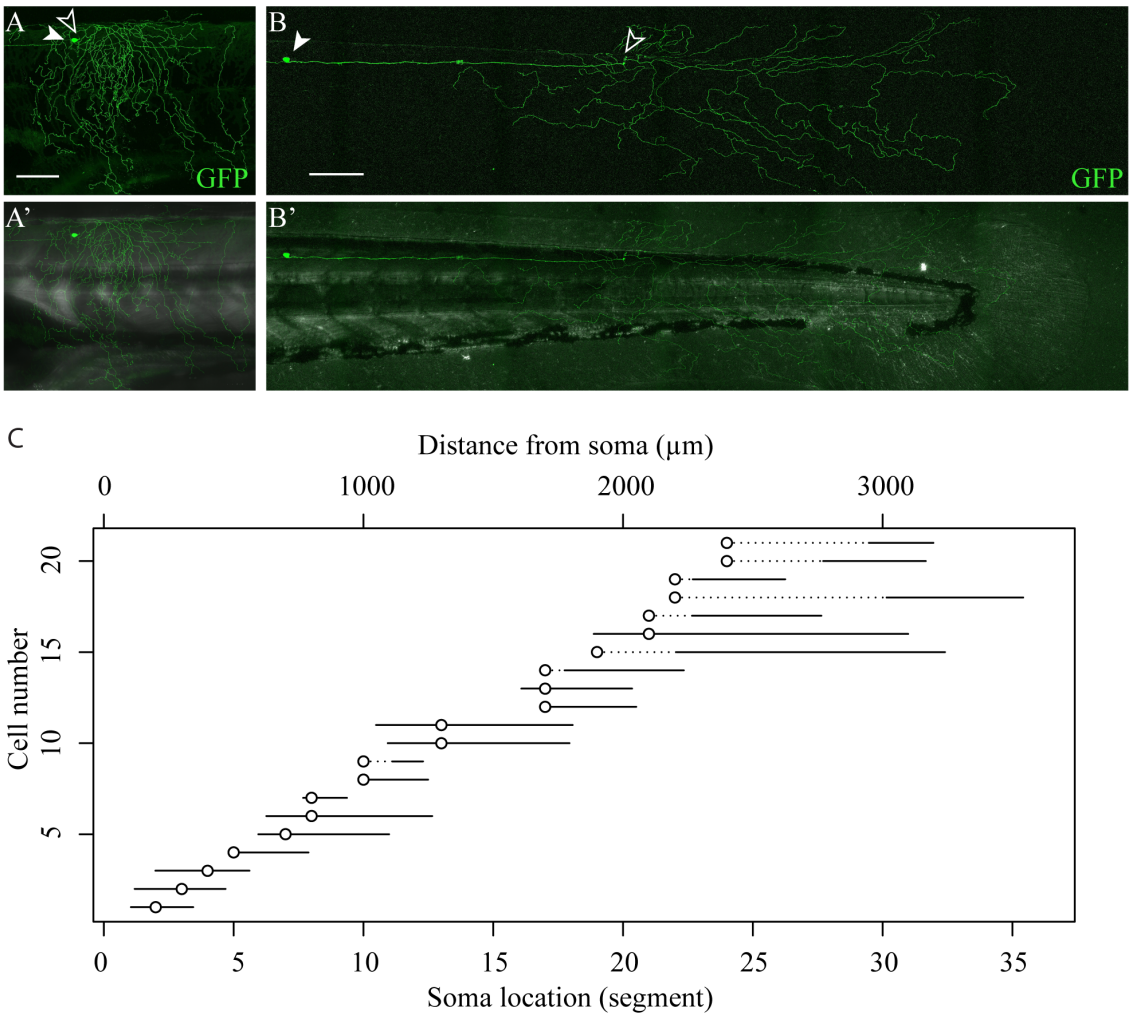

Figure 3.2: RB cells displayed morphological variation along the body axis. (A-B) Maximum intensity projections of two cells from islt2b:GAL4 zebrafish injected with a GFP label. (A) Example of a rostral cell (segment eight) which projects out of the spinal cord near the soma, and shows distinct rostrocaudal boundaries of the innervated area. (A') The brightfield image shows that the processes innervate the skin covering muscle, yolksac, and finfold. (B) Example of one caudal cell (segment 24) that projects 518.2µm caudally within the spinal cord before exiting to the skin. (B') The brightfield image shows the projections into the finfold and caudal fin. For A-B filled arrows denote soma location and open arrows note where the peripheral process exits the spinal cord (scale bars are 100µm). (C) Axial range of the peripheral projections within the skin measured from single RBs (n=21). The bottom x-axis indicates the segment that the soma is located and the top axis indicates the longitudinal distance in microns that the peripheral processes cover. Dotted lines indicate distance that the primary branch traveled before reaching the skin, and solid lines indicate the axial range of the peripheral processes at the skin.

Four out of 21 cells had two exit points out of spinal cord. Such cells have been described previously (Metcalfe et al. 1990), but we found that these cells also appeared to show rostrocaudal variation in morphology. Three out of 10 cells in the caudal region had one exit point near the soma and one further caudally (660.0µm±251.4). One out of the 11 rostral cells also had two projections out of the spinal cord, but both were close to the soma. This second exiting projection appeared to be the caudal projection that is usually described as terminating within the spinal cord. These findings lead to some interesting questions regarding the functionality of the caudal projection. Is this caudal projection relaying information to or from the soma?

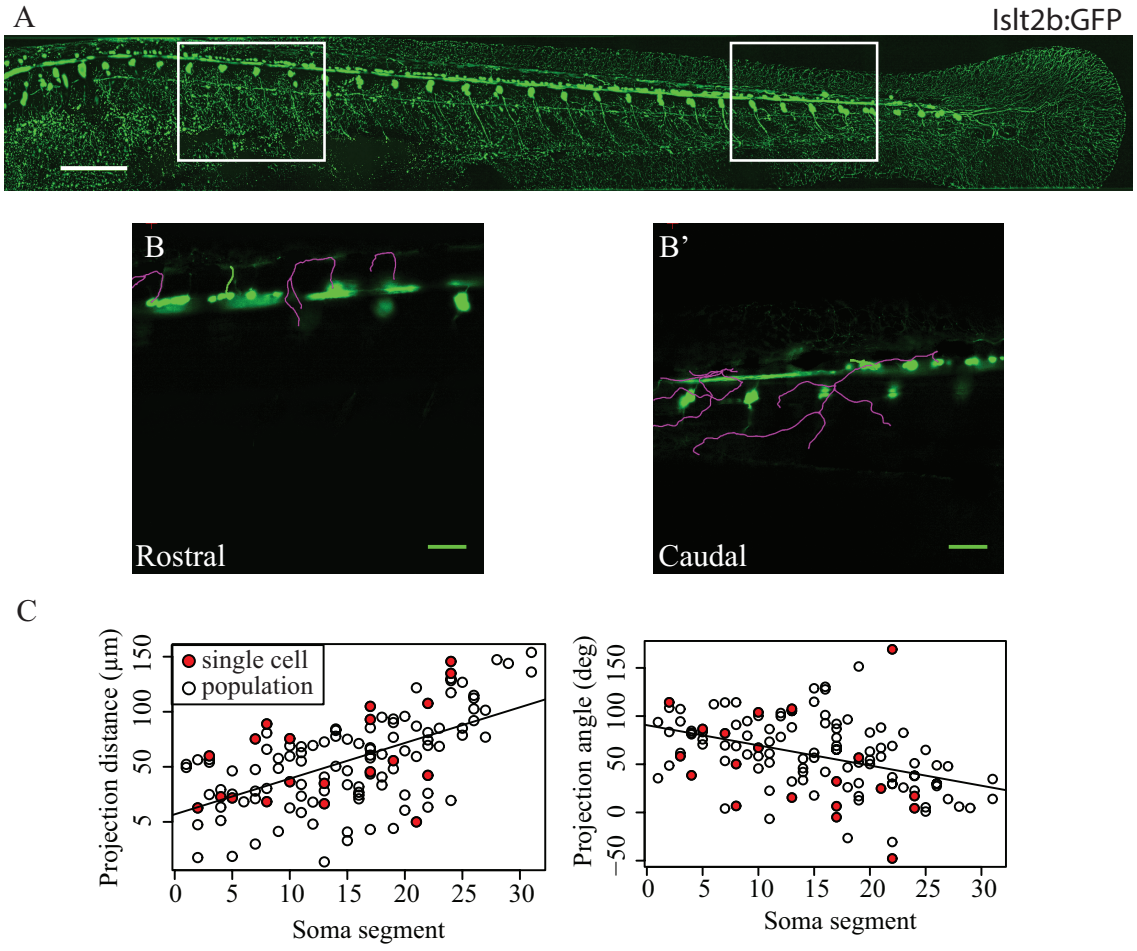

Figure 3.3: RB cells exhibit rostrocaudal variation in the projection angle and longitudinal distance of their peripheral processes in the skin.

Figure 3.3, continued. (A) Maximum intensity projection of islt2b:GFP zebrafish that were used to collect traces for analyzing population trends. Rectangles indicate areas highlighted with examples of traced cells. (B) Sample traces of RB cells from a rostral section of the fish, traced with Simple Neurite Tracer in Fiji. (B') Sample traces from a caudal section of the fish. (C, left) Longitudinal projection distance measured at 200μm from the soma increases significantly with soma location ($p<0.001$, $R^2 = 0.3704$). (C, right) Projection angle at the same location decreases significantly with soma location ($p<0.001$, $R^2 = 0.195$). Open circles are measurements taken from population measurements and closed circles are taken from single cell measurements.

In addition to this variation across individual cells, we surveyed variation across the RB population by examining the trajectory of peripheral processes shortly after they enter the skin, 200μm along the processes from the soma. From the 102 traces collected, we found variation along the body axis in the directionality of these processes (Figure 3.3). Cell bodies located further along the body projected further longitudinally towards the caudal end (Figure 3.3C, $p<0.001$, Pearson test). The projection angle was lower for cell bodies that were further caudal (Figure 3.3C, $p<0.001$, Pearson test), indicating that the peripheral processes of cells in the caudal region were projecting even further longitudinally beyond the point that we measured. These early trajectories suggest that cells bodies located more posterior along the body tend to project more towards the tail, while cells closer to the head tend to project more ventrally. Our population measurements were consistent with measurements taken from single cell traces (Figure 3.3C).

	RB cells			
	Caudal		Rostral	
	mean	sd	mean	sd
Input Resistance (MOhm)	618.4719	368.0319	575.1718	191.7438
Rheobase (pA)	209.4118	62.7964	198.2353	59.0800
Resting membrane potential (mV)	− 64.0256	5.1813	− 62.2420	5.1191
Threshold (mV)	− 28.5847	7.8511	− 25.9640	7.7095
Spike height	45.7428	21.9816	38.9645	17.4412
Spike half-width (ms)	0.6909	0.2233	0.6642	0.2629
Fast AHP (ms)	24.9750	6.8798	22.6239	7.6896
Slow AHP (ms)	3.0065	1.9980	2.6418	2.4838
Spike latency (ms)	2.1758	0.5589	2.0487	0.5327

Table 3.1: Mean and standard deviation (sd) of intrinsic values of RB cells (17 rostral and 17 caudal). No significant differences were identified between rostral and caudal cells (t-test and Mann-Whitney).

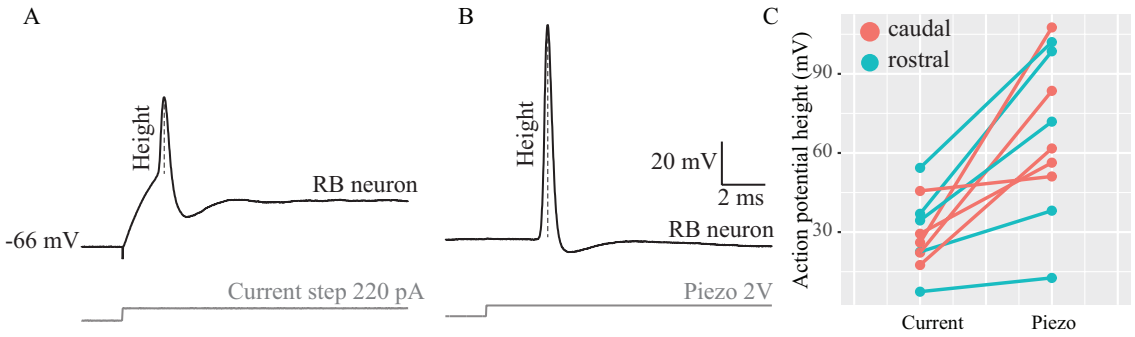

Figure 3.4: Action potential amplitude is higher in response to a tactile stimulus than in response to current injection. (A) Typical action potential elicited by current injection. (B) Typical action potential elicited from a tactile stimulus. Action potential height measurement is noted by the dotted line in both traces. (C) Action potential height was significantly greater in response to a piezo stimulus than a current injection for rostral (teal) and caudal (orange) cells (within-subject ANOVA, $p<0.001$).

Electrophysiology

After identifying this morphological variation we wanted to determine whether there were physiological differences at the rostral and caudal extremes. We first looked for rostrocaudal differences in the intrinsic physiological properties of RB somas that may be independent of afferent input. There were no differences in intrinsic properties between rostral (n=17; segments 10-16) and caudal (n=17; segments 21-26) RB cells (t-test,

$p>0.05$ for all variables, Table 3.1). Spikes elicited by current injection were significantly lower than spikes elicited by the piezo ($n=12$, repeated measures ANOVA, $p<0.05$ Figure 3.4), and the threshold for spiking was higher for current injections than for piezo-elicited spikes (repeated measures ANOVA, $p<0.05$). Like the current-evoked spikes, there were no significant differences identified in piezo-evoked spikes between rostral and caudal cells. These stimulus-based differences between action potential properties support our hypothesis that the peripheral processes play a major role in their activity.

To determine if RB physiology reflected the observed morphological trends, we identified the distance from the soma and range along the body where a stimulus could elicit a spike (Figure 3.5). For each cell, this analysis was done at the minimum stimulus intensity that could elicit spiking. The rostrocaudal variation observed in the peripheral morphology was reflected in the receptive fields of rostral ($n=6$) and caudal ($n=6$) cells tested electrophysiologically. Caudal cells tended to have receptive fields that were further caudal from the soma (506.4 μm±336.2), while rostral RB cells had receptive fields that were closer to the soma (121.6 μm±51.99; Figure 3.5C). Caudal cells also tended to spike at more locations than rostral cells (Figure 3.5C). Four out of six caudal cells spiked at more than one location, while only two out of six rostral cells spiked at more than one location. By ramping up the stimulus intensity some rostral and caudal cells responded to a wider range of stimulus positions. This could be due to the skin stretching and activating endings that are not directly beneath the stimulus.

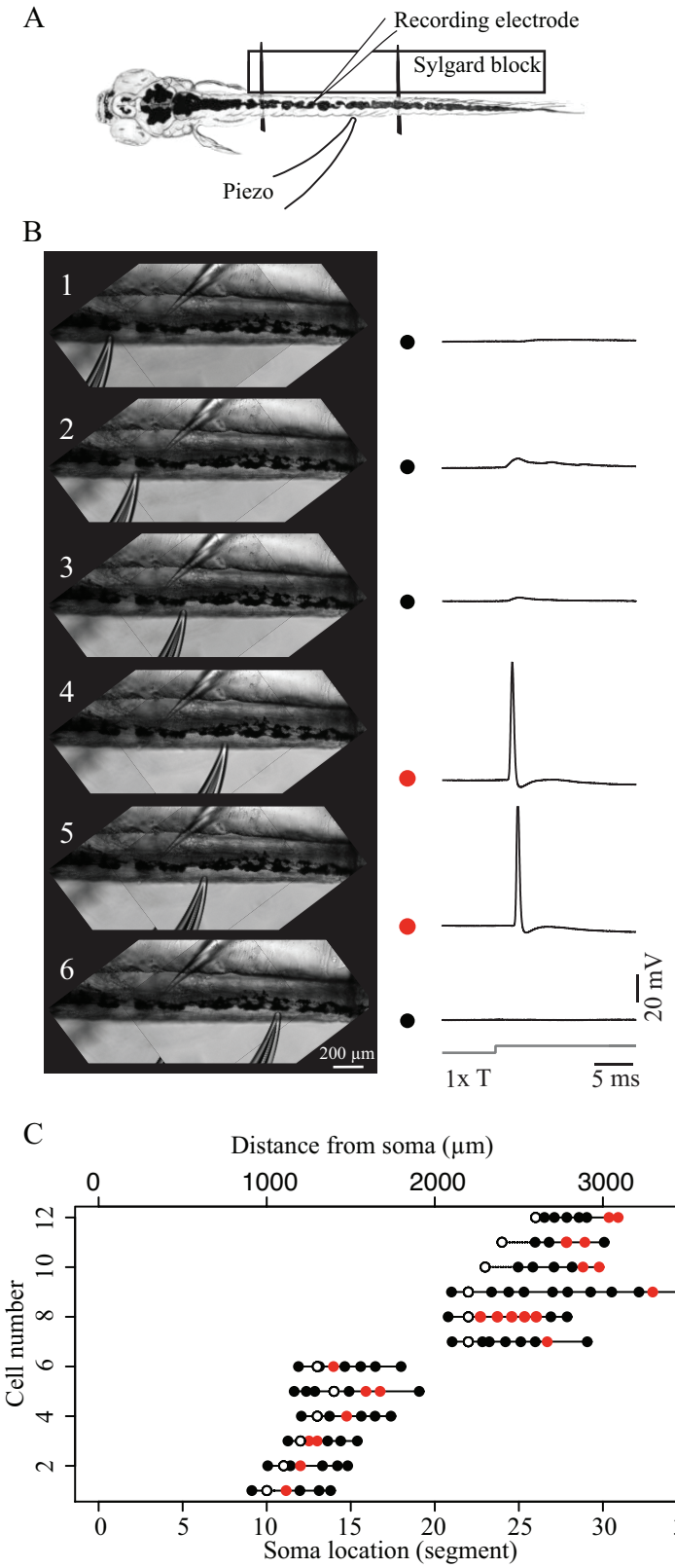

Figure 3.5: Receptive ranges of single cells varied between rostral and caudal cells.

Figure 3.5, continued. (A) Schematic of setup for single cell recordings where a tactile stimulus was presented. Fish were oriented dorsal side up against a block of Sylgard. (B) Example series of stimulus locations and corresponding traces for identifying the receptive range of each cell. Red dot indicates a spike was elicited and a black dot indicates no spike was elicited. (C) Sensitivity ranges for each cell examined. Filled circles denote sites of stimulation and the open circles indicate soma position. Red circles indicate a spike was elicited and black indicates no spike was elicited. The stimulus positions are relative to the soma.

In addition to identifying the receptive range of single cells, we examined sensitivity to stimulus features. We focused on two particular stimulus features: intensity (piezo displacement) and distance from the soma. We found that stimulus intensity was encoded by both spike number and latency. Spike number increased with stimulus intensity while spike latency decreased as stimulus intensity increased (Figure 3.6). We selected a subset of cells for further analysis. For each cell, we used the distance that exhibited the lowest latency at threshold. Any trial sets that had less than four intensity values were not included. We found a significant interaction effect between stimulus intensity and soma position ($p<0.001$, Mixed Model), where spike number increased more rapidly with stimulus intensity in caudal cells than rostral cells. The receptive fields of the cells that produced the highest spike numbers extended to the caudal fin, so this appears to be a particularly sensitive region. Spike latency decreased in a non-linear fashion with increasing stimulus intensity. An asymptotic non-linear regression fit for most of the stimulus data sets that had enough data points to fit a curve to (9 out of 13).

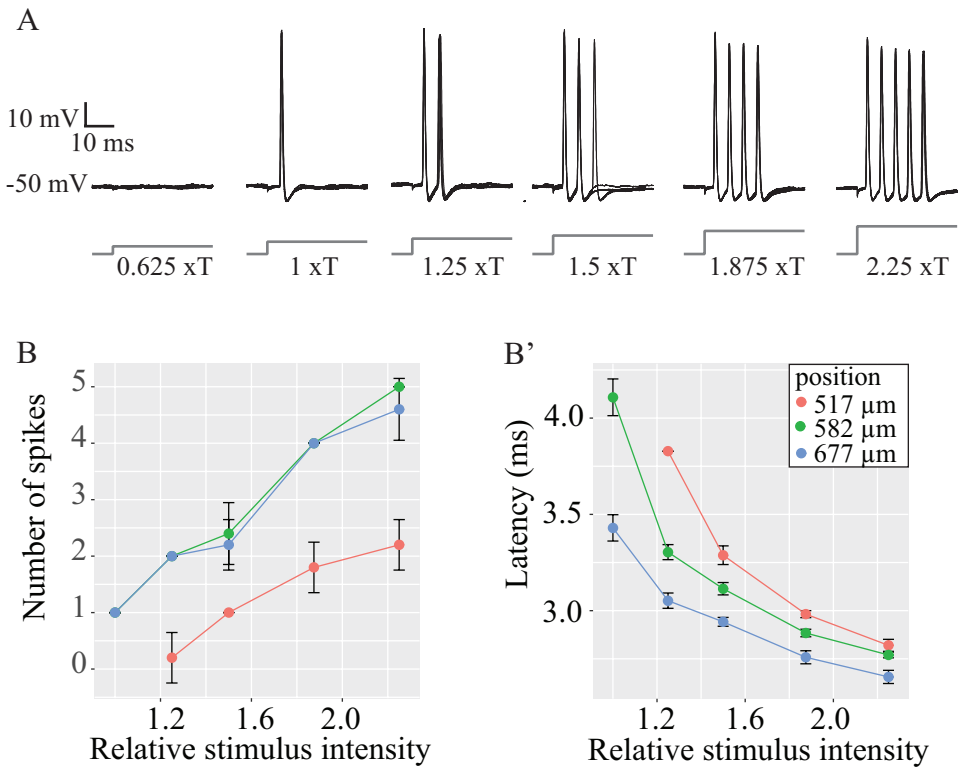

Figure 3.6: Spike number and latency varied with stimulus intensity. This figure shows data from one caudal cell, but the trends described here are consistent across our dataset. (A) Sample series of piezo intensity steps and corresponding increasing spike trains. Stimulus intensity values are relative to the lowest intensity to elicit spiking. (B) Spike number (y-axis) increased with stimulus intensity (y-axis). (B') Latency (y-axis) decreased with stimulus intensity (x-axis). Each point represents the average across five trials with standard deviations noted with the black lines. Colors on both plots indicate different distances from the soma that were stimulated. The spike trains from (A) are plotted in green.

RB cells showed no evidence of sensitivity to distance from the soma within their receptive ranges. If RB were sensitive to distance, we would expect a consistent trend in spike number or latency with distance, such as increasing latency with increasing distance from the soma. Instead, we found that a variety of relationships between latency/spike number and distance. For example in figure 3.6, the most sensitive (high spiking with low latency) distances were furthest from the soma, but in other cells, the closer positions were the most sensitive. From these results, we suspect that even within

the receptive range of a cell, response is sensitive to position. This could result from varied densities of receptors across the surface area that a cell innervates. Variable branching number also likely impacts the latency and spike number at different positions. One interesting feature that we found was that different distances that have similar spiking patterns can have different latency patterns (Figure 3.6B). This suggests that latency is a better indicator of position than spike number. Additional experiments would be necessary to test this hypothesis.

3.5 Discussion

We found that RB cells exhibit morphological and physiological variation along the rostrocaudal axis. By examining populations of RB cells, we found that cell bodies located further along the body tended to have projections that extended more longitudinally and caudally. We were also able to relate these trends in trajectory to overall morphology by performing the same measurements in our single cells. One of the most surprising differences was that several cells in the caudal region projected as far as 600μm in the spinal cord before exiting to the skin, while rostral cells always projected out of the spinal cord near the soma. To our knowledge, this type of morphological variation has not been described for RB cells. We suspect this is due to most studies focusing on one particular region of the body, presumably the rostral region based on our results. O'Brien et al. (2012) observed that primary afferent branches changed trajectory immediately after entering the skin, indicating that the trajectory of peripheral processes may be guided by external developmental cues early in development. The physiological responses to tactile stimuli were consistent with our morphological measurements.

Rostral cells responded to stimuli close to the soma, while caudal cells responded to stimuli further caudally and often had a wider receptive range.

The new physiological preparation we utilized allowed us to characterize RB responses to a biologically relevant tactile stimulus for the first time in zebrafish larvae. In the zebrafish literature, for single cell patch clamp recordings, RB cell activation is usually elicited by exciting the soma directly via a current injection. From these forms of stimulation, RBs have been characterized as producing a single spike in response to an internal electrical pulse (e.g. Knaffo et al. 2017). Using a tactile stimulus at the surface of the skin, we found a number of spike features that were distinct from spikes elicited by current injections. Tactile-elicited spikes had significantly higher depolarization peaks than current-elicited spikes (Figure 3.4). We also found that in response to a tactile stimulus, multiple spikes could be elicited. Both of these findings suggest that action potentials are initiated in the peripheral processes as opposed to the soma. For this reason, a response elicited by a current injection is not likely to be representative of a RB cell's response to a natural stimulus. The complex branching of the RB peripheral processes likely impacts the signal as it travels from the periphery to the soma (Peng et al. 1999; Branco et al. 2010). For example, if a stimulus excites multiple branches from the same cell, the two spikes may cancel each other out, hyperpolarization from the first spike may prevent other branches from spiking, or both spikes may reach the soma (Peng et al. 1999).

The spike pattern of RB cells in response to tactile stimuli resembled that of a rapidly adapting type cell in that they only spiked at the onset of the stimulus (Abraira and Ginty 2013). RB cells appear to encode stimulus intensity via number of spikes and

spike latency. The roles of spike number and latency as indicators of stimulus intensity is common across both vertebrate and invertebrate mechanosensory networks (Bensmaia 2008; Pirschel and Kretzberg 2016). Caudal RB cells appeared to have greater spike numbers than rostral cells for a given stimulus intensity. Again, these results suggest that the tail is a region of heightened sensitivity. We were surprised that we did not observe any rostrocaudal differences in latency. Based on the morphological results, we would have expected that caudal cells would have greater latencies because the stimulus site tends to be further from the soma than for a rostral cell.

There was no relationship between latency or number of spikes and stimulus distance from the soma. However each cell had locations of high and low sensitivity within the receptive range, indicating that these cells are sensitive to position and not distance. While the receptive ranges we identified showed a consistent trend with our morphology data, they were surprisingly narrow given the distance that the peripheral processes cover. We specifically stimulated along the midline for purposes of consistency, but the range of sensitivity would likely change for stimuli presented more dorsal or ventral. This is supported by the fact that stimulating at a higher intensity often resulted in a wider activation range. Greater displacement at the stimulus site results in greater displacement in the surrounding area (Srinivasan 1989; Elmi et al. 2017), which activates more nerve endings that are further from the stimulus site. There may also be variable distribution of receptor endings across RB cells. Some cells displayed more of a net-like morphology and seemed to fill the area within their boundary, while others appeared to have more specific targets such as the yolk sack, finfold, or caudal fin. It may be that sensory endings are localized to the target tissue as opposed to being distributed along the entire

process. In fact, portions of RB processes become encased in keratinocytes in the skin of zebrafish (O'Brien et al. 2012), which suggests that sensory endings may need to be located in specified regions that are not encased.

RB cells have been very broadly characterized as touch or mechanoreceptive neurons, but little is known about what these cells actually encode or how they relay information. From both vertebrate and invertebrate models, we know that there are many different ways to encode mechanosensory information. Our results indicate the RB cell spike patterns are consistent with rapidly adapting mechanoreceptors. The positional sensitivity within the receptive ranges is reminiscent of the receptive fields in primate hands comprised of regions of high and low sensitivity (Johansson 1976). These region-specific morphologies coupled with the greater spike numbers identified near the caudal fin suggest that larval fish may have regions of heightened sensitivity.

The regional variation in morphology and physiology of RB cells contrasts with the rostrocaudal consistency and segmental association of many other neurons of the spinal cord. An example of an animal with repeated segments that all have the same sensory organization is the leech. Similar to vertebrates, leeches have different types of cells for sensing various mechanosensory signals, however each cell exhibits the same pattern of innervation within each segment of the body (Nicholls and Baylor 1968). In leeches, inhibitory interactions between neighboring processes from the same type of sensory cell ensure that peripheral processes do not extend into neighboring segments (Gan and Macagno 1995). In zebrafish, RB cells that are more rostral tend to have peripheral processes with more defined boundaries around the field of arborization than

the cells that are more caudal. This could indicate that there are stronger inhibitory interactions in towards the rostral end of the animal.

The rostrocaudal variation in morphology and physiology provides a mechanism for regionalized motor output, such as the rostral and caudal bends observed in the S-start (Hale 2002, Liu et al. 2012, Liu and Hale 2017). Liu and Hale 2017 showed that the RB cells play a critical role in producing the zebrafish S-start by activating commissural contralateral inhibitory cells, which inhibit contralateral motor neurons before the startle signal reaches the hindbrain. This area of early contralateral inhibition is likely what designates where the rostral and caudal bends will occur. Because the cells that innervate the caudal fin initiate so far away, we would expect that a tactile stimulus at or near the caudal fin would excite a broad range of cells extending many segments rostral to the stimulus site. The same stimulus in the rostral region would likely only excite cells at or around the stimulus site. The wide range of RB cells that are likely activated when stimulating the caudal region of the body could be what produce the rostro-caudal designation for the S-start bends. Calcium imaging would be an ideal tool for testing this hypothesis. With a wide enough field of view, this method could allow us to visualize all of the cells responding to a given stimulus.

We have observed that the adult zebrafish do not perform the S-start, which could be related to the loss of RB cells through ontogeny. It is well established that RB cells undergo programmed cell death through ontogeny as the dorsal root ganglia (DRG) develop and become the primary mechanosensory network (Svoboda et al. 2001; Reyes et al. 2004) . However, the exact timing of this process remains unclear. Earlier studies on the subject found that the entire RB population died off between 2-4dpf (Williams et

al. 2000; Svoboda et al. 2001; Reyes et al. 2004). However, more recent studies have found evidence that these cells persist as late as 2 weeks post-fertilization (Patten et al. 2007; Palanca et al. 2012). It is still unclear exactly when, or even if, the RB cells are entirely lost. It is also possible this process of programmed cell death varies across species. While zebrafish do not perform S-starts as adults, some species of fish have been shown to perform S-starts as adults (Hale 2002, Schriefer and Hale 2004). If the RB cells are essential for producing the S-start, we would expect these species to retain these cells into adulthood, or for the DRG network to take over the role the RBs in the S-start circuit. It is currently unknown to what extent the DRG network "replaces" the functionality of the RB population. Future work on both RB and DRG systems in fish is necessary to better understand this transition.

In this study, we sought to identify variation in RB morphology along the rostrocaudal axis. RB cells have long been identified as the primary mechanosensory cells in larval fish, but we have only recently begun to get a sense of the specific role that they play in sensing touch. RB cells have been hypothesized to be a heterogeneous population of mechanosensory cells (Palanca et al. 2013; Umeda et al. 2016). Our work adds additional support to the hypothesis that there are functional subtypes within the RB population, and that these subtypes maybe reflected in the peripheral morphology. Our results show that there is clear rostrocaudal variation in RB peripheral morphology, and electrophysiology experiments showed that the observed morphology is reflected in the receptive field of the RB cells. This study begins to elucidate some of the specific characteristics of RB cells and the population as a whole. RB morphology exhibits rostrocaudal variation in morphology, which may be indicative of an early form of

regionalization that has expanded in amniotes. Additionally RB cell activity and receptive ranges appear to be comparable to those of other model mechanosensory systems. Because the zebrafish mechanosensory network undergoes the life history transition from RB to DRG, it also presents a unique opportunity to explore ontogenetic transitions in sensory motor integration.

CHAPTER 4

EXPLORING THE TRANSITION FROM AXIAL TO LIMB-BASED STARTLE THROUGH METAMORPHOSIS IN *XENOPUS LAEVIS*

4.1 Abstract

The startle response is vital to an organism's survival. Animals must perform startle throughout their life history as they undergo changes to their body shape and nervous system. Anurans (frogs and toads) undergo metamorphosis, during which time the limbs develop, the tail is lost, and the trunk stiffens. Here we ask how a critical function, startle, is maintained through a switch in its underlying morphology in the African clawed frog, *Xenopus laevis*. We examine how the performance of each head-directed response varies as limb-based startle develops, and axial startle is lost. Tadpoles have been shown to perform an axial-based C-start, similar to the startle response observed in fish. Maximum angular velocity did not significantly change until the C-start was lost around developmental stage 62. We found that *X. laevis* gradually integrates a limb-based "pushback" response into the startle repertoire starting at developmental stage 58. The pushback startle response consists of the frog rapidly extending its hindlimbs towards the head, resulting in a fast backwards movement away from the stimulus. For the pushback, we found that maximum velocity (in body lengths per second) increased from stage 59 to stage 64, but then dropped from stage 65 to post-metamorphic stages. *X. laevis* appears to transition startle modalities by maintaining a high performing C-start until the pushback performance has reached high performance levels, at which point the C-start is lost. We hypothesize that the drop in pushback performance is due to a change

in the functionality of the pushback response. Older post-metamorphic frogs may be utilizing the pushback as a re-orienting maneuver as opposed to a ballistic one.

4.2 Introduction

Behaviors that are essential for survival often appear early in development and are maintained throughout life history. In some instances, ontogenetic changes require the animal to use different strategies to perform the same behavior at later life stages. Such strategies may include utilizing different structures and/or different movements to perform the same behavior. For example, fish utilize their pectoral fins to aid cutaneous respiration as larvae while adult fish utilize gills for respiration (Green et al. 2013). Some animals, such as insects, undergo a period of inactivity during transitions between life stages, which allows them to cease most behavior as the body changes. Others must continue to behave throughout these transitional periods. Examining how animals maintain a particular behavior as the body is changing can give us insight into the evolution of behaviors. In this study, we utilize startle to examine how a behavior is maintained through a major life history transformation: anuran metamorphosis.

Tadpoles perform a classic axial C-start that is very similar to what is observed in fish (Rock 1981; Will 1991). The tadpole C-start consists of 2 stages: stage 1 is an initial bend away from the stimulus and stage 2 is a bend in the opposite direction that results in translation of the body (Will 1991). This behavioral response has been characterized in the tadpoles of several different species including the woodfrog, bullfrog, and African clawed frog (Will 1991; Eidietis 2005). Like fish, the tadpole C-start is driven by a pair of large reticulospinal neurons called Mauthner cells (Rock 1980). These cells resemble

those that are found in fishes both morphologically and physiologically (Rock 1980; Will 1986, 1991).

Aquatic frogs perform a limb-based startle response that has been qualitatively characterized by a handful of studies. Videler and Jorna (1985) referred to this response as a "surface dive," where the frog was startled at the surface of the water by visual stimulus and extended its hindlimbs forward and shortened its body length to rapidly move backwards down into the water column (Videler and Jorna 1985). Will (1991) described this same behavior in response to a vibratory stimulus. In this "back swim stoke," the animal was horizontal in the water column for the entire behavior (Will 1991). These studies provide evidence of a reproducible startle response in adult *X. laevis*, but do not quantitatively characterize the kinematic components of the response.

During metamorphosis, anurans undergo complete body plan reorganization, switching from an axial to a tetrapod body plan (Nieuwkoop and Faber 1994). During metamorphosis, the hindlimbs emerge first, followed by the forelimbs, and finally the tail degenerates. As the limbs develop, the animal transitions from axial- to limb-based locomotion. The startle response also transitions from the axial C-start to the adult limb-based movement. This is a unique model for examining Mauthner-based startle because unlike other amphibians such as salamanders (Landberg and Azizi 2010), anuran locomotion at the adult stage has virtually no axial component (based on Videler and Jorna 1985; Will 1991). This provides us with the unique opportunity to investigate how a behavior, startle, is maintained through life history as the body and physiology are changing.

In this study, we examine how each behavior, axial C-start and limb-based startle, is changing as the former is lost and the latter develops through metamorphosis in the aquatic frog *Xenopus laevis*. Here, we (1) describe the limb-based startle behavior, (2) evaluate the performance of each startle modality, axial- and limb-based, through metamorphosis, and (3) determine the timeline of the behavioral transition. We hypothesized that there is a period during metamorphosis where neither the tadpole startle or the adult startle are functioning at optimal performance and where the animal may be particularly susceptible to predation. Using *X. laevis* startle as a model, we can gain insight into different strategies that animals might use to maintain a behavior during dramatic morphological transitions through life history. Furthermore, by describing the transition of startle response, it provides us with a basis for examining how transitions in neural control are accomplished to maintain a behavior.

4.3 Methods

Husbandry

All frogs were housed and handled in the National Xenopus Resource center with animal care protocol approved by the Marine Biology Laboratory IACUC. Animal care protocols can be found on the National Xenopus Resource website (http://www.mbl.edu/xenopus/protocols). Strain J *X. laevis* were bred and raised in house. Some animals were housed in an incubator at 27^{o}C overnight to speed up metamorphosis. All animals used in this study were from the same clutch.

Behavior: Metamorphic animals

Frogs were between 2 months, 9 days and 2 months, 20 days old. Metamorphic staging referred to the normal tables assembled by Nieuwkoop and Faber (1994). Some animals were stored in an incubator at 27^{o}C in order to accelerate metamorphosis. These animals continued to be fed at their normal cycle. They did not appear to demonstrate any sort of unusual behavior when they were startled.

Individual animals (N=18) were placed in a filming tank (8" x 8" x 4") in approximately 2.5 inches of facility water at room temperature. Trials were filmed with a high-speed camera with a Tamron SP 90mm lens mounted on a tripod above the tanks at 500 fps. After an acclimation period of at least 10 minutes, we began startle trials. We elicited a startle response via a light tap on the head with a set of blunt forceps. We chose to stimulate at the head because head directed stimuli were the most likely to elicit a startle response. Additionally, head-directed attacks from a predator are more likely to be lethal (Van Buskirk and McCollum 2000; Johnson and Eidietis 2005). While taps were always at the head, we varied the stimulus location between three regions relative to the eyes: center, left, and right. We chose a tactile stimulus because it allowed us to target very specific regions of the body. After each startle, we allowed at least one minute between sequential trials in order to avoid desensitization. After completion of trials, animals were euthanized in ms-222.

Behavior: Adults

In addition to the metamorphic animals, we performed startle trials on 8 month-old animals (N=2). Because these adult animals were much larger than the metamorphic

animals, we used a larger filming tank (23" x 15" x 8") with a water depth of 3.5 inches. Additionally, we used a Nikon 28mm lens with a wider field of view. Otherwise, all behavioral methods were the same as metamorphic animals. We only startled the animal when it was completely submerged and parallel to the bottom of the tank.

Digitizing

We qualitatively categorized each startle response as either a C-start or pushback response. If an animal extended its hindlimbs toward its head, the behavior was characterized as a pushback response. In some instances, we observed an axial bend with pushback kinematic pattern in the hindlimbs. If the hindlimbs were fully extended before the axial bend, we analyzed the response as a pushback. We analyzed the response as a C-start if the bend initiated before the hindlimbs fully extended, the ankles never fully extended, and there was a clear stage 2. A maximum of three trials from of each behavior were selected for digitizing from each animal. Some of the criteria used to select trials include: the stimulus location was clear, the animal did not come into contact with forceps after stimulation, and the animal remained in focus for the duration of the video recording of the trial.

Landmarks were digitized in Fiji (Schindelin et al. 2012) every fourth frame (every 8ms) and exported into a csv file. We digitized the snout, eyes, anus, hips, knees, ankles, and toes. We did not digitize the tarsometatarsal because it was difficult to identify in the metamorphic animals with less-developed hindlimbs. See Figure 4.1 for a description of the landmarks digitized. All calculations and statistical analyses were performed in R (R Core Team 2013). Joint angles were smoothed with a lowpass spline

filter. Because the body sometimes obscured the hindlimbs during the startle response, we could not get kinematics for every joint of every animal that we digitized.

We used maximum velocity during stage 1 as a measure of performance (based on Walker et al. 2005). Linear velocity was calculated as the distance traveled by the snout between measured frames, divided by the time elapsed between the frames. Angular velocity was calculated as the change in angle of a line connecting the eyes divided by the time elapsed between frames. Joint angles were calculated for the hip, knee, and ankle (Figure 4.1).

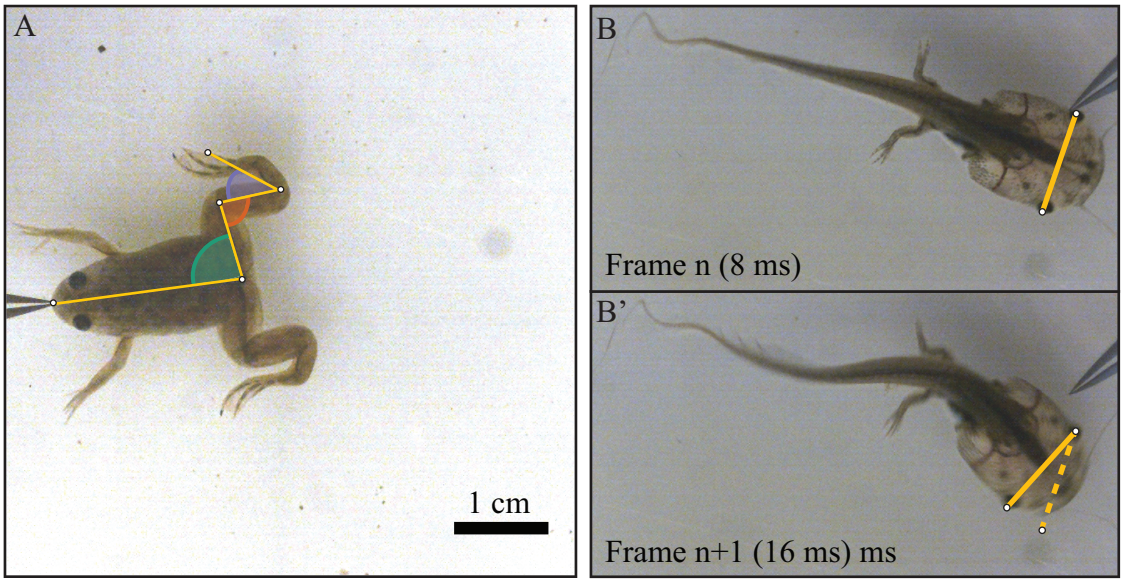

Figure 4.1: Snout, anus, ankle, toe, and eyes were digitized for each animal in Fiji. (A) Hindlimb joint angles were calculated from the two lines indicated in the image. Hip angle is indicated in turquoise, knee angle in orange, and ankle angle in purple. For performing the adult behavior, the linear velocity was calculated from snout displacement. (B-B') Angular velocity was calculated as the change in angle of a line connecting the eyes divided by the time elapsed between frames.

Statistics

Due to the small sample size of some developmental stages, we binned pushback data as follows: stages 59-60, stages 61-62, stages 63-64, and stages 65-66. C-start data

was binned as well: 57-58, 59, 60-61. Statistical tests were performed with these binned stages as groups. For comparisons of variance, we performed an F-test for normally distributed data and an Ansari-Bradley test for non-normal data. We performed a Kruskal-Wallis as a non-parametric equivalent to an ANOVA test with pairwise Wilcoxon rank sum (Mann-Whitney) tests for post-hoc analysis.

4.4 Results

Pushback

The limb-based startle response we observed in the late and post-metamorphic frogs were consistent with the behaviors described by Videler and Jorna (1985), and Will (1991). Here, we provide a more detailed, quantitative description of the limb-based frog startle. Adult frogs respond to a head-directed stimulus with a "pushback" startle response where they extend their hindlimbs towards their head. We found this to be a high performance behavior comparable to escape behaviors in other species (e.g. Arnott et al. 1998; Bierman et al. 2009; Landberg and Azizi 2010).

We identified two distinct stages within this behavior (Figure 4.2). Pushback stage 1 is defined as the duration from onset of movement until maximum ankle extension is achieved. Pushback stage 2 is the duration from maximum extension to the end of hindlimb retraction. Behavior during stage 2 is highly variable, and may include immediate retraction of the hindlimbs, a turn following extension, or preparation for a forward burst or second pushback. Because we are looking at performance, we focused our analysis on stage 1 where the power stroke occurs.

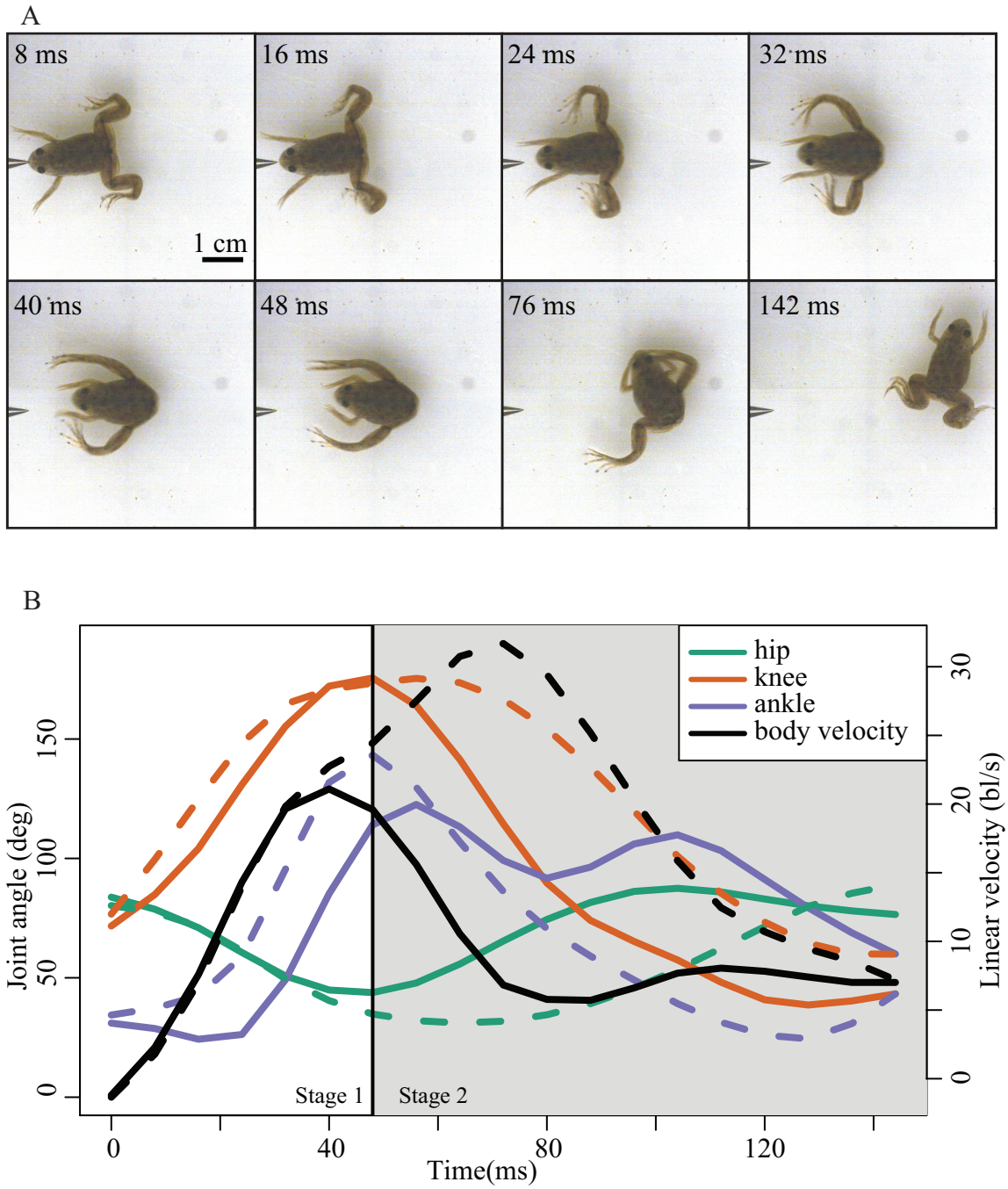

Figure 4.2: Limb-based pushback behavior can be broken down into two stages. (A) Stage 1 (1 – 48ms) and 2 (49 – 142ms) kinematics of the pushback response. (B) Example joint traces from the trial shown in A. Stage 1 kinematic pattern consisted of synchronous extension of the knee and flexion of the hip, with delayed extension of the ankle. An increased in joint angle is indicative of extension, while a decrease in angle corresponds to flexion. Hip flexion (green) and knee extension (orange) occur synchronously during stage 1.

Figure 4.2, continued. Colored solid and dashed lines correspond to left and right limbs, respectively. Black solid and dashed lines correspond to body velocity measured at the anus (solid) and head (dashed). While this is only one example trial, the joint kinematics during pushback stage 1 were consistent across individuals.

Stage 1 displayed a consistent pattern of hindlimb kinematics. The first movements observed are the synchronous extension of the knee and flexion of the hip. As the hindlimb is brought forward, the ankle extends (Figure 4.2B). The ankle extension occurred significantly later than hip flexion and knee extension. The onset of ankle extension was also significantly more variable than the hip and knee. This kinematic pattern was consistent from stages 59/60 to stages 65/66 ($p>0.05$, Kruskal-Wallis test). Preliminary measurements also suggest that stimulus location may impact right-left synchrony, particularly in the ankle joint. However, further analysis is needed to determine the impact of stimulus location on hindlimb coordination.

Pushback stage 1 performance changed significantly throughout anuran metamorphosis ($p<0.001$, Kruskal-Wallis test, Figure 4.3). Performance increased from stages 59/60 to 63/64 at which point it decreased through the adult stage (Table 4.1). We also observed increasingly wider ranges of performance values through stage 65. While the animals were able to achieve greater maximum velocities, they still exhibit lower-performance responses.

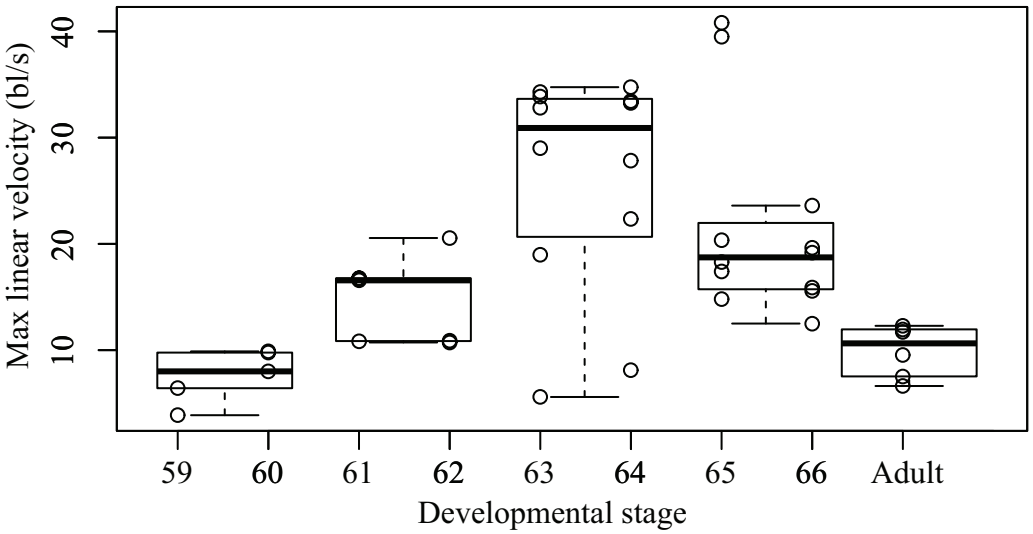

Figure 4.3: Maximum linear velocity (body lengths/second) for individuals at each metamorphic stage. Circles indicate individual trials (N=16, n=42), and boxplots show binned data sets that were used for analysis.

Stages	59/60	61/62	63/64	65/66
61/62	0.0084 *			
63/64	0.0234 *	0.0368 *		
65/66	0.0016 *	0.1187	0.2198	
Adult	0.2468	0.1267	0.0269 *	0.0011 *

Table 4.1: Paired comparisons of performance between metamorphic stages (Wilcoxon rank sum test). Asterisk denotes significantly different pairs ($p<0.05$).

In order determine why we still observed a range of high and low performance values at each given stage, we compared maximum velocity with a number of different morphological variables. We found that the range in performance within stages was likely due to the maximum extension the ankles achieved during the hindlimb extension. Animals displayed significantly greater performance values when maximum ankle

extension reached values greater than 160° (ANOVA, $p<0.05$, Figure 4.4). Therefore, we hypothesize that for any given stage, these animals can only reach their maximum performance by fully extending the ankle joint.

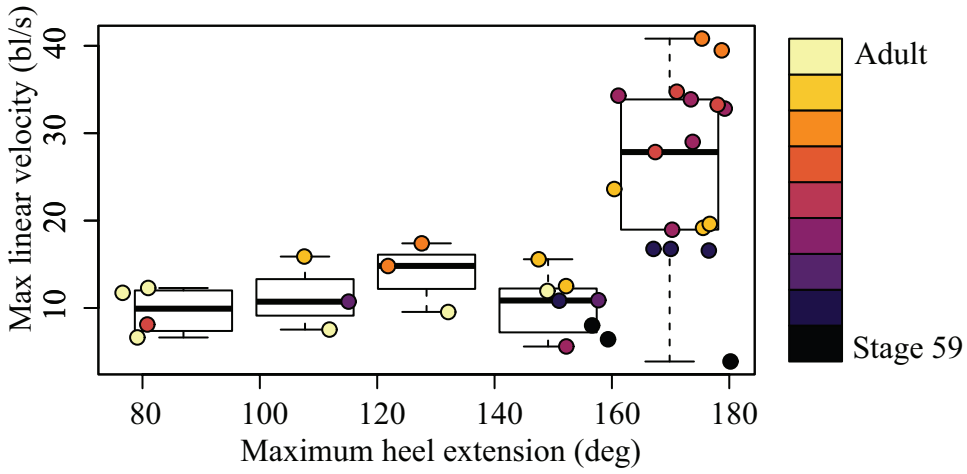

Figure 4.4: Maximum linear velocity plotted against maximum heel extension achieved at the end of stage 1 (N=16, n=34). Points represent a single trial and are color coded by developmental stage. Performance was significantly higher in trials where the ankle extension was greater that 160°.

Based on these results we examined the subset of trials where ankle extension reached at least 160°. Within this subset, we observed that performance decreased as body mass increased, and performance increased with relative foot length. Through metamorphosis, body mass in our sample set decreased through stage 65 and started increasing at stage 66. Similarly, relative foot length increased through stage 65 and decreased at stage 66. It appears that the pushback is able to achieve the highest performance values when the animal is at a low mass with high relative foot length. This would explain why performance drops so dramatically at stage 66 even when the animal fully extends its hindlimbs.

In addition to their much body greater mass and lower relative foot length, the adult frogs did not reach maximum extension in any of the trials that we examined (mean ankle extension was $104.96^{o} \pm 12.61$). These three factors likely contribute to the significantly lower performance values observed in these animals. While adult frogs performed a shallower pushback response, in 81% of trials the pushback was followed with a forward burst response. Burst swims were not observed as frequently in metamorphic ages. This could indicate a change in functionality of the pushback response, which we discuss in further detail in the discussion.

The C-start behavior we observed was comparable to what has been described in the literature previously for both tadpoles (Figure 4.5; Will 1991; Laura Eidietis 2006; L Eidietis 2005) and fish (Meager et al. 2006). In response to a head directed stimulus, the tadpole made a rapid turn away from the stimulus (stage 1), followed by a contralateral bend (stage 2). At the end of stage 2 the animal either glided or swam away.

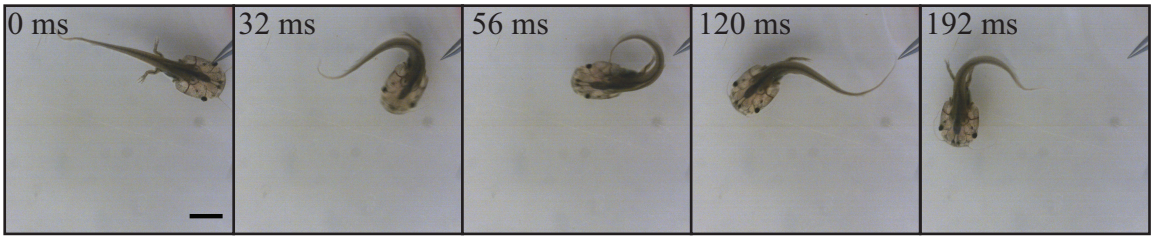

Figure 4.5: Tadpole C-start is similar to a fish C-start. Stage 1 occurs from 0-55ms and stage 2 is from 56-192ms. This animal is at developmental stage 57, before the forelimbs have emerged. Scale bar is 1cm.

We found no significant change in C-start performance through metamorphosis (ANOVA, Figure 4.6). We did not observe any size related variation (Eidietis 2005; Wilson and Franklin 2013), but we also had a relatively narrow range in sizes for our

tadpoles (snout-vent length = 2.255±0.1457). During early metamorphic stages, hindlimbs were kept close to the body during a C-start (Figure 4.5). This is the same way the legs are positioned during steady swimming at this stage (Combes et al. 2004). At later stages, hindlimb movement was more variable. They may be held along the body or incorporate a kick, which may assist the animal in turning.

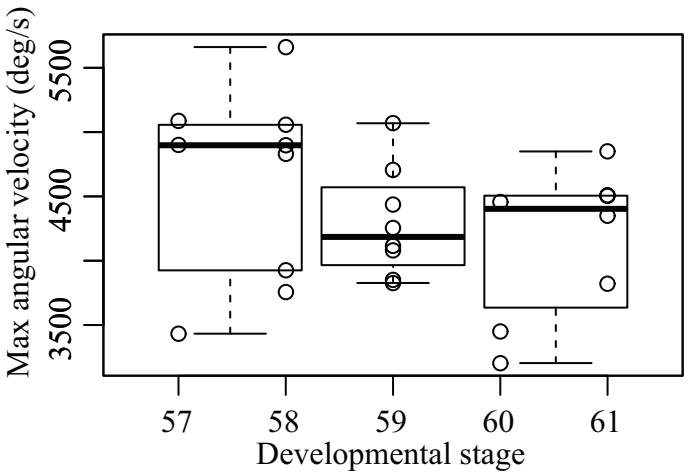

Figure 4.6: Maximum angular velocity (degrees/second) during Stage 1 of the C-start for individuals at each metamorphic stage. Circles indicate individual trials (N=9, n=25), and boxplots show binned data sets that were used for analysis.

There is a very clear gradual transition in the frequency of each behavior (Figure 4.7). The pushback first appears at stage 58 and becomes increasingly more prevalent, as the C-start becomes less common until it is almost entirely lost by stage 61 (Figure 4.7A). We did see a response resembling a C-start at stage 63, but it went out of the frame before the end of stage 1. It was also unclear whether it was truly a C-start or more of a forward burst swim. When the pushback first appears, it has low performance values, but by the time the C-start is lost, the pushback is able to achieve higher performance values

(Figure 4.7B). The C-start may be able to compensate for the pushback behavior as performance improves through metamorphosis.

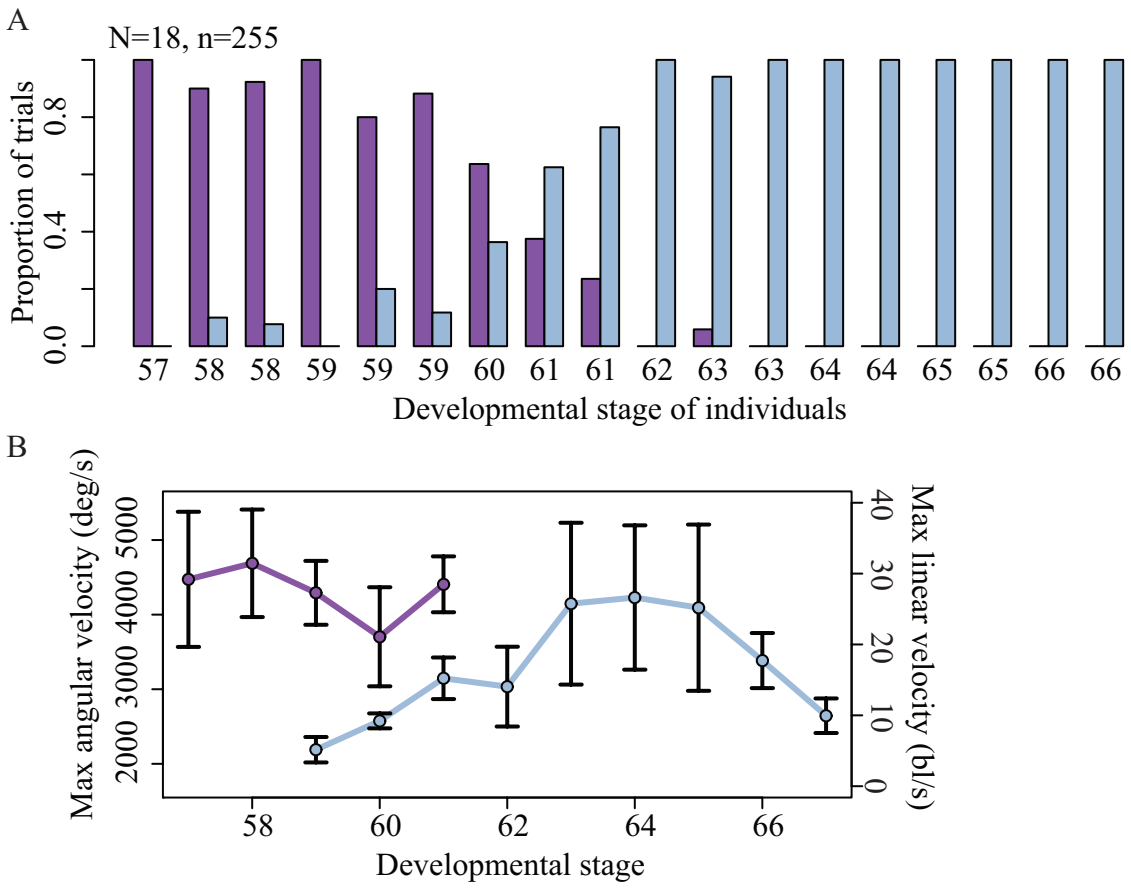

Figure 4.7: The startle response in *X. laevis* gradually transitions from the C-start to pushback response. (A) Proportion of trials that were C-start (purple) or pushback (blue) startle responses. The pushback gradually becomes the more prevalent startle response through metamorphosis until the C-start is lost. The x-axis includes individual animals which is why some stages have multiples. (B) C-start performance (left y-axis) does not change significantly through metamorphosis until the response is lost. Pushback performance (right y-axis) increases through metamorphosis, and reaches peak performance values shortly after the C-start is lost.

4.5 Discussion

In this study, we utilized the frog startle response as a model to investigate how a behavioral is maintained through a dramatic ontogenetic change in body structure. *X.*

laevis appears to transition startle modalities by forming the neural connections necessary for pushback startle before the hindlimbs are developed enough to generate effective thrust. Early in this transition, the performance level of the tadpole C-start is maintained, presumably until the adult behavior is sufficient. This suggests that the neural circuit that facilitates this behavior is in place before the necessary morphological components have been established. We know from previous work that the hindlimb muscles are active by stage 58 (Combes et al. 2004). From our observations, we would expect that the hindbrain components of this circuit are also in place at this time.

The consistent performance of the C-start through metamorphosis contradicted our initial hypothesis. We expected that C-start performance would decrease as the hindlimbs developed and the skeleton ossified given that these factors would likely increase drag and limit axial bending. The delayed ossification of the postsacral region of the vertebral column (Ročková and Roček 2005) may allow the animal to continue to perform deep axial bends through stage 61. This region seems to be consistent with where the axial bend is centered during a C-start (Figure 4.5). It could be that the hindlimbs are able to assist in turning, or that they do not add as much drag during turning as initially predicted. We also expected to observe the turn angle to become shallower, but we did not observe any significant difference in turn angle. This may be because the pelvis does not develop until stage 63.

We found that maximum ankle extension was a significant factor in pushback performance. Variability in extension angle suggests that it could be a modulatory mechanism, similar to the turn angle for a C-start. Because ankle extension occurs with a delay, it is unlikely to be directly initiated by reticulospinal cells, such as Mauthner cells.

The contribution of ankle angle to performance is consistent with previous work showing that rotational velocity is the primary contributor to thrust in *X. laevis* and other aquatic species (Richards 2010; Robovska-Havelkova et al. 2014). Ankle extension is a major contributor to rotational velocity, while knee extension results in translational velocity. Ecological niche has been shown to impact locomotion more than phylogenetic relationships in anurans (Robovska-Havelkova et al. 2014). Because terrestrial species rely more on translational velocity for thrust, it would be worth examining whether these species also perform a pushback response and compare their joint coordination pattern to that of the aquatic *X. laevis*. It is important to note that our "ankle" measurements combine the ankle and tarsometatarsal (tmt) joints. Both of these joints contribute to rotational velocity, but the tmt was challenging to measure in the younger animals. In the future, we plan examine the individual contributions of these two joints to the pushback response in late metamorphic animal where the tmt can be more easily tracked.

While the pushback response has been characterized as an adult behavior, it appears to reach the highest performance values during late metamorphosis. We looked at velocity in body lengths per second to compare performance across stages without confounding body size. However, even comparing velocity in centimeters per second, there was no significant difference between stages 65-66 and adults. This means that late metamorphic animals can move as quickly, in absolute distance per time, as conspecifics that are 2-3 times their size. The drop in performance of mature animals could be due, in part, to post-metamorrphic changes in the body. Qualitatively, we observed that *X. laevis* undergoes further development from post-metamorphic to sexually mature life stages. They become more triangle -shaped and their mass increases dramatically. All of these

changes would add drag and limit the performance of the pushback. Additionally there is a possibility that this decrease in performance could be the result of the animals growing in captivity. In captivity, *X. laevis* have less space in which to startle as they increase in size, so they might not be performing an optimal pushback in order to avoid hitting a wall. The same behavioral trials would need to be performed on wild-caught animals for comparison to determine if this behavior varies with environment.

Our behavioral results show that between stages 58 and 61, *X. laevis* can perform both unilateral (C-start) and bilateral (pushback) startle responses. Based on our findings, we hypothesize that the adult startle neural circuit is in place and active relatively early in metamorphosis. Furthermore, the circuit appears to allow the animal to alternate between two patterns of activation, perhaps similar to how the larval zebrafish can perform both S- and C-starts. By the time the animals begin to lose the tail, we see no behavioral evidence of a unilateral component, though this needs to be confirmed physiologically.

The startle response in *X. laevis* tadpoles is mediated by Mauthner cells, and exhibits a similar pattern of activation as the fish Mauthner cell circuit (Rock 1980). Physiological studies confirmed in *R. catesbeiana* tadpoles that direct Mauthner cell stimulation produces the contralateral muscle response associated with the C-start (Rock 1980). This same study showed that bilateral stimulation of the eighth cranial nerves elicits action potentials in both cells, indicating a lack of contralateral M-cell inhibition that is found in zebrafish and goldfish. Depending on the inter-stimulus interval, the muscle response may be either bilateral or unilateral. This work from Rock (1980) indicated that tadpoles exhibit contralateral inhibition within the spinal cord, but that it may not be all or none. The lack of contralateral M-cell inhibition is likely related to the

simple axon cap structure found in anurans (Bierman, Zottoli, and Hale 2009). This type of axon cap lacks the inhibitory interneurons that are found in the composite cap structures that zebrafish have. The lack of M-cell contralateral inhibition may allow the animal to transition more easily through metamorphosis. The loss of the unilateral axial response could simply result from the loss of inhibitory interneurons in the spinal cord through metamorphosis.

It was long thought that Mauthner cells were lost through metamorphosis until Will (1986) showed that they persist in adults of some anuran species. We confirmed the presence of Mauthner cells in all of our adult frogs (Figure 4.8). While we know that the Mauthner cells are retained in adult *X. laevis* frogs, physiological studies are still necessary to confirm whether these cells drive the startle response at this stage. However, it has been shown in *Rana catesbeiana* (bullfrog) that the Mauthner cell projections to the lumbar region are maintained through metamorphosis (Davis and Farel 1990). This would suggest that Mauthner cells have the potential to form synapses with hindlimb motor neurons.

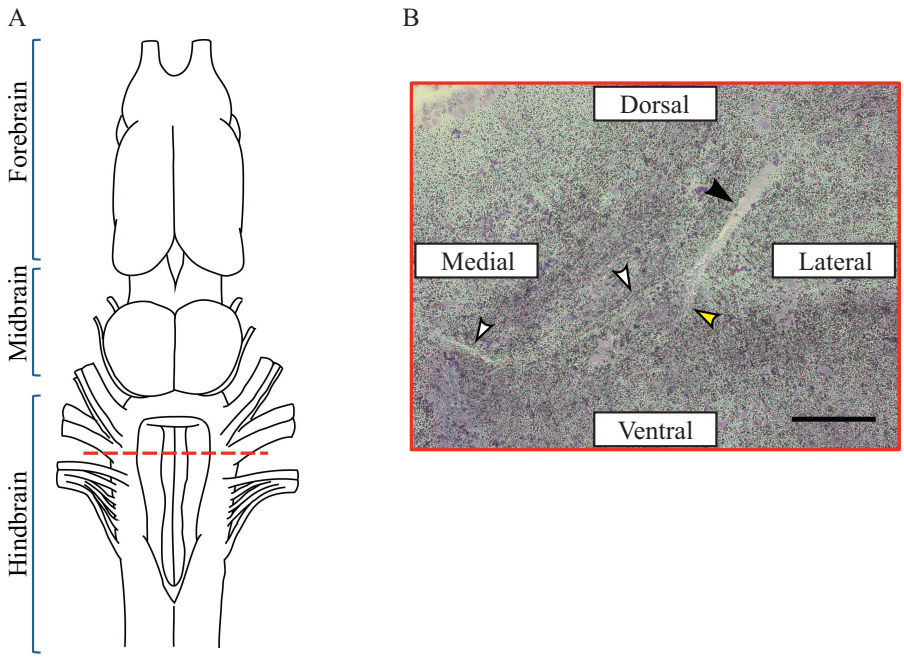

Figure 4.8: Mauthner cells identified via cryosectioning and cresyl violet staining in the post-metamorphic frogs. (A) A dorsal view schematic of the *X. laevis* frog brain modified from Nikundiwe and Nieuwenhuys (1983). We were able to find Mauthner cells at the level of the VIIIth cranial nerve in the hindbrain. The approximate location of the sections where we found Mauthner cells is indicated by the red dashed line. (B) Coronal cryosection stained with cresyl violet. The black arrow indicates the soma, white arrows indicate what we suspect to be the axon, and the yellow arrow indicates a suspected dendritic branch. Scale bar is 150µm.

We hypothesize that the pushback response may be undergoing a shift in functionality in post-metamorphic adult animals. During late metamorphosis, the pushback seems to act as an escape response, while in adults it is more of a preparatory response to re-orient the animal. This transition makes sense from an ecological standpoint. *X. laevis* has few natural predators, and one of their primary predators are conspecifics (Tinsley and Kobel 1996; Lobos and Jaksic 2005; Faraone et al. 2008), which likely makes it more advantageous for late metamorphic frogs to out-perform adult startles. In addition to conspecifics, depending on their geographical location their

predators may include fish (Prinsloo, Schoonbee, and Nxiweni 1981) and birds (Lobos and Jaksic 2005), Adult frogs are likely most vulnerable to predation when they go to the surface to breath (Baird 1983). Videler and Jorna (1985) showed that frogs performed a pushback, or "surface dive" when a shadow stimulus was presented at the surface. Videler and Jorna (1985) did not report behavior beyond stage 1 and we did not look at behavior at the surface, but we would expect that a burst swim after the pushback would allow the animal to more rapidly dive into the substrate. Based on burst swim performance measurements from other studies, it appears that a burst swim is more likely to out-perform a pushback response (based on Wilson et al. 2002).

The startle response is just one example of a vital behavior that is maintained through metamorphosis. In this study, we have characterized the behavioral transition from axial- to limb-based startle. In addition to the behavioral shifts associated with a metamorphic body transformation, we observed variation within the pushback modality that may be related to changes in ecology. Because the startle neural circuit is well characterized, it is an ideal model for examining how mechanisms of sensorimotor integration are maintained through metamorphosis.

CHAPTER 5

DISCUSSION

Here, I have examined morphological, neural, and behavioral features of the startle response in order to gain insight into how relationships between structure and function can change through life history. In fish, I studied two factors that have been shown to impact startle behavior: body shape and the Rohon-Beard (RB) mechanosensory network. In my second chapter, I found that most ray-finned fish transition to a less elongate body form, which suggests that the S-start startle modality is common across fish, but primarily at the larval stage. In my third chapter, I found variation in the morphology and physiology of RB mechanosensory cells along the rostrocaudal axis of zebrafish. This regionalization may play a role in how the startle modality relates to body shape. In frogs, I examined how startle is maintained as these animals transition from axial- to limb-based locomotion through metamorphosis. In chapter four, I showed that as *X. laevis* gradually transition from a C-start to a pushback response, and go through a period when they can alternate between the two behavioral modalities. Here, I discuss my results across chapters and propose future experiments that could provide further insight into ontogenetic relationships between structure and function, and their corresponding impact on behavior.

A potential stage-specific adaptation in larval fish

Body elongation is closely related to locomotor strategy across adult fish (Webb 1984). An elongate body axis is more ideal for undulatory axial movements, while a

rounded body shape is ideal for oscillatory fin movement (Webb 1984). Because most fish undergo a dramatic ontogenetic change in body shape, we would expect locomotor strategies to also change through life history. Due to their elongate shape and undeveloped fins, I expect that most larvae use undulatory locomotion similar to what we see in larval zebrafish. With the greater variation in body elongation, the addition of developed fins, and increased overall size; the locomotor strategies in adults are likely to exhibit more diversity than in larvae.

In zebrafish, we found that RB cells exhibit rostrocaudal differences in morphology and physiology. We suspect that this variation within the mechanosensory system could facilitate the regionalized motor output observed during the S-start. As discussed in chapter three, it has been generally accepted that RB cells undergo programmed cell death during early post-hatching life history (Williams et al. 2000; Svoboda et al. 2001; Reyes et al. 2004). If RB cells are necessary to produce an S-start response, we would expect the S-start motor pattern to disappear as the cells die off. These animals would then only perform a C-start response, as we see in zebrafish. Based on the relationship between startle and body shape, I would expect the timing of the ontogenetic decrease in elongation ratio to correlate with the progression of RB cell death. In summary, I hypothesize that RB cell death and decrease in elongation ratio occur within the same time period, and contribute to the loss of the S-start.

It is still unknown exactly when or whether RB cells die off entirely. Over the years, RB cell bodies have continued to be identified in the spinal cord at later and later stages (Metcalfe et al. 1990; Svoboda et al. 2001; O'Brien et al. 2012; Palanca et al. 2013). Recently they have been identified as late as 14 dpf (Palanca et al. 2013). It may

be that some RB cells are retained in the adult stage. They have also been hypothesized to be retained in lampreys and newts (Nakao and Ishizawa 1987; Reyes et al. 2004). As zebrafish become more pigmented and the vertebral column develops, it becomes much more challenging to identify cells within the spinal cord. Some species of fish have been shown to perform S-starts as adults (e.g. Hale 2002). Perhaps in species that perform S-starts as adults enough RB cells remain at the adult stage to retain the ability to elicit an S-start through the same basic mechanism as in larvae.

A question that still remains is why a larval-specific mechanosenory network even exists. What distinguishes RB cells from dorsal root ganglion cells? We have found that RB activity in response to tactile stimuli resembles that of fast-adapting mechanoreceptors, and that RB cells encode stimulus intensity and position. The identified regionalization and its proposed role in regionalized motor output suggest they play a specialized role startle and potentially, more broadly, in locomotion. This hypothesis is further supported by work from Knafo et al. (2017) that indicates RB cells play a role in modulating swimming speed, and thus may sensing stretch. We also have not tested whether RB cells could be multimodal. Larval fish respire cutaneously, and have chemoreceptors distributed across the entire body (Coccimiglio and Jonz 2012). Like RB cells, these receptors gradually die off, however they can be found in adult fish in the gills (Coccimiglio and Jonz 2012; Porteus et al. 2015). If chemoreceptors interact with the peripheral processes of RB cells, then RB cells could relay chemosensory information in addition to mechanical information. Additional studies on both RB cells and DRG cells are necessary to understand how the transition between these two networks impacts behavior.

Based on our findings on body elongation and RB cells, I hypothesize that the S-start response is common across fishes. However, it is likely that this behavioral modality is most prevalent across fish at the larval stage. The S-start may have evolved as a larval-specific startle modality, and is only retained in a subset of adults. Looking only in adults, the S-start could be viewed as a specialized, possibly derived, startle modality found only in a handful of species. However, we expect that, like the zebrafish, many species that do not perform an S-start as adults could perform the response as larvae. In fact, because bilateral Mauthner cell (M-cell) activation is necessary to produce the S-start (Liu et al. 2012), this response may not be limited to fish species that have contralateral inhibition at the level of the M-cell. RB cells are also highly conserved across species that have M-cells. Additional work will be necessary to elucidate the evolutionary history of this behavioral modality.

Maintaining a behavior through ontogenetic body plan reorganization

My work has filled in some of the few gaps in our knowledge pertaining to stage-specific components of Mauthner cell-driven startle in fish. We can utilize this very detailed picture of the fish startle system as a guide as we explore this circuit in frogs. While the presence of M-cells in tadpoles has been well established for many decades (Stefanelli 1951), Will (1986) was the first to show that the M-cells have been observed to be retained post-metamorphosis in some species of frogs. However, since this discovery, very little has been done to examine the M-cells or startle behavior in post-metamorphic frogs. In my fourth chapter, I examined how the startle behavior is maintained through anuran metamorphosis in *X. laevis*, a species that is known to have

M-cells in adults. I found that the startle modality gradually shifts from axial-based to limb-based through development. C-start performance is consistent through metamorphosis until the response is lost, while limb-based startle performance changes both through and post-metamorphosis. Using this behavioral transition as a guide, we can start to examine the neural components that underlie this change in modality.

Anurans present an ideal model for examining more extreme ontogenetic changes in body and behavior. How do these animals continue to behave at a performance level that is sufficient to keep them from getting eaten despite massive reorganization of propulsive systems? In the case of locomotion, the overlapping pre- and post-metamorphic components appear to allow the animal to fine-tune the adult movement before the tadpole locomotor strategy is lost. When the pushback kinematic pattern first appears, it performs very poorly. At this time, the C-start is still the more prevalent startle modality. Pushback performance gradually improves as the hindlimbs develop and the more common startle modality shifts from the C-start to the pushback. This indicates that the neural circuitry is in place before the body is developed enough to perform the behavior.

This is consistent with other studies that utilized an *ex vivo* prep to examine the transition in *X. laevis* from motor output along the body axis to motor output in the hindlimbs (Combes et al. 2004). These studies show that there is motor output to the hindlimbs before the hindlimbs are developed enough to generate propulsion. They found that at stage 58, these animals exhibit simultaneous activation of extensor and flexor muscles, which likely acts to hold their limbs against the body during swimming. As the hindlimbs develop and the frogs start to utilize them for propulsion, the motor output

patterns become more complex (Combes et al. 2004). Both in swimming and startle, the hindlimbs are incorporated into the behavior before they are sufficiently developed to generate propulsion. This indicates that the frog nervous system overlaps with the tadpole system, at least within the spinal cord. The timing and changes that occur in the hindbrain are still unclear

Electrophysiological M-cell recordings in bullfrog tadpole indicate that an action potential is necessary and sufficient to produce contralateral motor output (Rock 1980). However these tadpoles do not exhibit the contralateral M-cell inhibition that has been shown in zebrafish and goldfish. As a result, stimulating both M-cells may result in unilateral or bilateral motor output, depending on the relative timing of the stimuli. In adults, the startle response is characterized by bilateral, synchronous movement that is indicative of bilateral motor output. If M-cells play a role in adult startle as we hypothesize, we would expect that both M-cells must fire to produce the response. In some of the stages where the animals performed both C-starts and pushbacks, we observed what seemed to be an incomplete pushback with a deep axial bend. In such instances, I would hypothesize that the contralateral inhibition in the spinal cord does not extend to the hindlimbs. I have been able to reliably locate and identify M-cells in adult frog brain sections, so that in the future we might be able to target these cells for *in vivo* recording.

Previous work has already identified some of the differences between the zebrafish and frog systems that could allow for this bilateral M-cell activity. M-cells have a structure known as the axon cap that surrounds the axon hillock and influences the excitability of the cell. There are multiple types of axon caps found across ray-finned

fishes (Bierman et al. 2009). Zebrafish have what is known as a composite axon cap, while tadpoles have a simple axon cap (Bierman et al. 2009). This simple structure lacks input from passive hyperpolarizing inhibitory cells. In zebrafish, these cells play a role in contralateral M-cell inhibition. The simple structure could be what allows for the higher probability of bilateral M-cell firing in tadpoles, just as the lack of axon caps likely promote bilateral firing in animals that perform a retraction response (Currie 1991; Zottoli and Faber 2000). If the limb circuit develops without the contralateral spinal inhibition seen in tadpoles, then bilateral M-cell activity would always result in bilateral motor output.

While *X. laevis* animals achieve their adult body plan by the end of metamorphosis, they do not become sexually mature until several months later. Qualitatively, the animals appeared to undergo further changes in body shape beyond growth. In these mature animals, we observed a decrease in pushback performance as well as a decrease in ankle extension. We did not examine ages in between stage 66 and the eight-month-old animals, but if we did, more extensive morphological measurements might elucidate what adult features are changing and impacting performance. This period of post-metamorphic development is almost reminiscent of the morphological changes we might see in fish, where the body shape is changing, but the fundamental body plan is the same. A study examining cranial characters in post-metamorphic anurans found that these characters vary based on the selective influence of the climate that the adult inhabits and are in independent of the tadpole features (Simon and Marroig 2017). *X. laevis* have been known to be able to inhabit a diverse range of habitats, so it is possible that post-metamorphic environments could influence differences in startle performance or strategy.

In fish, the motor and interneuron components of the spinal cord are essentially established at the larval stage. RB cells are the only spinal cell type involved in the startle circuit that has been shown to change in number through ontogeny. In contrast, the frog experiences cell proliferation and cell death throughout the spinal cord during metamorphosis. The changes in behavior could be explained entirely by these changes spinal cord, but are the M-cells also changing? Based on the images from Will (1986) and my own observations from stained sections, the M-cells change their shape through metmorphosis. Could this morphological change correspond to a functional change? In the future, we plan to use single cell transcriptomics to determine whether there are different patterns of gene expression in pre- and post-metamorphic animals. By looking at components such as receptors and ion channels, we could potentially gain insight into particular aspects of excitability might be changing in the cells.

Conclusions

Many animals undergo dramatic body transformations through ontogeny, and may inhabit completely different environments at these stages (e.g. Fuiman and Higgs 1997; Leis and McCormick 2002). To cope with these different pressures, many species have stage-specific adaptations that are distinct from the adult stage. To understand an animal's entire behavioral repertoire, it must be examined across life history. Certain stage-specific behavioral modalities may allow us to investigate questions that others cannot. For example, the S-start and RB cells have facilitated our examination of regionalization in the zebrafish spinal cord, which we would not have looked for if we had only considered the C-start. In addition to studying stage specific traits, examining

the transition between these stage-specific modalities can provide insights into the developmental coordination between body shape and the nervous system. Characterizing the transition from axial to limb-based startle in anurans has allowed us to develop new hypotheses on how the nervous system facilitates this shift in startle modality. The work that I have presented on startle demonstrates some of the insights that can be gained by considering an ontogenetic perspective, and adds to the growing body of work that highlights the significance of these intermediate life-history stages.

References

Abraira VE, & Ginty DD. 2013. The sensory neurons of touch. Neuron, 79(4):618–639.

Arnott SA, Neil DM, & Ansell AD. 1998. Tail-flip mechanism and size-dependent kinematics of escape swimming in the brown shrimp Crangon crangon. Journal of Experimental Biology, 201:1771–1784.

Bagnall MW, & McLean DL. 2014 Modular organization of axial microcircuits in zebrafish. Science, 343(6167):197–200.

Baird TA. 1983. Influence of Social and Predatory Stimuli on the Air-Breathing Behavior of the African Clawed Frog , Xenopus laevis Author (s): Troy A . Baird Published by : American Society of Ichthyologists and Herpetologists (ASIH)

Bensmaia SJ. 2008. Tactile intensity and population codes. Behavioural Brain Research, 190(2):165–173.

Bernhardt RR, Patel CK, Wilson SW, & Kuwada JY. 1992. Axonal trajectories and distribution of GABAergic spinal neurons in wildtype and mutant zebrafish lacking floor plate cells. Journal of Comparative Neurology, 326(2):263–272.

Bhatt DH, McLean DL, Hale ME, & Fetcho JR. 2007. Grading Movement Strength by Changes in Firing Intensity versus Recruitment of Spinal Interneurons. Neuron, 53(1):91–102.

Bierman HS, Schriefer JE, Zottoli SJ, & Hale ME. 2004. The effects of head and tail stimulation on the withdrawal startle response of the rope fish (Erpetoichthys calabaricus). Journal of Experimental Biology, 207(22):3985-3997.

Bierman HS, Zottoli SJ, & Hale ME. 2009. Evolution of the Mauthner axon cap. Brain, Behavior and Evolution, 73(3):174–187.

Buchanan JT. 2001. Contributions of identifiable neurons and neuron classes to lamprey vertebrate neurobiology. Progress in Neurobiology, 63(4):441–466.

Carter S, & Fox H. 1994. Rohon-Beard cells and associated neural components in some larval amphibians and fishes: arrangement, measurements and comparisons. European Archives of Biology, 105:81-94.

Clarke JDW, Hayes BP, Hunt SP, & Roberts A. 1984. Sensory physiology, anatomy and immunohistochemistry of Rohon-beard neurones in embryos of Xenopus laevis. Journal of Physiology, 348:511–525.

Claverie T, & Wainwright PC. 2014. A morphospace for reef fishes: Elongation is the dominant axis of body shape evolution. PLoS ONE, 9(11): e1128732.

Coccimiglio ML, & Jonz MG. 2012. Serotonergic neuroepithelial cells of the skin in developing zebrafish: morphology, innervation and oxygen-sensitive properties. Journal of Experimental Biology, 215(22):3881–3894.

Combes D, Merrywest SD, Simmers J, & Sillar KT. 2004. Developmental segregation of spinal networks driving axial- and hindlimb-based locomotion in metamorphosing Xenopus laevis. The Journal of Physiology, 559(1):17–24.

Currie S, & Carlsen RC. 1985. A rapid startle response in larval lampreys. Brain Research, 358(1-2):367-371.

Currie SN. 1991. Vibration-evoked startle behavior in larval lampreys. Brain, Behavior and Evolution, 37(5):260-271.

Davis GR, & Farel, PB. 1990. Mauthner cells maintain their lumbar projection in adult frog. Neuroscience Letters, 113(2):139–143.

Djouhri L, Bleazard L, & Lawson SN. 1998. Association of somatic action potential shape with sensory receptive properties in guinea-pig dorsal root ganglion neurones. Journal of Physiology, 513(3):857–872.

Eschmeyer WN, Fricke R, van der Laan R (eds). 201. Catalog of Fishes: Genrta, Species, References. (http://researcharchive.calacademy.org/research/ichthyology/catalog/fishcatmain.asp). Electronic version accessed 1 January 2015.

Eidietis L. 2005. Size-related performance variation in the wood frog (Rana sylvatica) tadpole tactile-stimulated startle response. Canadian Journal of Zoology, 83:1117–1127.

Eidietis L. 2006. The Tactile-Stimulated Startle Response of Tadpoles: Acceleration Performance and its Relationship to the Anatomy of Wood Frog (Rana sylvatica), Bullfrog (Rana catesbeiana), and American Toad (Bufo americanus) Tadpoles. Journal of Experimental Zoology, 305(9):672–682.

Fang X, McMullan S, Lawson SN, & Djouhri L. 2005. Electrophysiological differences between nociceptive and non-nociceptive dorsal root ganglion neurones in the rat in vivo. Journal of Physiology, 565(3):927–943.

Faraone FP, Lillo F, Giacalone G, & Valvo MLo. 2008. The large invasive population of Xenopus laevis in Sicily, Italy. Amphibia-Reptilia, 29(3):405–412.

Feilich KL, & Lauder GV. 2015. Passive mechanical models of fish caudal fins: Effects of shape and stiffness on self-propulsion. Bioinspiration and Biomimetics, 10(3).

Fuiman LA. 1979. Descriptions and comparisons of catostomid fish larvae: northern

Atlantic drainage species. The American Fisheries Society, 108(6):560-603.

Fuiman LA & Higgs DM. 1997. Ontogeny, growth and the recruitment process. In *Early life history and recruitment in fish populations.* Springer, Dordrecht (pp. 225-249).

Furukawa T and Furshpan EJ. 1963. Two inhibitory mechanisms in the neurons of goldfish. Journal of Neurophysiology 26 (1): 140-176.

Green MH, Curet OM, Patankar NA, & Hale ME. 2013. Fluid dynamics of the larval zebrafish pectoral fin and the role of fin bending in fluid transport. Bioinspiration and Biomimetics, 8(1).

Hale ME, Ritter DA, & Fetcho JR. 2001. A confocal study of spinal interneurons in living larval zebrafish. Journal of Comparative Neurology, 437(1):1–16.

Hale ME. 2002. S- and C-start escape responses of the muskellunge (Esox masquinongy) require alternative neuromotor mechanisms. The Journal of Experimental Biology, 205(Pt 14):2005–2016.

Hale ME. 2014. Developmental change in the function of movement systems: transition of the pectoral fins between respiratory and locomotor roles in zebrafish. Integr Comp Biol, 54(2):238-249.

Hale ME, Katz HR, Peek MY, & Fremont RT. 2016. Neural circuits that drive startle behavior, with a focus on the Mauthner cells and spiral fiber neurons of fishes. Journal of Neurogenetics, 30(2):89–100.

Hasegawa H, & Wang F. 2008. Visualizing mechanosensory endings of TrkC-expressing neurons in HS3ST-2-hPLAP mice. Journal of Comparative Neurology, 511(4):543–556.

Herrel A, Choi HF, Dumont E, De Schepper N, Vanhooydonck B, Aerts P, et al. 2011. Burrowing and subsurface locomotion in anguilliform fish: behavioral specializations and mechanical constraints. Journal of Experimental Biology, 214(8):1379-1385.

Inoue JG, Miya M, Miller MJ, Sado T, Hanel R, Hatooka K, et al. 2010. Deep-ocean origin of the freshwater eels. Biol. Lett.; 6:363-366.

Johansson RS. 1976. Receptive field sensitivity profile mechanosensitive units innervating the glabrous skin of the human hand. Brain Research, 104(2):330–334.

Johnson KE, & Eidietis L. 2005. Tadpole Body Zones Differ with Regard to Strike Frequencies and Kill Rates by Dragonfly Naiads. Copeia, 2005(4):909–913.

Jones PW, Martin FD, Hardy JD, Johnson GD, Fritzsche RA, & Drewry GE. 1978. Development of fishes of the Mid-Atlantic Bight. An atlas of egg, larval and juvenile stages. Fish and Wildlife Service, U.S. Department of the Interior.

Knafo S, Fidelin K, Prendergast A, Tseng PEB, Parrin A, Dickey C, et al. 2017. Mechanosensory neurons control the timing of spinal microcircuit selection during locomotion. ELife, 6:1–21.

Korn H, & Faber DS. 2005. The Mauthner cell half a century later: a neurobiological model for decision-making? Neuron, 47(1):13–28.

Koyama M, Kinkhabwala A, Satou C, Higashijima SI, & Fetcho J. 2011. Mapping a Sensory-motor Network onto a Structural and Functional Ground Plan in the Hindbrain. Proceedings of the National Academy of Sciences. 108(3):1–6.

Landberg T, & Azizi E. 2010. Ontogeny of escape swimming performance in the spotted salamander. Functional Ecology, 24(3):576–587.

Lavoué S, & Sullivan JP. 2004. Simultaneous analysis of five molecular markers provides a well-supported phylogenetic hypothesis for the living bony-tongue fishes (Osteoglossomorpha: Teleostei). Molecular Phylogenetics and Evolution, 33(1):171-185.

Leis JM, & McCormick MI. 2002. The biology, behavior, and ecology of the pelagic, larval stage of coral reef fishes. Coral Reef Fishes - Dynamics and Diversity in a Complex Ecosystem, 171–199.

Li L, Rutlin M, Abraira VE, Cassidy C, Kus L, Gong S, et al. 2011. The functional organization of cutaneous low-threshold mechanosensory neurons. Cell, 147(7):1615–1627.

Liu YC, Bailey I, & Hale ME. 2012. Alternative startle motor patterns and behaviors in the larval zebrafish (Danio rerio). Journal of Comparative Physiology. A, Neuroethology, Sensory, Neural, and Behavioral Physiology, 198(1):11–24.

Liu YC, & Hale ME. 2014. Alternative forms of axial startle behaviors in fishes. Zoology, 117(1):36–47.

Liu YC, & Hale ME. 2017. Local Spinal Cord Circuits and Bilateral Mauthner Cell Activity Function Together to Drive Alternative Startle Behaviors. Current Biology, 27(5):697–704.

Lobos G, & Jaksic FM. 2005. The ongoing invasion of African clawed frogs (Xenopus laevis) in Chile: Causes of concern. Biodiversity and Conservation, 14(2):429–439.

Longair MH, Baker DA, & Armstrong JD. 2011. Simple neurite tracer: Open source

software for reconstruction, visualization and analysis of neuronal processes. Bioinformatics, 27(17):2453–2454.

Mauthner L. 1859. Untersuchungen über den Bau des Rückenmarkes der Fische: Eine vorläufige Mittheilung. H-& Stts-Dr. (SCbC Gerold's Sohn).

Marshall KL, Clary RC, Baba Y, Orlowsky RL, Gerling GJ, & Lumpkin EA. 2016. Touch Receptors Undergo Rapid Remodeling in Healthy Skin. Cell Reports, 17(7):1719–1727.

McEachran JD, & Fechhelm JD. 1998. Fishes of the Gulf of Mexico, volume 1: *Myxiniformes* to *Gasterosteiformes*. University of Texas Press.

Mchenry MJ, & Lauder GV. 2006. Ontogeny of Form and Function : Locomotor Morphology and Drag in Zebrafish (Danio rerio), Journal of Morphology 267(9):1099–1109.

Meager JJ, Domenici P, Shingles A, & Utne-Palm AC. 2006. Escape responses in juvenile Atlantic cod Gadus morhua L.: the effects of turbidity and predator speed. Journal of Experimental Biology, 209(20):4174–4184.

Menelaou E, & McLean DL. 2012. A Gradient in Endogenous Rhythmicity and Oscillatory Drive Matches Recruitment Order in an Axial Motor Pool. Journal of Neuroscience, 32(32):10925–10939.

Metcalfe WK, Myers PZ, Trevarrow B, Bass MB, & Kimmel CB. 1990. Primary neurons that express the L2/HNK-1 carbohydrate during early development in the zebrafish. Development, 110:491–504.

Metcalfe WK, Myers PZ, Trevarrowt B, Bass MB, & Kimmel CB. 1990. Primary neurons that express the L2 / HNK-1 carbohydrate during early development in the zebrafish, 504:491–504.

Miller MJ. 2009. Ecology of Anguilliform leptocephali: remarkable transparent fish larvae of the ocean surface layer. Aqua-BioSci Monogr, 2(4):1-94

Miya M, Friedman M, Satoh TP, Takeshima H, Sado T, Iwasaki W, et al. 2013. Evolutionary origin of the Scombridae (Tunas and Mackerels): members of a paluogene adaptive radiation with 14 other pelagic fish families. PLOS ONE, 8(9): e73535.

Muller UK, & van Leeuwen JL. 2004. Swimming of larval zebrafish: ontogeny of body waves and implications for locomotory development. Journal of Experimental Biology, 207(5):853–868.

Nakao T, & Ishizawa A. 1987. Development of the spinal nerves in the lamprey: I.

Rohon-beard cells and interneurons. Journal of Comparative Neurology, 256(3):342–355.

Near TJ, Eytan RI, Dornburg A, Kuhn KL, Moore JA, Davis MP, et al. 2012. Resolution of ray-finned fish phylogeny and timing of diversification. PNAS, 109(34): 1398-13703.

Near TJ, Dornburg A, Eytan RI, Keck BP, Smith WL, Kuhn KL, et al. 2013. Phylogeny and tempo of diversification in the superradiation of spiny-rayed fishes. PNAS, 110(31): 12738-12743.

Nicholls JG, & Baylor Da. 1968. Specific modalities and receptive fields of sensory neurons in CNS of the leech. J Neurophysiol, 31(5):740–756.

Nieuwkoop P, & Faber J. (1994). Normal Table of Xenopus Laevis (Daudin): A Systematical & Chronological Survey of the Development from the Fertilized Egg till the End of Metamorphosis. Http://Www.Xenbase.Org/Anatomy/Alldev.Do.

Nikundiwe AM, & Nieuwenhuys R. 1983. The cell masses in the brainstem of the South African clawed frog Xenopus laevis: A topographical and topological analysis. Journal of Comparative Neurology, 213(2):199–219.

O'Brien GS, Rieger S, Wang F, Smolen GA, Gonzalez RE, Buchanan J, & Sagasti, A. 2012. Coordinate development of skin cells and cutaneous sensory axons in zebrafish. Journal of Comparative Neurology, 520(4):816–831.

Palanca AMS, Lee SL, Yee LE, Joe-Wong C, Trinh LA, Hiroyasu E, et al. 2013. New transgenic reporters identify somatosensory neuron subtypes in larval zebrafish. Developmental Neurobiology, 73(2):152–167.

Parichy DM, Elizondo MR, Mills MG, Gordon TN, & Engeszer RE. 2009. Normal table of postembryonic zebrafish development: staging by externally visible anatomy of the living fish. Dev Dynam, 238(12):2975–3015.

Peng YB, Ringkamp M, Campbell JN, & Meyer RA. 1999. Electrophysiological Assessment of the Cutaneous Arborization of Aδ-Fiber Nociceptors. Journal of Neurophysiology, 82(3):1164–1177.

Pirschel, F, & Kretzberg J. 2016. Multiplexed Population Coding of Stimulus Properties by Leech Mechanosensory Cells. The Journal of Neuroscience, 36(13):3636–3647.

Porteus CS, Pollack J, Tzaneva, V, Kwong RWM, Kumai Y, Abdallah SJ, et al. 2015. A role for nitric oxide in the control of breathing in zebrafish (Danio rerio). Journal of Experimental Biology, 218(23):3746–3753.

Preibisch S, Saalfeld S, & Tomancak P. 2009. Globally optimal stitching of tiled 3D

microscopic image acquisitions. Bioinformatics, 25(11):1463–1465.

Prinsloo JF, Schoonbee HJ, & Nxiweni J. 1981. Some Observations on Biological and Other Control Measures of the African Clawed Frog Xenopus laevis (Daudin) (Pipidae, Amphibia) in Fish Ponds in Transkei. Water SA. 7(2):88-96

R Core Team. 2013. R: A language and environment for statistical computing. R foundation for Statistical Computing, Vienna

Reyes R, Haendel M, Grant D, Melancon E, & Eisen, JS. 2004. Slow Degeneration of Zebrafish Rohon-Beard Neurons during Programmed Cell Death. Developmental Dynamics, 229(1):30–41.

Richards WJ (Ed.). 2005. Early stages of Atlantic fishes: an identification guide for the western central north Atlantic, Two Volume Set (Vol. 2). CRC Press.

Richards, C. T. (2010). Kinematics and hydrodynamics analysis of swimming anurans reveals striking inter-specific differences in the mechanism for producing thrust. Journal of Experimental Biology, 213(4), 621–634.

Roberts A, & Hayes BP. 1977. The anatomy and function of "free" nerve endings in an amphibian skin sensory system. Proceedings of the Royal Society B: Biological Sciences, 196(1125):415–429.

Robovska-Havelkova P, Aerts P, Rocek Z, Prikryl T, Fabre AC, & Herrel A. 2014. Do all frogs swim alike? The effect of ecological specialization on swimming kinematics in frogs. Journal of Experimental Biology, 217(20):3637–3644.

Rock MK. 1980. Functional properties of Mauthner cell in the tadpole Rana catesbeiana. Journal of Neurophysiology, 44(1):135–150.

Rock MK, Hackett JT, & Les Brown D. 1981. Does the Mauthner cell conform to the criteria of the command neuron concept? Brain research, 204(1):21-27.

Ročková H, & Roček Z. 2005. Development of the pelvis and posterior part of the vertebral column in the anura. Journal of Anatomy, 206(1):17–35.

Rovainen CM. 1967. Physiological and anatomical studies on large neurons of central nervous system of the sea lamprey (Petromyzon marinus). I. Müller and Mauthner cells. Journal of Neurophysiology, 30(5):1000-1023.

Rovainen CM. 1974. Synaptic interactions of identified nerve cells in the spinal cord of the sea lamprey. Journal of Comparative Neurology, 154(2):189–206.

Schindelin J, Arganda-Carreras I, Frise E, Kaynig V, Longair M, Pietzsch T, et al. 2012. Fiji: An open source platform for biological image analysis. Nature Methods,

9(7):676–682.

Scott JW, Zottoli SJ, Beatty NP, & Korn H. 1994. Origin and Function of Spiral Fibers Projecting to the Goldfish Mauthner Cell. Journal of Comparative Neurology. 339(1):76–90.

Schneider CA, Rasband WS, Eliceiri KW. 2012. NIH to ImageJ: 25 years of image analysis. Nature Methods. 9:671-675.

Selzer ME. 1979. Variability in maps of identified neurons in the sea Lamprey spinal cord examined by a wholemount technique. Brain Research, 163(2):181–193.

Simon MN, & Marroig G. 2017. Evolution of a complex phenotype with biphasic ontogeny: Contribution of development versus function and climatic variation to skull modularity in toads. Ecology and Evolution, 7(24):10752–10769.

Stefanelli A. 1951. The mauthnerian apparatus in the Ichthyopsida; its nature and function and correlated problems of neurohistogenesis. The Quarterly Review of Biology, 26(1):17–34.

Strauss RE, & Fuiman LA. 1985. Quantitative comparisons of body form and allometry in larval and adult Pacific sculpins (Teleostei: Cottidae). Can J Zoology, 63(7):1582-1589.

Sullivan JP, Lundberg JG, & Hardman MA. 2006. phylogenetic analysis of the major groups of catfishes (Teleostei: Siluriformes) using rag1 and rag2 nuclear gene sequences. Molecular Phylogenetics and Evolution, 41:636-662.

Svoboda KR, Linares AE., & Ribera AB. 2001. Activity regulates programmed cell death of zebrafish Rohon-Beard neurons. Development, 128(18):3511–3520.

Talbot WH, Darian-Smith I, Kornhuber HH, & Mountcastle VB. 1968. The sense of flutter-vibration: comparison of the human capacity with response patterns of mechanoreceptive afferents from the monkey hand. Journal of Neurophysiology, 31(2):301–334.

Tinsley RC, & Kobel HR. 1996. The biology of Xenopus. Zoological Society of London.

Toline CA, & Baker AJ. 1993. Foraging tactic as a potential selection pressure influencing geographic differences in body shape among populations of dace (Phoxinus eos). Can J Zoolog, 71(11):2178-2184.

Umeda K, Ishizuka T, Yawo, H, & Shoji W. 2016. Position- and quantity-dependent responses in zebrafish turning behavior. Scientific Reports, 6:27888.

Van Buskirk J, & McCollum SA. 2000. Influence of tail shape on tadpole swimming

performance. The Journal of Experimental Biology, 203(14):2149–2158.

Videler J, & Jorna J. 1985. Functions of the sliding pelvis in Xenopus laevis. Copeia, (1):251–254.

Walker JA, Ghalambor, CK, Griset OL, McKenney D, & Reznick DN. 2005. Do faster starts increase the probability of evading predators? Functional Ecology, 19(5):808–815.

Walsh CM, Bautista DM, & Lumpkin EA. 2015. Mammalian touch catches up. Current Opinion in Neurobiology, 34:133–139.

Wang X, Gan X, Li J, Mayden RL, & He S. 2012. Cyprinid phylogeny based on Bayesian and maximum likelihood analysis of partitioned data: implications for Cyprinidae systematics. Science China Life Sciences, 55(9): 761-773.

Ward AB, & Azizi E. 2004. Convergent evolution of the head retraction escape response in elongate fishes and amphibians. Zoology, 107(3):205–217.

Ward AB, & Brainerd EL. 2007. Evolution of axial patterning in elongate fishes. Biological Journal of the Linnean Society, 90: 97-116.

Ward AB, & Mehta RS. 2010. Axial elongation in fishes: using morphological approaches to elucidate developmental mechanisms in studying body shape. Integrative and Comparative Biology, 50(6):1106-1119.

Webb PW. 1984. Form and Function in Fish Swimming. Scientific American, 251:72–82.

Webb PW, & Weihs D. 1986. Functional locomotor morphology of early life history stages of fishes. The American Fisheries Society, 115(1):115-127.

Weiss SA, Preuss T, & Faber DS. 2008. A Role of Electrical Inhibition in Sensorimotor Integration. 105 (46):18047–18052.

Westneat MW. 2004. Evolution of levers and linkages in the feeding mechanisms of fishes. Integrative and Comparative Biology, 44(5):378–389.

Will U. 1986. Mauthner neurons survive metamorphosis in anurans: A comparative HRP study on the cytoarchitecture of Mauthner neurons in amphibians. Journal of Comparative Neurology, 244(1):111–120.

Will U. 1991. Amphibian Mauthner Cells. Brain, Behavior and Evolution, 37:317–332.

Wilson RS, & Franklin CE. 2013. Effect of ontogenetic increases in body size on burst swimming performance in tadpoles of the striped marsh frog, Limnodynastes peronii. Physiological and Biochemical Zoology : PBZ, 73(2):142–152.

Wilson RS, James RS, & Van Damme R. 2002. Trade-offs between speed and endurance in the frog Xenopus laevis: a multi-level approach. The Journal of Experimental Biology, 205(8):1145–1152.

Yoon M, Kim KY, Bang IC, Nam YK, & Kim DS. 2011. Complete mitogenome sequence of the Chinese medaka Oryzias sinensis (Teleostei: Beloniformes) and its phylogenetic analysis. Genes and Genomics, 33:307-312.

Zimmermann K, Hein A, Hager U, Kaczmarek JS, Turnquist BP, Clapham DE, & Reeh PW. 2009. Phenotyping sensory nerve endings in vitro in the mouse. Nature Protocols, 4(2):174–196.

Zottoli SJ, & Faber DS. 2000.Review: The Mauthner Cell: What has it taught us? The Neuroscientist, 6(1):26-38

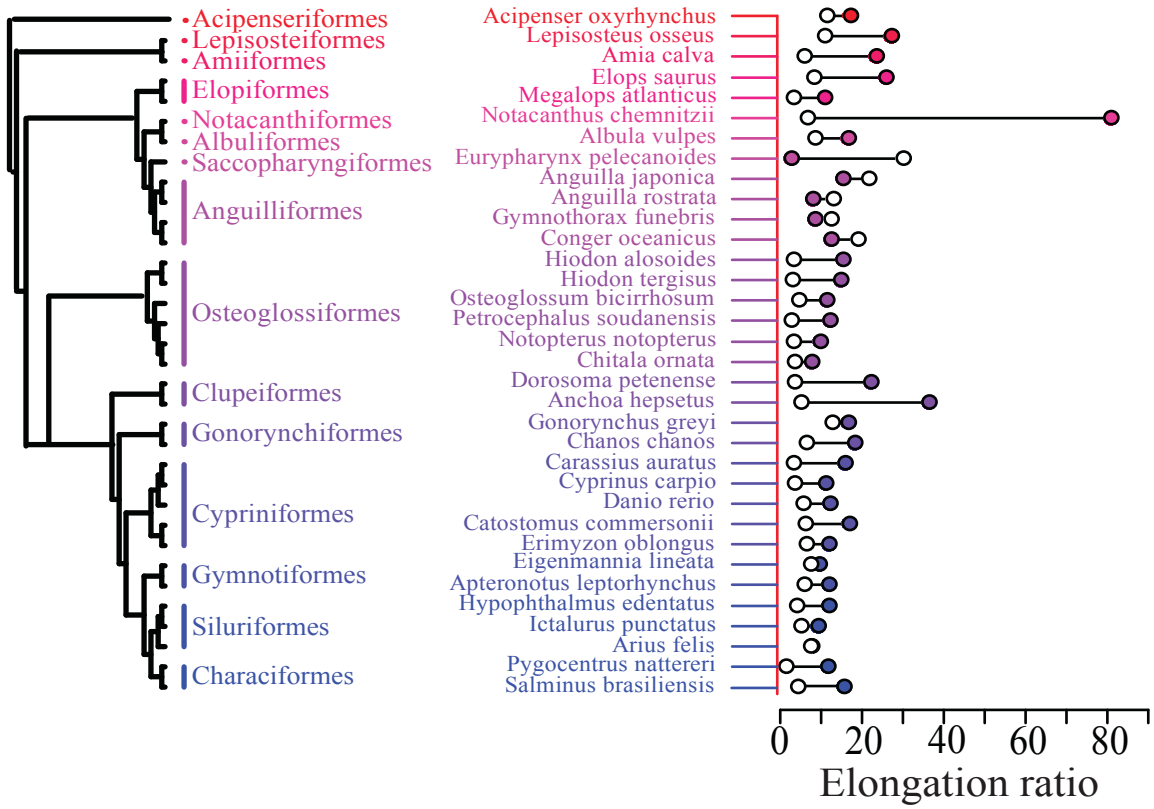

Figure S2.1: Individual larval and adult elongation ratios (Part 1). Genus and species name for a subset of species measured in this study with corresponding larval (filled circle) and adult (open circle) elongation ratios (see S1 Table for exact values). The measurements plotted are the same as those used for statistical analyses (see methods section for selection criteria). Colors correspond to the orders from which the species were selected. Modified from Figure 2.1.

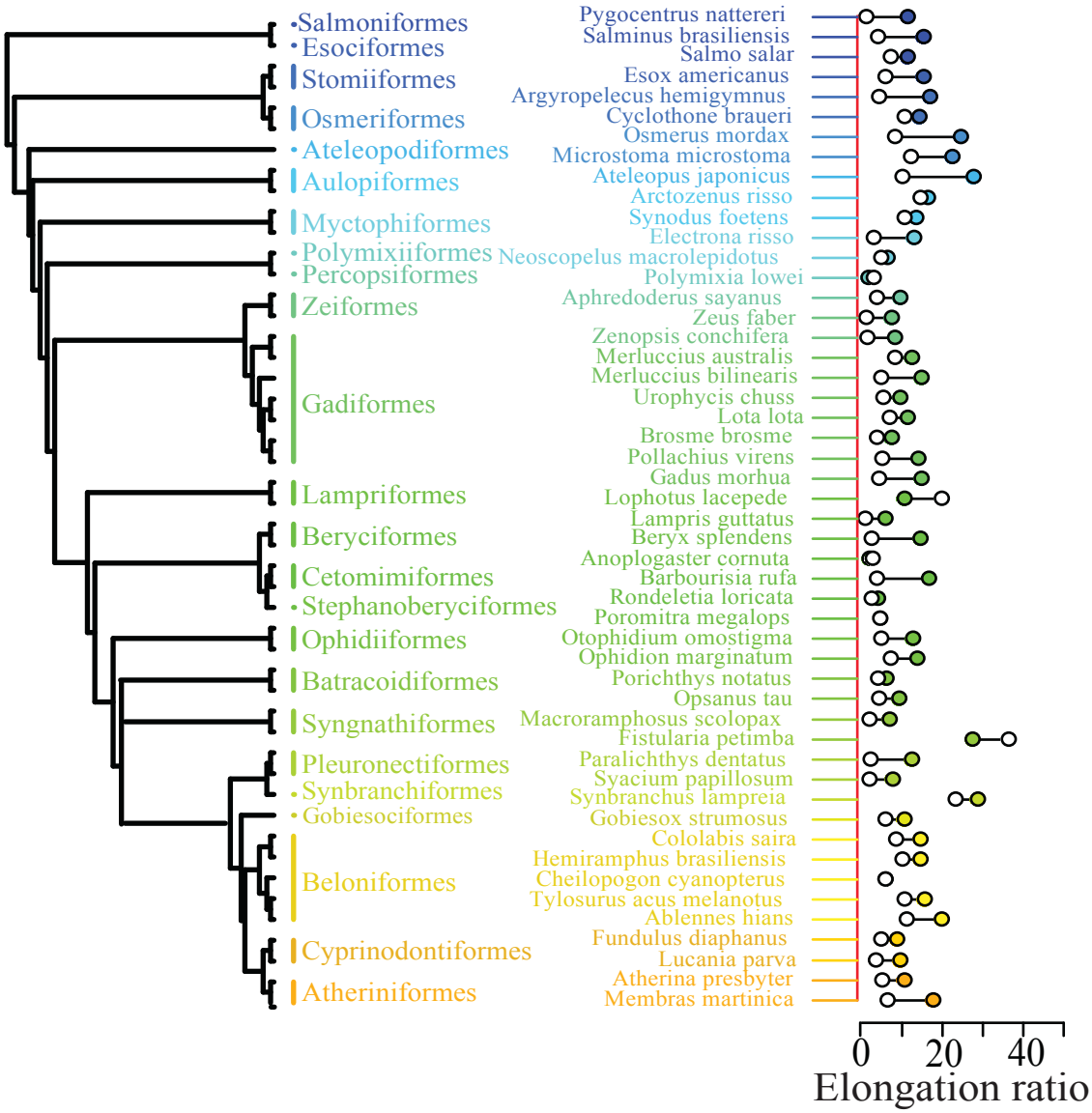

Figure S2.2: Individual larval and adult elongation ratios (Part 2). Genus and species name for a subset of species measured in this study with corresponding larval (filled circle) and adult (open circle) elongation ratios (see S1 Table for exact values). The measurements plotted are the same as those used for statistical analyses (see methods section for selection criteria). Colors correspond to the orders from which the species were selected. Modified from Figure 2.1.

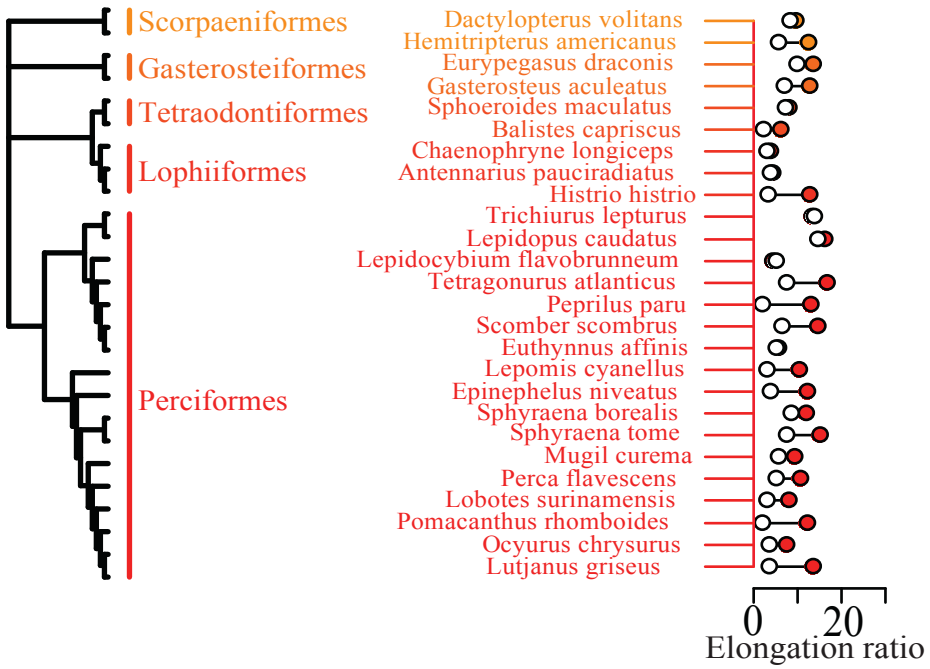

Figure S2.3: Individual larval and adult elongation ratios (Part 3). Genus and species name for a subset of species measured in this study with corresponding larval (filled circle) and adult (open circle) elongation ratios (see S1 Table for exact values). The measurements plotted are the same as those used for statistical analyses (see methods section for selection criteria). Colors correspond to the orders from which the species were selected. Modified from Figure 2.1.

Table S2.1: Primary elongation measurements and image sources. (left to right) Species, larval and adult elongation ratio values, larval image source, and adult image source for every specimen analyzed in this study. These raw elongation values were used for all statistical tests described in this study. MAB stands for Jones et al. (1987).

Species	larval, adult elongation ratio	Larval source	Adult Source
Acipenser oxyrhyncus	17.97, 12.07	O'Connor JM, Alber JB, Arvidson LG. 1981 Development and identification of larval Atlantic sturgeon (*Acipenser oxyrhynchus*) and shortnose sturgeon (*A. brevirostrum*) from the Hudson River estuary, New York. *Copeia*. 711-717.	MAB I: Goode GB, and a Staff of Associates. 1884
Lepisosteus osseus	27.93, 11.53	MAB I: Mansueti AJ, Hardy Jr. JD, after Kerr JG. 1919	MAB I: Suttkus RD. 1963
Amia calva	24.21, 6.50	MAB I: Dean B. 1896	MAB I: Goode GB, and a Staff of Associates. 1884
Elops saurus	26.46, 8.96	MAB I: Gehringer JW. 1959a	MAB I: Goode GB, and a Staff of Associates.1884
Megalops atlanticus	11.48, 4.00	Fahay MP. 2007 *Early stages of fishes in the Western North Atlantic Ocean*. NAFO. From Smith. 1980	fishbase: Meatl_u1.jpg by Garcia CB.
Notacanthus chemnitzii	81.74, 7.29	Fahay MP. 2007 *Early stages of fishes in the Western North Atlantic Ocean*. NAFO. From Moser, Charter. 1996a	fishbase: Noche_u1.jpg by Dolgov A.
Albula vulpes	17.24, 9.07	fishbase: Alvule_10.jpg by Sazima I.	MAB I: Goode GB, and a Staff of Associates. 1884
Eurypharynx pelecanoides	3.27, 30.67	Miller MJ. 2004 An Introduction to Leptocephali Biology and Identification. Ocean Research Institute, University of Tokyo	NMNZ P. 38952 by McPhee R.
Anguilla japonica	16.06, 22.30	Miller MJ. 2009 Ecology of Anguilliform leptocephali: remarkable transparent fish larvae of the ocean surface layer. Aqua-*BioSci. Monogr*. 2(4),1-94	fishbase: Anjap_u0.jpg Shao KT.
Anguilla rostrata	8.62, 13.68	Fahay MP. 2007 *Early stages of fishes in the Western North Atlantic Ocean*. redrawn from Vladykov. 1955	http://txstate.fishesoftexas.org/anguilla%20rostrata.htm: photo by Thomas C.
Gymnothorax funebris	9.14, 12.97	MAB II: Eldred B. 1970	fishbase: Gyfun_u0.gif Ref No 9358
Conger oceanicus	13.03, 19.73	Bell GW, Witting, DA, and Able, KW. 2003 Aspects of metamorphosis and habitat use in the Conger Eel, Conger oceanicus. *Copeia*. 3, 544-552	MAB VII: Bigelow HB, Schroeder WC. 1953
Hiodon alosoides	15.91, 3.84	Battle HI, Sprules WM. 1960 A description of the semi-buoyant eggs and early stages of the goldeye, hiodon-alosoides (Rafinesque) *J Fish Board Can*. 17(2), 245-266.	Stewart K, Watkinson D. 2004 *Freshwater fishes of Manitoba*. Univ. of Manitoba Press
Hiodon tergisus	15.40, 3.71	Snyder DE, Douglas SC. 1987 Description and identification of mooneye, Hiodon tergisus, protolarvae, *T Am Fish Soc*. 107(4), 590-594	Stewart K, Watkinson D. 2004 *Freshwater fishes of Manitoba*. Univ. of Manitoba Press

Table S2.1, continued.

Osteoglossum bicirrhosum	12.08, 5.18	Yanwirsal H. 2013 Reproductive styles of Osteoglossomorpha with emphasis on *Notopterus notopterus* and *Osteoglossum bicirrhosum* (Doctoral dissertation, Humboldt-Universität zu Berlin, Landwirtschaftlich-Gärtnerische Fakultät)	fishbase: Osbic_u0.jpg by IBAMA
Petrocephalus soudanensis	12.71, 3.45	Kirschbaum F, Schugardt C. 2002 Reproductive strategies and developmental aspects in mormyrid and gymnotiform fishes. *J Physiol*. 96, 557-566	Moritz T, Engelmann J, Linsenmair KE, von der Emde G. 2009 The electric organ discharges of the *Petrocephalus*species (Teleostei: Mormyridae) of the upper volta system. *J Fish Biol*. 74, 54-76
Notopterus notopterus	10.36, 3.86	Termvidchakorn A, Hortle KG. 2013 A guide to larvae and juveniles of some common fish species from the Mekong River Basin. MRC Technical Paper No. 38. Mekong River Commission, Phnom Penh. 234pp.	fishbase: Notopterus_notopterus.jpg by Mahalder B
Chitala ornata	8.30, 4.14	Termvidchakorn A, Hortle KG. 2013 A guide to larvae and juveniles of some common fish species from the Mekong River Basin. MRC Technical Paper No. 38. Mekong River Commission, Phnom Penh. 234pp.	fishbase: Chorn_u4.jpg by Baird IG.
Dorosoma petenense	22.84, 4.18	MAB I: Taber CA. 1961	http://txstate.fishesoftexas.org/dorosoma%20petenense.htm
Anchoa hepsetus	37.03, 5.69	MAB I: Hildebrand SF. 1963b	fishbase: Anhep_u0.jpg by Flescher D.
Gonorynchus greyi	17.29, 13.25	Leis JM, Trnski T, Bruce B. 1989 *The larvae of Indo-Pacific shorefishes*. Honolulu: University of Hawaii Press.	fishbase: Gogre_u9.jpg by Randall JE.
Chanos chanos	18.82, 6.93	Bagarinao TU. 1991 Biology of milkfish (Chanos chanos Forsskal). Iloilo, Philippines: Aquaculture Department, Southeast Asian Fisheries Development Center	fishbase: Chcha_u2.jpg by Randall JE
Carassius auratus	16.62, 3.93	Battle HI. 1940 The embryology and larval development of the goldfish (*Carassius Auratus L.*) from Lake Erie. *Ohio J Sci*. 40(2), 82-93	fishbase: Caaurau1.jpg by Winter TJ
Cyprinus carpio	11.75, 4.15	Cole NJ, Hall TE, Martin CI, Chapman MA, Kobiyama A, Nihei Y, Watabe S, and Johnston IA. 2004 Temperature and the expression of myogenic regulatory factors (MRFs) and myosin heavy chain isoforms during embryogenesis in the common carp Cyprinus carpio L. *JEB*. 207, 4239-4248	fishbase: Cyprinus.jpg by Kibria M, Asma GSM, Arafeen S.
Danio rerio	12.96, 6.30	Kimmel CB, Ballard WW, Kimmel SR, Ullmann B, and Schilling TF. 1995 Stages of Embryonic development of the zebrafish. *Dev Dynam*. 203, 253-310	photo by Hilary Katz
Catostomus commersonii	17.55, 6.79	Fishbase: Cacom_I0.gif by Faber DJ	http://gallery.nanfa.org/v/members/Uland/Family+Catostomidae/Catostomus/Catostomus+commersoni++White+Sucker+.jpg.html?g2_imageViewsIndex=1

Table S2.1, continued.

Erimyzon oblongus	12.47, 7.02	Fuiman LA. 1979 Descriptions and Comparisons of Catostomid Fish Larvae: Northern Atlantic Drainage Species, *T Am Fish Soc*. 108(6), 560-603,	MAB I: Trautman MB. 1957
Eigenmannia lineata	10.29, 8.10	Kirschbaum F, Schugardt C. 2002 Reproductive strategies and developmental aspects in mormyrid and gymnotiform fishes. *J Physiol - Paris*. 96, 557-566	Kirschbaum F, Schugardt C. 2002 Reproductive strategies and developmental aspects in mormyrid and gymnotiform fishes. *J Physiol - Paris*. 96:557-566
Apteronotus leptorhynchus	12.47, 6.51	Kirschbaum F, Schugardt C. 2002 Reproductive strategies and developmental aspects in mormyrid and gymnotiform fishes. *J Physiol - Paris*. 96, 557-566	Kirschbaum F, Schugardt C. 2002 Reproductive strategies and developmental aspects in mormyrid and gymnotiform fishes. *J Physiol - Paris*. 96, 557-566
Hypophthalmus edentatus	12.66, 4.72	Nakata K, Baumgartner G, Latini JD. 1998 Morphological description of larvae of the mapara *Hypophthalmus edentatus* (spix) (Osteichthyes, Hypophthalmidae) in the Itaipu reservoir (Parana river, Brazil)	fishbase: H_edentatus.jpg by Ferreira ES.
Ictalurus punctatus	10.00, 5.73	MAB I: Greeley JR, Bishop SC. 1932	MAB I: Trautman MB. 1957
Arius felis	8.22, 8.07	MAB I: Mansueti AJ, Hardy JD. 1967	fishbase: Arfel_u0.jpg by Flescher D.
Pygocentrus nattereri	12.43, 2.14	Bender A, Moritz T. 2013 Developmental residue and developmental novelty - different modes of adipose-fin formation during ontogeny. *Zoosyst. Evol.* 89(2), 209-214	fishbase: Pynat_u9.jpg by Timm CD.
Salminus brasiliensis	16.29, 4.83	Santos JE, Godinho HP. 2002 Ontogenic events and swimming behavior of larvae of the characid fish Salminus brasiliensis (Cuvier) (Characiformes, Characidae) under laboratory conditions. *Revta. bras. Zool*. 19(1), 163-171	fishbase: Sabra_u6.jpg by Sverlij S.
Salmo salar	12.31, 7.99	Gorodilov YN. 1996 Description of the early ontogeny of the Atlantic salmon, *Salmo salar*, with a novel system of interval (state) identification, *Env. Biol. Fish.* 47:109-127	fishbase: Sasal_u5.jpg by McDowall RM.
Esox americanus	16.15, 6.65	Leslie JK, Gorrie JF, 1985 Distinguishing features for separating protolarvae of three species of esocids. *Can. Tech. Rep. Fish. Aquat. Sci.* 1359:82 p.	MAB I: Mansueti AJ and Hardy JD. 1967
Argyropelecus hemigymnus	17.72, 5.29	Richards WJ. (Ed.). 2004 Early stages of Atlantic fishes: an identification guide for the western central north Atlantic, Two Volume Set. CRC Press.	fishbase: Arhem_u6.jpg by Fischer LG.
Cyclothone braueri	15.16, 11.43	Fahay MP. 2007 *Early stages of fishes in the Western North Atlantic Ocean*. NAFO. From Sanzo 1931a	MCZbase: The database of zoological collections: Cat Num: 143600
Osmerus mordax	25.56, 9.26	Cooper JE. 1978 Identification of eggs, larvae, and juveniles of the rainbow smelt, *Osmerus mordax*, with comparisons to larval alewife, *Alosa pseudoharengus*, and gizzard shad, *Dorosoma cepedianum*. *T Am Fish Soc*, 107(1), 56-62	Osmor_u2.jpg by Lyons J.
Microstoma microstoma	23.47, 13.16	Fahay MP. 2007 *Early stages of fishes in the Western North Atlantic Ocean*. NAFO. From Olivar and Fortuno 1991, redrawn from Sanzo, 1931a	fishbase: mimic_u0.gif Ref. No. 3978

Table S2.1, continued.

Ateleopus japonicus	28.67, 11.07	Amaoka K. 2003 *Preliminary Guide to the Identification of the Early Life History Stages of Ateleopodid Fishes of the Western Central North Atlantic*. US Department of Commerce, NOAA, NMFS, Southeast Fisheries Science Center.	fishbase: Atjap_u3.jpg by Ho HC.
Arctozenus risso	17.26, 15.48	Richards WJ. (Ed.) 2004 Early stages of Atlantic fishes: an identification guide for the western central north Atlantic, Two Volume Set. CRC Press. From Ege 1930	fishbase: Arris_u0.jpg by Dolgov.
Synodus foetens	14.53, 11.40	Richards WJ. (Ed.) 2004 Early stages of Atlantic fishes: an identification guide for the western central north Atlantic, Two Volume Set. CRC Press. From Able and Fahay 1998	fishbase: syfoe_u0.jpg by Flescher D.
Electrona risso	13.98, 3.84	Richards, W. J. (Ed.). 2004 Early stages of Atlantic fishes: an identification guide for the western central north Atlantic, Two Volume Set. CRC Press.	fishbase: Elris_u1.jpg by Costa F.
Neoscopelus macrolepidotus	7.26, 5.84	Richards, W. J. (Ed.). 2004 Early stages of Atlantic fishes: an identification guide for the western central north Atlantic, Two Volume Set. CRC Press. From Okiyama 1988c	fishbase: Nemac_u1.jpg by JAMARC
Polymixia lowei	2.66, 3.90	Fahay MP. 2007 *Early stages of fishes in the Western North Atlantic Ocean*. NAFO. From Bond PJ (Lyczkowski-Shultz 2006)	fishbase: Polow_u0.jpg by Flescher D.
Aphredoderus sayanus	10.54, 4.54	Minton AL, Osteen DV, Snyder DE. 1985 Description of larval pirate perch, *Aphredoderus sayanus* (Gilliams), from the Savannah River. Can. Tech. Rep. Fish. Aquat. Sci. 1359:82 p.	fishbase: Apsay_f0.jpg by Burkhead N and Jenkins R
Zeus faber	8.26, 1.94	fishbase: Zefab_I1.gif Ref. No. 63	fishbase: Zefab_f0.jpg by Cambraia Duarte PMN
Zenopsis conchifera	9.08, 2.27	Fahay MP. 2007 *Early stages of fishes in the Western North Atlantic Ocean*. NAFO. From Weiss et al. 1987	fishbase: Zecon_f0.jpg by Cambraia Duarte PMN.
Merluccius australis	13.28, 9.16	Bustos CA, Landaeta MF. 2005 Development of eggs and early larvae of the Southern hake, *Merluccius australis* reared under laboratory conditions. *Gayana*. *69*, 402-408	fishbase: Meaus_u0.jpg by SeaFIC.
Merluccius bilinearis	15.60, 5.81	MAB II: Kuntz A, Radcliffe L. 1918	fishbase: Mebil_u0.jpg by Flescher D.
Urophycis chuss	10.39, 6.25	fishbase: from Scotton, L.N., R.E. Smith, N.S. Smith, K.S. Price and D.P. de Sylva, 1973. Pictorial guide to fish larvae of Delaware Bay: with information and bibliographies useful for the study of fish larvae. Delaware Bay Report Series. Vol. 7. College of Marine Studies, University of Delaware. 205 p.	MAB II: Goode GB. 1884

Table S2.1, continued.

Lota lota	12.20, 7.91	Palińska-Żarska K, Żarski D, Krejszeff S, Nowosad J, Biłas M, Trejchel K, Kucharczyk D. 2014 Dynamics of yolk sac and oil droplet utilization and behavioural aspects of swim bladder inflation in burbot, *Lota lota* L., larvae during the first days of life, under laboratory conditions. *Aquacul Int*. *22*(1), 13-27	fishbase: Lota_ua.jpg by Artaev O.
Brosme brosme	8.34, 4.74	fishbase: Brbro_I1.gif by Faber DJ.	fishbase: Brbro_u0.jpg by Flescher D.
Pollachius virens	14.91, 6.05	Scotton LN, Smith RE, Smith NS, Price KS, de Sylva DP. 1973 Pictorial guide to fish larvae of Delaware Bay. Univ. Delaware, Del. Bay Rept. Ser, 7, 205: Bigelow and Schroeder, 1953	Povir_u0.jpg by Flescher D.
Gadus morhua	15.65, 5.20	Norman T Nicoll/ Natural Visions, image reference: NN_86_01_15	fishbase: Gamor_ub.jgp by Nilsson K.
Lophotus lacepede	11.40, 20.65	Fahay MP. 2007 *Early stages of fishes in the Western North Atlantic Ocean*. NAFO. From Sanzo 1940b	Lolac_u0.jpg by Ragonese S.
Lampris guttatus	6.81, 1.70	Ahlstrom EH. 1984 Ontogeny and systematics of fishes: Based on an International Symposium Dedicated to the Memory of Elbert Halvor Ahlstrom. American Society of Ichthyologists and Herpetologists. MCZ 58990	fishbase: 6760_full_107cm.jpg by Raulsinho R.
Beryx splendens	15.54, 3.40	Fahay MP. 2007 *Early stages of fishes in the Western North Atlantic Ocean*. NAFO. From Munday, 1990	fishbase: Bespl_f0.jpg by Duarte C, P.M.N.
Anoplogaster cornuta	2.74, 3.74	Fahay MP. 2007 *Early stages of fishes in the Western North Atlantic Ocean*. NAFO. From Richards et al., 2003	fishbase: Ancor_u1.jpg by Diaz B.
Barbourisia rufa	17.64, 4.54	Paxton JR, Johnson GD, Trnski T. 2001 Larvae and juveniles of the deepsea "whalefishes" Barbourisia and Rondeletia (Stephanoberyciformes: Barbourisiidae, Rondeletiidae), with comments on family relationships. *Records-Australian Museum*, 53(3), 407-426	fishbase: Baruf_u0.jpg by JAMARC
Rondeletia loricata	4.89, 3.46	Paxton JR, Johnson GD, Trnski T. 2001 Larvae and juveniles of the deepsea" whalefishes" Barbourisia and Rondeletia (Stephanoberyciformes: Barbourisiidae, Rondeletiidae), with comments on family relationships. *Records-Australian Museum*, 53(3), 407-426	fishbase: Rolor_u0.jpg by Garazo Fabregat A.
Poromitra megalops	5.47, 5.32	Fahay, M. P. (2007). *Early stages of fishes in the Western North Atlantic Ocean*. NAFO. From Sandknop and Watson, 1996a	fishbase: Pomeg_u0.jpg by Garazo Fabregat A./ Roman Marcote E.
Otophidium omostigma	13.55, 5.70	Richards WJ. (Ed.) 2004 Early stages of Atlantic fishes: an identification guide for the western central north Atlantic, Two Volume Set. CRC Press. From Jordan & Gilbert 1882	fishbase: Otomo_u0.jpg by JAMARC

Table S2.1, continued.

Ophidion marginatum	14.80, 8.19	MAB V: Scotton LN, etal. 1973	fishbase: Opmar_u0.jpg by Flescher D.
Porichthys notatus	7.00, 5.05	Richards WJ. (Ed.) 2004 Early stages of Atlantic fishes: an identification guide for the western central north Atlantic, Two Volume Set. CRC Press. From Watson 1996f	fishbase: Ponot_u0.gif, Ref. No. 12204
Opsanus tau	10.07, 5.24	MAB VI: Dovel W. 1960	MAB VI: Bigelow HB, Schroeder WC. 1953
Macroramphosus scolopax	7.71, 2.89	Kuranaga I, Sasaki K. 2000 Larval development in a snipefish (*Macroramphosus scoplopax*) from Japan with notes on eastern Pacific and Mediterranean Macroramphosus larvae (*Gasterosteiformes, Macroramphosidae*). *Ichthyol Res*. 47(1), 101-106	http://australianmuseum.net.au/image/A-Common-Bellowsfish-trawled-off-Norah-Head/ by Ken Graham
Fistularia petimba	28.47, 37.39	Barros FBAGD, Castro MSD, Bonecker ACT. 2007 Description and distribution of the larvae of two species of Fistulariidae (Teleostei, Syngnathiformes) in the southeastern Brazil. *Biota Neotropica*, 7(1)	fishbase: Fipet_u2.jpg by Randall JE.
Paralichthys dentatus	13.25, 3.21	Martinez GM, Bolker JA. 2003 Embryonic and larval staging of summer flounder (*Paralichthys dentatus*). *J Morphol*. 255(2), 162-176	fishbase: Paden_u0.jpg by Flescher D.
Syacium papillosum	8.52, 2.88	MAB VI: Futch CR, Hoff FH Jr., 1971	fishbase: Sypap_u2.jpg by NOAA/NMFS/Mississippi Laboratory
Synbranchus lampreia	29.63, 24.23	Favorito SE, Zanata AM, Assumpção MI. 2005 A new Synbranchus (Teleostei: Synbranchiformes: Synbranchidae) from ilha de Marajó, Pará, Brazil, with notes on its reproductive biology and larval development. *Neotrop Ichthyol*. 3(3), 319-328	Favorito SE, Zanata AM, Assumpção MI. 2005 A new Synbranchus (Teleostei: Synbranchiformes: Synbranchidae) from ilha de Marajó, Pará, Brazil, with notes on its reproductive biology and larval development. *Neotrop Ichthyol*. *3*(3), 319-328
Gobiesox strumosus	11.62, 6.86	Fahay MP. 2007 *Early stages of fishes in the Western North Atlantic Ocean*. NAFO. From Runyan, 1961	fishbase: Gostr_u0.gif Ref. No. 9358
Cololabis saira	15.38, 9.33	fishbase: Cosai I0.gif, Ref. No. 265	fishbase: CosaiU0.jpg by Miyahara H.
Hemiramphus brasiliensis	15.53, 10.95	Hardy JD, Johnson RK. 1974 Descriptions of halfbeak larvae and juveniles from Chesapeake Bay (Pisces: Hemiramphidae). *Chesapeake Science*. *15*(4), 241-246.	MAB II: Jordan DS, Evermann BW. 1896-1900
Cheilopogon cyanopterus	6.73, 6.85	Fahay MP. 2007 *Early stages of fishes in the Western North Atlantic Ocean*. NAFO. From T.N. Steyker (Kovalevskaya, 1977)	fishbase: Chcya_u3.jpg by Hermosa GV Jr.
Tylosurus acus melanotus	16.43, 11.47	Fahay MP. 2007 *Early stages of fishes in the Western North Atlantic Ocean*. NAFO. From Mito, 1958 (redrawn)	fishbase: Tyacu_u0.jpg by Shao KT.
Ablennes hians	20.63, 11.93	Fahay MP. 2007 *Early stages of fishes in the Western North Atlantic Ocean*. NAFO. From Chen 1988	MAB II: Bigelow HB, Schroeder WC. 1953

Table S2.1, continued.

Fundulus diaphanus	9.56, 5.84	Jones GG, Tabery MA, Turnpike G. 1980 Larval development of the banded killifish (*Fundulus diaphanus*) with notes on the distribution in the Hudson River estuary. In *Proceedings of the Fourth Annual Larval Fish Conference, February 27-28, 1980, Oxford, Mississippi* (p. 25). Fish and Wildlife Service, US Department of the Interior.	fishbase: Fudia_f0.jpg by Burkhead N, Jenkins R, courtesy of VDGIF
Lucania parva	10.39, 4.28	Crawford SS, Balon EK. 1994 Alternative life histories of the genus Lucania: 1. Early ontogeny of *L. parva*, the rainwater killifish. *Environ Biol Fishes*. 40(4), 349-389	MAB II: Bean TH. 1888
Atherina presbyter	11.50, 6.00	Bamber RN, Henderson PA, Turnpenny AWH. 1985 The early life history of the sand smelt (*Atherina presbyter*). *J Mar Biol Assoc UK,* 65(03), 697-706.	fishbase: MNHN 2004-1491
Membras martinica	18.65, 7.29	MAB VI: Wang JCS. 1974	fishbase: Memar_u1.jpg by Thomas C.
Dactylopterus volitans	9.41, 8.15	Fahay MP. 2007 *Early stages of fishes in the Western North Atlantic Ocean*. NAFO. From Padoa 1956c	fishbase: Davol_u3.jpg by Cambraia Duarte, PMN.
Hemitripterus americanus	12.23, 5.57	Fahay MP. 2007 *Early stages of fishes in the Western North Atlantic Ocean*. NAFO. From Fuiman 1976	MAB V: Goode GB. 1884
Eurypegasus draconis	13.37, 9.72	Herold D, Clark E. 1993 Monogamy, spawning and skin-shedding of the sea moth, *Eurypegasus draconis* (Pisces: Pegasidae). *Environ Biol Fishes*. 37(3), 219-236	fishbase: Eudra_u7 by Randall JE.
Gasterosteus aculeatus	12.67, 6.79	fishbase: Gaacu_I0.jpg by Pinder AC.	fishbase: Gaacu_u7.jpg by Miyahara H.
Sphoeroides maculatus	7.95, 6.91	MAB VI: Welsh WW, Brender CM Jr. 1922	fishbase: Spmac_u0.jpg by Flescher D.
Balistes capriscus	5.91, 2.03	Matsuura Y, Katsuragawa M. 1981 Larvae and juveniles of grey triggerfish, *Balistes capriscus*, from Southern Brazil. *Jap J Ichthyol*. 28(3), 267-275	fishbase: Bacar_u1.jpg by Flescher D.
Chaenophryne longiceps	3.49, 2.88	Fahay MP. 2007 *Early stages of fishes in the Western North Atlantic Ocean*. NAFO. From Bertelsen, 1951	Australian Museum CSIRO H6022-01
Antennarius pauciradiatus	4.19, 3.52	Baldwin CC. 2013 The phylogenetic significance of colour patterns in marine teleost larvae. *Zool J of Linnean Soc*. 168(3), 496-563	Williams JT, Carpenter KE, Van Tassell JL, Hoetjes P, Toller W, Etnoyer P, Smith M. 2010 Biodiversity assessment of the fishes of Saba Bank atoll, Netherlands Antilles. *PloS one*. 5(5), e10676
Histrio histrio	12.67, 3.15	MAB VI: Fujita S, Uchida K. 1959	fishbase: Hihis_u5.jpg by Randall JE.
Trichiurus lepturus	13.08, 13.59	fishbase: Trlep_I3.gif Ref No. 44342	fishbase: Trlep_u1.jpg by Flescher D.
Lepidopus caudatus	15.98, 14.38	fishbase: Lecau_I0.gif, Ref. No. 29072	fishbase: Lecau_f0.jpg by Cambraia Duarte, PMN.

Table S2.1, continued.

Lepidocybium flavobrunneum	4.02, 4.96	Nishikawa Y. 1982 Early development of the fishes of the family Gempylidae I. Larvae and juveniles of escolar, *Lepidocybium flavobrunneum* (Smith). *Bull Far Seas Fish Res Lab*. 19, 1-19.	fishbase: Lefla_u1.jpg by Camraia Duarte, PMN.
Tetragonurus atlanticus	16.64, 7.42	MAB VI: Ahlstrom EH, Butler JL, and Sunida BY. 1976	fishbase: Teatl_u0.gif, Ref. No. 4415
Peprilus paru	12.92, 1.70	MAB VI: Pearson JC. 1941	fishbase: Pepar_u1.jpg by Ramjohn DD.
Scomber scombrus	14.36, 6.29	fishbase: Scsco_I0.jpg by Mendiola D.	fishbase: NRM 49614b from Swedish Museum of Natural History
Euthynnus affinis	5.32, 4.95	National Bioresource Development Board, Dept. of Biotechnology, Government of India, New Delhi. Reproduced from Gorbunova, 1974	fishbase: Euaff_u1.jpg by Randall JE.
Lepomis cyanellus	10.24, 2.77	Taubert BD. 1977 Early morphological development of the green sunfish, *Lepomis cyanellus*, and its separation from other larval Lepomis species. *T Am Fish Soc*. 106(5), 445-448	fishbase: Lecya_m6.jpg by Burkhead N, Jenkins R, courtesy of VDGIF
Epinephelus niveatus	11.92, 3.49	Powell AB, Tucker JW. 1992 Egg and larval development of laboratory-reared Nassau grouper, *Epinephelus striatus* (Pisces, Serranidae). *Bull Mar Sci*. 50(1), 171-185	fishbase: Epniv_u0.jpg by Flescher D.
Sphyraena borealis	11.65, 8.34	MAB VI: Houde ED. 1972	fishbase: Spbor_u0.jpg by Flescher D.
Sphyraena tome	14.85, 7.40	Matsuura Y, Suzuki K. 1997 Larval development of two species of barracuda, *Sphyraena guachancho* and *S. tome* (Teleostei: Sphyraenidae), from southeastern Brazil. *Ichthyol Res*. 44(4), 369-378	fishbase: sphyraenatome.jpg by Vaske T Jr.
Mugil curema	9.18, 5.37	MAB VI: Anderson WW. 1957	fishbase: Mucur_u1.jpg by CENAIM
Perca flavescens	10.57, 4.81	Mansueti AJ. 1964 Early development of the yellow perch, *Perca flavescens*. *Chesapeake Science*. 5(1-2), 46-66	fishbase: Pefla_m0.jpg by Burkhead N, Jenkins R, courtesy of VDGIF
Lobotes surinamensis	7.79, 2.74	Ditty JG, Shaw RF. 1994 *Lobotes surinamensis* (Pisces: Lobotidae), and their spatial and temporal distribution in the northern Gulf of Mexico. *Fish Bull*. 92(1), 33-45	fishbase: Losur_u0.jpg by Jimenez PP.
Pomacanthus rhomboides	11.98, 1.79	Baldwin CC. 2013 The phylogenetic significance of colour patterns in marine teleost larvae. *Zool J Linnean Soc*. 168(3), 496-563	fishbase: Porho_u0.jpg by Randall JE.
Ocyurus chrysurus	7.39, 3.27	Riley CM, Holt GJ, Arnold CR. 1995 Growth and morphology of larval and juvenile captive bred yellowtail snapper, *Ocyurus chrysurus*. *Fish Bull*. *93*, 179-185	fishbase: Occur_u8.jpg by Macieira RM.
Lutjanus griseus	13.36, 3.38	Richards WJ, Saksena VP. 1980 Description of larvae and early juveniles of laboratory-reared gray snapper, *Lutjanus griseus* (Linnaeus)(Pisces, Lutjanaidae). *Bull Mar Sci*. *30*(2), 515-521	fishbase: Lugri_u0.jpg by Flescher D.

Table S2.2: Secondary elongation measurements and image sources. These values were not included in the statistical analyses since we were not able to find a second source for every study. We chose to include these sources for the benefit of individuals looking to find multiple online sources for larval and adult stages.

Species	larval adult elongation	larval source	adult source
Acipenser oxyrhyncus	15.00, x	MAB I: Ryder JA. 1890	x
Lepisosteus osseus	x, 13.82	x	Official gallery of NANFA: Longnose gar 1500
Amia calva	x, 5.93	x	http://txstate.fishesoftexas.org/amia%20calva.htm
Elops saurus	x, 9.23	x	NOAA photo library: fish4201 by Noble B
Megalops atlanticus	x, x	x	x
Notacanthus chemnitzii	x, x	x	x
Albula vulpes	35.95, 7.91	MAB I: Alexander EC. 1961	Marinebio.org species database
Eurypharynx pelecanoides	x, x	x	x
Anguilla japonica	14.81, x	Miller MJ. 2004 An Introduction to Leptocephali Biology and Identification. Ocean Research Institute, University of Tokyo	x
Anguilla rostrata	x, x	x	x
Gymnothorax funebris	x, 17.26	x	fishbase: Gyfun_u4.jpg by Hofinger E.
Conger oceanicus	17.92, x	MAB VII: Bigelow HB, Schroeder WC. 1953	x
Hiodon alosoides	x, x	x	x
Hiodon tergisus	x, 4.05	x	ODNR Division of Wildlife by Zimmerman B
Osteoglossum bicirrhosum	x, x	x	x
Petrocephalus soudanensis	x, 2.84	x	Moritz T, Engelmann J, Linsenmair KE, von der Emde G. 2009 The electric organ discharges of the *Petrocephalus* species (Teleostei: Mormyridae) of the upper volta system. *J Fish Biol*. 74, 54-76
Notopterus notopterus	x, x	x	x
Chitala ornata	x, x	x	x
Dorosoma petenense	x, 4.78	x	MAB I: Miller RR. 1963
Anchoa hepsetus	x, 7.05	x	MAB I: Hildebrand SF, Cable LE. 1930
Gonorynchus greyi	x, x	x	x
Chanos chanos	19.00, 7.41	fishbase: Chcha_I0.gif, Ref No 41564	fishbase: Chcha_u0.jpg by Shao KT.

Table S2.2, continued.

Carassius auratus	x x	x	x
Cyprinus carpio	17.67, 5.60	MAB I: Taber CA. 1969	MAB I: Smith HM. 1896
Danio rerio	x, x	x	x
Catostomus commersonii	x, x	x	x
Erimyzon oblongus	19.47, 6.20	MAB I: Carnes WC Jr. 1958	fishbase: Erbol_u1.jpg by Lyons J.
Eigenmannia lineata	x, 8.20	x	fishbase: Eivir_u4.jpg by Holm E.
Apteronotus leptorhynchus	x x	x	x
Hypophthalmus edentatus	x 4.72	x	fishbase: MNHN A-896A
Ictalurus punctatus	x, 6.57	x	mid-atlantic stocking: http://www.midatlanticstocking.com /images/Channel%20Catfish.gif
Arius felis	x, 8.52	x	MAB I: Goode GB, etal. 1884
Pygocentrus nattereri	x, 2.44	x	fishbates: Pynat_u3.jpg by Ostergaard T
Salminus brasiliensis	x, 4.82	x	fishbase: Sabra_ub.jpg by Timm CD.
Salmo salar	10.61, x	von Schalburg KR, Yasuike M, Yazawa R, De Boer JG, Reid L, So S, Robb A, Rondeau EB, Phillips RB, Davidson WS, Koop BF. 2011. Regulation and expression of sexual differentiation factors in embryonic and extragonadal tissues of Atlantic salmon. *BMC genomics*. 12(1), 31	x
Esox americanus	16.00, x	MAB I: Mansueti AJ, Hardy JD Jr, 1967	x
Argyropelecus hemigymnus	x, 4.94	x	fishbase: Arhem_u1.jpg by Costa F.
Cyclothone braueri	x, 11.87	x	fishbase: Cybra_u0.jpg by Costa F.
Osmerus mordax	x, x	x	x
Microstoma microstoma	x, 12.08	x	fishbase: Mimic_u1.jpg by Costa F.
Ateleopus japonicus	x, 19.06	x	Amaoka K. 2003 *Preliminary Guide to the Identification of the Early Life History Stages of Ateleopodid Fishes of the Western Central North Atlantic*. US Department of Commerce, NOAA, NMFS, SFSC.
Arctozenus risso	x, x	x	x
Synodus foetens	16.74, 13.55	MAB I: Mansueti AJ, Hardy JD Jr. 1967	MAB I: Anderson WW, Gehringer JW, Berry FH. 1966
Electrona risso	x, 3.35	x	fishbase: Elris_u0.jpg by JAMARC
Neoscopelus macrolepidotus	x, 6.33	x	World Register of Marine Species: Noères, Claude
Polymixia lowei	x, 4.02	x	fishbase: Polow_u1.gif Ref. No. 9358

Table S2.2, continued.

Aphredoderus sayanus	15.26, 5.17	MAB III: Drawn from photographs, Peters ER	MAB III: Trautman MB. 1957
Zeus faber	x, 2.15	x	fishbase: Zefab_uc.jpg by Dijkstra K.
Zenopsis conchifera	x, 1.87	x	fishbase: PA034125.jpg by Winkler M.
Merluccius australis	15.30, x	fishbase: Meaus_I1.jpg by Chile F.	x
Merluccius bilinearis	9.32, 6.20	fishbase: Mebil_I0.gif by Faber DJ	MAB II: Goode GB. 1884
Urophycis chuss	x, x	x	x
Lota lota	x, x	x	x
Brosme brosme	x, x	x	x
Pollachius virens	x, x	x	x
Gadus morhua	13.34, 4.39	MAB II: M'Intosh WC, Masterman AT. 1897	MAB II: Goode GB. 1884
Lophotus lacepede	x, 20.65	x	Dulčić, J, Ahnelt H. 2007 How many specimens of the crested oarfish, *Lophotus lacepede Giorna*, 1809 (Pisces: Lophotidae), were caught in the Adriatic Sea? *Acta adriatica*. 48(1), 39-43.
Lampris guttatus	x, 1.86	x	fishbase: Lagut_ua.jpg by Mincarone MM
Beryx splendens	x, 4.84	x	fishbase: Bespl_ud.jpg by Labbe J, Ahumada M.
Anoplogaster cornuta	x, 3.98	x	fishbase: Ancor_u0.jpg by JAMARC
Barbourisia rufa	x, 5.44	x	fishbase: Baruf_u0.gif, Ref. No. 4249
Rondeletia loricata	x, 2.74	x	fishbase: Rolor_u0.gif, Ref. No. 4246
Poromitra megalops	x, 4.47	x	fishbase: Pomeg_u0.gif, Ref. No. 4241
Otophidium omostigma	x, 5.28	x	eol.org: Cat num 167777 from Museum of Comparative Zoology, Harvard
Ophidion marginatum	x, 8.21	x	MAB V: Hildebrand SF, Schroeder WC. 1928
Porichthys notatus	x, x	x	x
Opsanus tau	x, x	x	x
Macroramphosus scolopax	14.03, 3.25	MAB II: Sparta A. 1936	MAB II: Kamohara T. 1967
Fistularia petimba	28.08, 30.21	MAB II: Mito S. 1961	fishbase: Fipet_u3.jpg by Cambraia Duarte, PMN
Paralichthys dentatus	12.38, 3.41	MAB VI: Smith WG, Fahay MP. 1970	MAB VI: Norman JR. 1934
Syacium papillosum	x, 2.99	x	MAB VI: Futch CR, Hoff FH Jr. 1971
Synbranchus lampreia	x, x	x	x
Gobiesox strumosus	x, x	x	x

Table S2.2, continued.

Cololabis saira	x, x	x	x
Hemiramphus brasiliensis	14.73, x	MAB II: Hardy JD, Johnson RK. 1974	x
Cheilopogon cyanopterus	x, x	x	x
Tylosurus acus melanotus	x, x	x	x
Ablennes hians	20.84, x	MAB II: Original drawing by Smith NS.	x
Fundulus diaphanus	10.19, 5.36	www.fishbabies.ca/frwspecies.html	fishbase: Fdiaphanusmale.jpg by Terceira AC.
Lucania parva	10.15, x	MAB II: Foster N. 1974	x
Atherina presbyter	16.50, 6.51	Palmer CJ, Culley MB. 1984 The egg and early life stages of the sandsmelt, Atherina presbyter Cuvier. *J Fish Biol*. 24(5), 537-544.	fishbase: Atpre_u0.jpg by Ostergaard T.
Membras martinica	x, 6.61	x	http://txmarspecies.tamug.edu/
Dactylopterus volitans	x, 7.11	x	fishbase: Davol_m0.jpg by Freitas R.
Hemitripterus americanus	x, 5.20	x	World Register of Marine Species: Fisheries and Oceans Canada, Wiele H.
Eurypegasus draconis	x, 6.67	x	fishbase: Eudra_u5.jpg by Randall JE.
Gasterosteus aculeatus	18.69, 6.52	MAB II: Swarup H. 1958	MAB II: Hildebrand SF, Schroeder WC. 1928
Sphoeroides maculatus	7.83, 6.79	www.jeffbloom.net by Jeffrey Bloom 2010	MAB VI: Welsh WW, Breder CM Jr. 1922
Balistes capriscus	3.46, 2.25	Lyczkowski-Shultz J, Ingram GW. 2003 *Preliminary guide to the identification of the early life stages of balistid fishes of the western Central North Atlantic*. US Department of Commerce, NOAA, NMFS, Southeast Fisheries Science Center, Mississippi Laboratory.	fishbase: Bacar_u6.jpg by Cambraia Duarte, PMN.
Chaenophryne longiceps	x, 2.77	x	fishbase: Chlon_u1.jpg by Dolgov A.
Antennarius pauciradiatus	x, x	x	x
Histrio histrio	x, 2.56	x	MAB VI: Jordan DS. 1905
Trichiurus lepturus	x, x	x	x
Lepidopus caudatus	x, x	x	x
Lepidocybium flavobrunneum	x, x	x	x
Tetragonurus atlanticus	x, 7.24	x	MAB VI: Jordan DS, Evermann BW. 1896-1900
Peprilus paru	x, 1.78	x	MAB VI: Hilebrand S, Schroeder WC. 1928
Scomber scombrus	x, x	x	x
Euthynnus affinis	x, x	x	x

Table S2.2, continued.

Lepomis cyanellus	x, 3.00	x	MAB III: Trautman MB. 1957
Epinephelus niveatus	x, 3.88	x	MAB II: Smith CL. 1971
Sphyraena borealis	x, 8.37	x	MAB VI: Goode GB. 1884
Sphyraena tome	x, x	x	X
Mugil curema	x, 5.37	x	MAB VI: Goode GB. 1884
Perca flavescens	13.78, 4.81	MAB III: Fish MP. 1929	MAB III: Goode GB, etal. 1884
Lobotes surinamensis	x, 2.81	x	MAB III: Goode GB, etal. 1884
Pomacanthus rhomboides	x, 1.62	x	fishbase: Porhu_u1.jpg by Randall JE.
Ocyurus chrysurus	x, 4.09	x	MAB III: Jordan DS, Evermann BW. 1896-1900
Lutjanus griseus	x, x	x	x